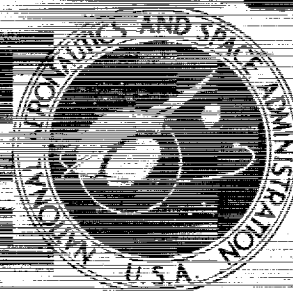


Available from NASA to U. S.
Government agencies and U. S.
Government contractors only.

X67 12811

NASA CONTRACTOR REPORT



UB
NASA CR-698

UB
NASA CR-698

CASE FILE
COPY

CLASSIFICATION CHANGED
UNCLASSIFIED

TO

By Authority of

NASA ID 70-37-1-28-70

12-5-69

PRELIMINARY CONCEPTUAL DESIGN STUDY OF A SPECIFIC VORTEX-STABILIZED GASEOUS NUCLEAR ROCKET ENGINE

by G. H. McLafferty, H. E. Bauer, and D. E. Sheldon

Prepared by
UNITED AIRCRAFT CORPORATION
East Hartford, Conn.
for

Declassified by authority of NASA
Classification Change Notices No. 191
Dated ** 28 FEB 1970

NATIONAL AERONAUTICS AND SPACE ADMINISTRATION • WASHINGTON, D. C. • MARCH 1967



PRELIMINARY CONCEPTUAL DESIGN STUDY OF
A SPECIFIC VORTEX-STABILIZED GASEOUS
NUCLEAR ROCKET ENGINE

By G. H. McLafferty, H. E. Bauer, and D. E. Sheldon

Distribution of this report is provided in the interest of
information exchange. Responsibility for the contents
resides in the author or organization that prepared it.

Prepared under Contract No. NASw-847 by
UNITED AIRCRAFT CORPORATION
East Hartford, Conn.

for

NATIONAL AERONAUTICS AND SPACE ADMINISTRATION

UNCLASSIFIED

UNCLASSIFIED

UNCLASSIFIED

UNCLASSIFIED

UNCLASSIFIED

Preliminary Conceptual Design Study

of a Specific Vortex-Stabilized Gaseous Nuclear Rocket Engine (U)

TABLE OF CONTENTS

	<u>Page</u>
SUMMARY	1
RESULTS	2
INTRODUCTION	4
DESCRIPTION OF ENGINE CONFIGURATION	5
CAVITY CONDITIONS	6
HEAT BALANCE	8
CHARACTERISTICS OF MODERATOR REGION	11
Inner Liner Region	11
Beryllium Oxide and Graphite Moderator Regions	12
Heavy-Water Moderator Region	15
CHARACTERISTICS OF EXTERNAL REGION	16
External Piping	16
Heat Exchangers	16
Turbopumps	17
Pressure Vessel	18
ENGINE WEIGHT	21
ENGINE PERFORMANCE	23
LIMITATIONS OF DESIGN STUDY	25

CONFIDENTIAL

TABLE OF CONTENTS (cont'd)

	<u>Page</u>
EFFECT OF SELECTED DESIGN MODIFICATIONS ON ENGINE CHARACTERISTICS	26
Elimination of Helium Circuit	26
Use of Bleed Turbopump Cycle	26
Increase in Helium Temperature	27
Increase in Critical Mass of Nuclear Fuel	28
REFERENCES	29
LIST OF SYMBOLS	35
APPENDIXES	
A - APPROXIMATE CONDITIONS DURING ENGINE START-UP	38
B - EFFECT OF CHANGES IN CRITICAL MASS AND AVERAGE CAVITY PROPELLANT ENTHALPY ON ENGINE CHARACTERISTICS	41
C - MODERATOR CONFIGURATION WITH SPIRAL HOLES	43
TABLES	49
FIGURES	65

CONFIDENTIAL

CONFIDENTIAL

Preliminary Conceptual Design Study

of a Specific Vortex-Stabilized Gaseous Nuclear Rocket Engine (U)

SUMMARY

A study of a specific gaseous nuclear rocket engine configuration was made to determine the approximate weight of the primary components of the engine and to determine the dimensions necessary for the determination of the critical mass of nuclear fuel required. The vortex-stabilized engine concept considered is based on the transfer of heat by thermal radiation from gaseous nuclear fuel suspended in a vortex to seeded propellant passing axially over the fuel-containment region. The configuration employed in the study is assumed to have both a cavity diameter and cavity length of 6 ft and a moderator composed of successive layers of beryllium, beryllium oxide, graphite, and heavy water. The energy deposited in the moderator is assumed to be removed by a helium coolant and transferred through external heat exchangers to the propellant. The engine is estimated to have the following characteristics: specific impulse, 2186 sec; thrust, 1.45×10^6 lb; and weight of major components, between 113,000 and 211,000 lb. The analysis of the engine configuration covered only design-point operation.

The appendixes to the report include results of studies of the following: the approximate conditions in the engine during the start-up process; the effect of changes in critical mass and average cavity propellant enthalpy on engine characteristics; and a criteria for laminar-flow instability in the spiral-hole configuration employed for cooling the moderator.

RESULTS

1. The nuclear rocket engine is estimated to have a thrust of 1.45×10^6 lb, a specific impulse of 2186 sec, and a weight of major components between 113,000 and 211,000 lb.

2. The largest uncertainty in the weight of the engine considered in the design study is due to uncertainties in the weight of the pressure vessel. The estimated pressure vessel weight varies from 30,600 lb for a cylindrical, filament-wound configuration employing filaments having a strength-to-density ratio of 5.0×10^6 in., to 125,000 lb for a spherical configuration made from maraging steel having a strength of 240,000 psi.

3. The estimated weights of the major components other than the pressure vessel are: moderator region, 50,700 lb; external heat exchanger, 13,500 lb; and turbopumps and ducting, between 18,600 and 21,900 lb.

4. The structural surface area in the moderator region requiring protection from hot hydrogen is 410 ft²: 170 ft² of cavity surface area; and 240 ft² in the ducts through which the hydrogen passes through the moderator. Since helium is employed to remove the energy deposited in the moderator, no protection is required in the moderator coolant ducts.

5. The use of tungsten-184 to protect the moderator region from hydrogen attack requires the use of 1170 lb of tungsten-184: 565 lb in a series of small-diameter coolant tubes located on the inside surface of the moderator; 50 lb in the injection nozzles through which the hydrogen is injected into the cavity; and 555 lb in the hydrogen ducts passing through the moderator. The presence of the tungsten-184 causes an increase of approximately 60 percent in the critical mass required due to neutron absorption in the tungsten.

6. The use of graphite coated with a 0.002-in. thick layer of niobium carbide to protect the moderator region from hot hydrogen results in the requirement for 34 lb of niobium carbide: 14 lb on the surface of the small tubes employed at the cavity surface; and 20 lb in the passages used to duct the hydrogen through the moderator region. This configuration also requires the use of 50 lb of tungsten-184 in the nozzles employed to inject the hydrogen into the cavity. Although the weight difference between the niobium carbide and tungsten tube configurations is negligible with respect to the total system weight, the use of the niobium carbide configuration would eliminate most of the increase in critical mass which would result from the use of tungsten-184.

7. The average total void fraction required in the moderator region is 12 percent: 3 percent due to coolant passages in the beryllium, beryllium oxide, and graphite portions of the moderator; 4 percent due to ducting and plenums for the helium and hydrogen; and 5 percent due to the annulus leading from the cavity to the exhaust nozzles.

8. The total mass of moderator material employed in the engine is 49,500 lb: 18,100 lb of graphite; 18,750 lb of heavy water; 9530 lb of beryllium oxide; and 3120 lb of beryllium.

9. The pressure drops in the cooling passages, ducts, and heat exchangers are 35 atm, 30 atm, and 5 atm for the helium, hydrogen, and heavy-water systems, respectively.

10. The use of a spiral-coolant-hole configuration results in a reduced pressure drop relative to a straight-coolant-hole configuration, permits the use of radial ducting for the gases passing through the moderator region, and reduces the possibility of laminar-flow instability at low power levels. A spiral-coolant-hole configuration could be made by employing circular cylinders with spiral grooves cut in the outside of the cylinder, and inserting these cylinders into cylindrical holes in a containing block.

11. The calculated engine specific impulse for an assumed hydrogen injection temperature of 4300 R and an average fuel density ratio of 5.0 is 2186 sec, including allowance for a finite-area-ratio nozzle, nozzle recombination losses, nozzle friction and flow nonuniformity losses, and transpiration coolant flow.

INTRODUCTION

The feasibility of a vortex-stabilized gaseous nuclear rocket engine has been under investigation at the Research Laboratories of United Aircraft Corporation since 1959. This work has been supported under a NASA Contract monitored by the Space Nuclear Propulsion Office (Contract NASw-847); under Air Force Contracts monitored by Edwards Air Force Base (Contracts AF 04(611)-7448 and AF 04(611)-8189); and under Corporate sponsorship. Reports issued under these contracts are listed in chronological order as Refs. 1 through 41. The present report is one of a series of six reports (see Refs. 37 through 41) which describe portions of the work conducted during the period from September 1965 through September 1966.

Studies of the performance characteristics of a vortex-stabilized gaseous nuclear rocket engine made to date (Refs. 4, 10, and 36) have been conducted to obtain general information on the effect of size and pressure on engine performance. The results of these studies give only approximate indications of engine weight because of the simplifications made in specifying the engine design. The studies described in the following sections were initiated to determine a more realistic engine design for a specific set of input conditions and assumptions which have been chosen on the basis of the more generalized work of Ref. 36. The specific engine configuration described in the following sections has also been employed in the studies of Ref. 40 to obtain a more accurate estimate of the mass of nuclear fuel required for criticality. Although the configuration described in the following sections has been chosen on the basis of that required for a vortex-stabilized gaseous nuclear rocket, many of the results obtained also apply to the design of the coaxial-flow gaseous nuclear rocket now being investigated at the NASA Lewis Research Center. Work on the coaxial-flow reactor is described in Refs. 42 through 52.



DESCRIPTION OF ENGINE CONFIGURATION

The engine configuration chosen for study is, in general, similar to that employed in preceding studies of vortex-stabilized gaseous nuclear rockets (Refs. 4, 10, and 36). However, several changes have been made, and both new and old configurations are illustrated in Fig. 1. The primary difference in the two configurations is that a series of six nozzles has been employed in the engine for the present study versus the single nozzle assumed for preceding studies. The change in nozzle configuration was made because the surface area downstream of the primary cavity is reduced and because it resulted in a more simple configuration for use in the criticality studies of Ref. 40. In addition, curved end walls were substituted for the flat end walls assumed in preceding studies in order to minimize stresses due to pressure differences between the gases in the moderator and the gases in the cavity.

A simplified layout drawing of the design configuration devised during the present study is shown in Fig. 2, and a sketch showing the various regions of the structure surrounding the cavity is given in Fig. 3. Discussions of each of the regions shown in Fig. 3 are given in the following sections of this report. A total of 1100 injection ports are employed to inject propellant into the cavity. Since the structural section shown in Fig. 3 is approximately that associated with a single cavity injection port, a complete engine would be made up of 1100 sections substantially similar to that shown in Fig. 3. It should be pointed out that the design configuration shown in Figs. 2 and 3 has not been optimized, but is intended for use in making preliminary estimates of engine weight and critical mass. The design is based on a cavity having a length of 6 ft and a diameter of 6 ft. Radial dimensions to each of the regions shown in Figs. 2 and 3 are given in Table I.

Nuclear fuel is assumed to be injected into the cavity through a port in the nonaxial-flow end wall. Discussions of the design of this injection port are contained in Refs. 35 and 40. It is also assumed that the secondary flow near the end walls of the cavity is made to flow radially outward by injecting this flow with high angular momentum (see Ref. 29).

Specifications for the analyses described in the following sections of this report were determined from Figs. 42 through 50 of Ref. 36 on the basis of a cavity diameter of 6 ft, a cavity pressure of 1000 atm, an engine thrust-to-weight ratio of 10, and a fuel density ratio, $\bar{\rho}_F/\rho_6$, of 5.0. According to the simplified studies of Ref. 36, the resulting engine would have a weight of 124,000 lb and a thrust of 1.24×10^6 lb. A comparison of these results from Ref. 36 with results obtained from the present study are also given in following sections of this report.

CAVITY CONDITIONS

Flow conditions in the cavity of the engine under consideration determined from Ref. 36 are given in Table II. As noted on this Table, the average axial velocity approaching the axial-flow annulus is 508 ft/sec, and this velocity corresponds to a dynamic pressure of 3.82 atm for the density corresponding to an injection temperature of 4300 R. Tests conducted to date (see, for example, Refs. 26, 28, 29, and 30) have indicated that stability is enhanced in the cavity of a rocket by superimposing a rotational component to the flow, although the required ratio of tangential to axial velocity to obtain a given degree of stability has not as yet been determined. For the studies outlined in the following sections of this report, it is assumed that the tangential velocity near the peripheral wall of the cavity is 2.7 times the average exit axial velocity, or 1370 ft/sec. The dynamic pressure associated with this tangential velocity is 27.9 atm. The propellant flow injected into the cavity must have a velocity higher than the required vortex tangential velocity in order to overcome friction between the rotating flow and the cavity peripheral wall. Preliminary analysis has indicated that the ratio between injection velocity and tangential velocity should be approximately 1.75 for the conditions considered, leading to an injection dynamic pressure of 86 atm. Therefore, the total pressure at the entrance to the ducts used to inject the cavity propellant into the cavity must be approximately 1086 atm. Although the resulting injection velocity is relatively high (2400 ft/sec), the corresponding Mach number is low, only approximately 0.35. This is the highest Mach number existing at any position in the cavity. The Mach number near the center of the cavity is substantially less than that near the outside of the cavity because of the high speed of sound at the high temperatures in the fuel-containment region. Therefore, the radial pressure gradient resulting from flow rotation is small, and the difference in static pressure between the periphery of the tube and the tube axis is on the order of only 3 atm.

The studies of Ref. 36 were made on the basis of a required critical fuel mass of 18.1 lb for a cavity having a diameter of 6 ft. The corresponding average fuel density based on the entire volume within the cavity, $\bar{\rho}_F$, is 0.107 lb/ft³, and is 0.190 lb/ft³ based on the volume within the fuel-containment region. The average partial pressure of the fuel within the fuel-containment region is approximately 250 atm on the basis of the curves in Ref. 39 determined from ionization potentials from Ref. 34.

The density of hydrogen at a pressure of 1000 atm and the edge-of-fuel temperature of 102,000 R is 0.0068 lb/ft³. Therefore, if hydrogen were employed as the cavity propellant, the average fuel density ratio $\bar{\rho}_F/\rho_6$ would be 0.107/0.0068 = 15.8. As noted in Ref. 36, it is often desirable in a vortex-stabilized gaseous nuclear rocket engine to employ a cavity propellant which has a higher molecular weight than hydrogen in order to reduce unstable density gradients between the

CONFIDENTIAL

fuel-containment region and the propellant region. Such an increased molecular weight could be obtained by the addition of a very-high-molecular-weight seed to the hydrogen passing into the cavity. For the configuration considered, the average cavity propellant molecular weight was assumed to be 3.16 times that of hydrogen (i.e., $K_p = 3.16$) in order to obtain the value of fuel density ratio, ρ_F / ρ_6 , of 5.0 specified in the preceding section. Therefore, the density of the propellant at the edge of the fuel, ρ_6 , is assumed to be $(3.16) (0.0068) = 0.0215 \text{ lb/ft}^3$, as indicated in Table II.

CONFIDENTIAL

HEAT BALANCE

The over-all heat balance in the engine under consideration is illustrated in Table III. The hydrogen propellant flow into the cavity of 75 lb/sec is assumed to be augmented by 161 lb/sec of effectively infinite-molecular-weight diluent to obtain the total cavity propellant flow of 236 lb/sec. The cavity propellant flow is heated to a very high temperature and, as noted in Ref. 36, must be diluted by bypass propellant flow in order to obtain an enthalpy at the nozzle entrance compatible with an over-all heat balance. Stating the requirement for bypass flow in another way: the bypass propellant flow is necessary to aid in removing the energy from the moderator which cannot be removed by the small quantity of cavity propellant flow. The cavity propellant flow, because of its increased molecular weight, has a lower enthalpy at a given temperature than the bypass propellant flow. It is assumed that both the cavity propellant flow and the bypass flow are heated to a temperature of 4300 R before injection. As can be seen from Table III, the cavity propellant flow removes only 18 percent of the total energy removed from the moderator.

As noted in Table III, the total energy absorbed by the propellant flow before injection is composed of energy which has been deposited within the wall by neutrons and gamma rays and transferred to the surface of the wall by convection and thermal radiation. The heat assumed to be transferred to the surface of the wall, 0.4×10^6 Btu/sec, represents a heat flux to the cavity surface of 2360 Btu/sec-ft². Such a heat flux is almost twice as great as the heat flux at the throat of a hydrogen-oxygen chemical rocket such as the RL-10.

The energy deposited within the walls by neutrons and gamma rays, 6.56×10^6 Btu/sec, is assumed to be 7.6 percent of the total reactor power. Such a power fraction is compatible with fuel retention times on the order of 20 to 40 sec according to Ref. 53 (see also Fig. 4 of Ref. 10) if beta particles are prevented from hitting the walls by the use of a magnetic field in the cavity. If no magnetic fields are employed and there is no attenuation of beta particle energy in the cavity, 7.6 percent of the total energy released represents the energy which would be deposited by neutrons, gamma rays, and beta particles for a fuel retention time of approximately 3 sec. In this latter case, the energy deposited by beta particles (approximately 0.7 percent of the total energy created) would be deposited close to the surface of the cavity.

The total heating rate in the various moderating and structural regions is shown in Table IV. All of the internal heat generated is removed by flowing helium and is transferred to the cavity propellant and bypass hydrogen in a series of heat exchangers located between the outer shell of the heavy-water region and the pressure vessel.

CONFIDENTIAL

A schematic diagram of the helium circulation system is shown in Fig. 4. The total flow rate of helium is 1325 lb/sec and the total system pressure drop is 35 atm. The temperature and pressure levels in the helium circuit are listed in Table V. The station numbers correspond to the locations shown in Figs. 3 and 4. The helium leaves the pump and passes through an annular space adjacent to the inner pressure vessel wall to remove a portion of the heat deposited in the pressure vessel. The helium then absorbs the heat from the heavy water in a heat exchanger and is manifolded to 1100 helium inlets which are annular in cross section and surround the cavity propellant inlets. The helium is manifolded from the inlets to the inner liner tubes and then passes radially outwards through the solid moderators. The hot helium is collected and piped to the high-temperature heat exchangers in the lower, or nozzle end of the reactor. After passing through the high-temperature heat exchangers, the helium is piped to the low-temperature heat exchangers in the upper end of the reactor and from the low-temperature heat exchangers it returns to the pump.

In this study, the temperature increase in the helium which would occur in the pump was neglected since it is a very small value compared to the over-all system temperature variations. In the helium pumps the temperature rise was on the order of 5.4 R compared to an over-all temperature rise of 4200 R in the entire system.

The power to drive the hydrogen pump, the helium pump, and the heavy-water circulation pump is derived from a hydrogen turbine using a conventional topping cycle. The temperature rise between the hydrogen pump exit and the turbine inlet is obtained via the low-temperature heat exchanger from the recirculating helium. According to Ref. 35, a turbine pressure drop on the order of 500 atm is required to obtain a turbine exit pressure of 1086 atm. The hydrogen leaving the turbine exit is then further heated via the high-temperature heat exchanger using energy provided by the helium.

The process of energy absorption by the hydrogen as a function of temperature is complex because of the variable specific heat of hydrogen and because of the temperature rise through the pump and the temperature drop through the turbine. To simplify the calculations, it was assumed that the heat-sink capacity of the hydrogen can be represented by a fluid having a specific heat of 4 Btu/lb-deg R and operating between a temperature of 100 R and 4300 R. A schematic diagram of the hydrogen system based on these assumptions is shown in Fig. 5. The temperatures and pressures in the hydrogen circuit are listed in Table VI, and the station numbers in this table correspond to the locations shown in Figs. 3 and 5.

The total hydrogen flow of 414 lb/sec, after passing through the pump, the low-temperature heat exchanger, the turbine, and the high-temperature heat exchanger, is split into two separate ducts. The cavity propellant flow of 216 lb/sec is made up of 75 lb/sec of hydrogen flow discharging from the high-temperature heat exchanger plus 161 lb/sec of diluent assumed to be made up of a fluid having

effectively an infinite molecular weight. The ducting for this infinite-molecular-weight fluid was not considered in the analysis. The remaining hydrogen flow of 339 lb/sec is injected into the region upstream of the nozzle as bypass propellant flow.

Two separate locations were considered for the high-temperature heat exchangers: at the nozzle end of the configuration, and at the pump end of the configuration. It was decided to locate the high-temperature heat exchangers near the nozzle end of the configuration in order to minimize the length of piping which would be required to carry the hot (approximately 4500 R) gases.

It is assumed that the exhaust nozzle will require some form of transpiration cooling (see Ref. 54), and a finite heat-sink capacity is available in the transpiration coolant flow before it is injected into the exhaust nozzle region. A portion of this heat-sink capacity is assumed to be used to remove some of the neutron and gamma energy deposited in the pressure shell.



CHARACTERISTICS OF MODERATOR REGION

The moderator region is assumed to be composed of the following: an inner liner region, beryllium oxide and graphite moderator regions, and a heavy-water moderator region (see Fig. 3). The characteristics of each of these regions are described in the following subsections.

Inner Liner Region

The inner liner region consists of tungsten liner tubes, a beryllium wall, flow baffles, plenums and propellant injection ducts. A sketch of this region showing dimensions, materials and operating temperatures and pressures is given in Fig. 6, and a detailed drawing of the same region showing the actual design configuration is presented in Fig. 7. The helium coolant enters the inner liner region through the annulus surrounding the propellant injection duct. The helium passes from the headers through the liner tubes and is then baffled so that it flows circumferentially around the inside of the beryllium walls and into the plenum. The bends in the liner tubes shown in Fig. 7 are necessary in order to stagger the penetrations in the beryllium liner and maintain a reasonable ligament thickness.

The walls of the reactor cavity are formed by a series of tungsten tubes which protect the beryllium wall from direct radiation or convection from the cavity region. The tungsten tubes are assumed to have an inside diameter of 0.165 in. and a wall thickness of 0.010 in. They are fabricated from tungsten-184 to reduce the neutron capture cross section. The majority of the temperature drop between the temperature of the hot gases near the cavity wall (~5000 R) and the helium coolant in the tubes (~1100 R) occurs in the gas film inside the tube. A considerable temperature difference exists in the tube wall around the circumference of the tube. Because of the large circumferential temperature variation, an analysis was performed to determine the effect of thermal cycling on the tungsten liner tubes. The assumptions used in the analysis were: the tube is clamped at its ends at the length associated with a uniform temperature of 750 R; one half of the tube, circumferentially, remains at 750 R while the other half is cycled to 5000 R. The number of cycles to failure was calculated as a function of tensile elongation of tungsten at 5000 R. Values of tensile elongation for the tungsten at 5000 R between 5 percent and 40 percent have been reported in the literature, and it is not possible to determine a good representative value. If the tensile elongation is on the order of 5 percent, the number of cycles to failure will be approximately 15, which would represent a minimum value. If the tensile elongation is as high as 40 percent, the number of cycles to failure would increase to over 700.

The use of tungsten tubes for forming the cavity wall causes a significant increase in the critical mass of fuel required because of the high absorption cross

section of tungsten. Even if the tungsten is highly enriched in the tungsten-184 isotope, which has the smallest absorption cross section of all the tungsten isotopes, an increase in critical mass is necessary. The effect of the tungsten on criticality is discussed in detail in Ref. 40. The use of tungsten-184 in the liner tubes, propellant inlet ducts, and propellant injection nozzles would lead to an increase in critical mass of approximately 60 percent on the basis of calculations of critical mass reported in Ref. 40.

An alternate liner tube configuration has been considered to eliminate the need for the tungsten tubes and is shown in Fig. 8. The liner tubes in this alternate configuration are constructed from metallic beryllium. Due to the high cavity temperature, the beryllium must be insulated with a pyrolytic graphite coating on the outer surfaces. A niobium carbide surface coating must be applied to the pyrolytic graphite in order to keep the graphite from being chemically attacked by the propellant flow. The use of the beryllium liner tubes would also eliminate the problem of the bimetallic joint between the tungsten tubes and the beryllium liner which exists in the tungsten tube configuration shown in Figs. 6 and 7.

The beryllium wall behind the tubes is cooled by the helium after it has been discharged from the liner tubes. The maximum temperature in the beryllium wall was calculated using the assumption that all of the internal heat generated in the beryllium must be removed through the surface of the wall furthest from the cavity and that no heat could be rejected to the tungsten tubes. Under these conditions the maximum beryllium temperature was calculated to be 1500 R.

The cavity propellant flow passes through the moderator region in a 0.2-in.-diameter duct as shown in Fig. 7. The cavity propellant, which enters the cavity at a temperature of 4300 R, is shielded from the cold helium flow (~900 R) by 0.1 in. of pyrolytic graphite. As noted in a preceding section, the stagnation pressure of this cavity propellant flow is 1086 atm as compared to a cavity static pressure of 1000 atm. The diameter of each of the 1100 nozzles is 0.090 in.

Beryllium Oxide and Graphite Moderator Regions

The methods of analysis used to determine the cooling requirements and operating conditions in the solid moderator regions are similar to those presented in Ref. 20. The variation of frictional pressure loss, dynamic pressure, Reynolds number and the required slope of the cooling holes with coolant volume fraction and cooling hole diameter is shown in Figs. 9 through 12 for the beryllium oxide region and in Figs. 13 through 16 for the graphite region. In both regions, the calculations were based on a constant average value of the volumetric heat deposition in the two materials, and a surface-to-coolant temperature difference of 200 R.

The assumption of a constant average heat generation rate rather than an exponential heat generation rate which decreases with radial distance from the cavity leads to a cooling configuration which is conservative. In the region closest to the cavity where the actual heat generation rate would exceed the average, the temperature difference between the coolant passage walls and the coolant fluid would be greater than 200 R. Conversely, at the outlet end of each moderator region, the internal heat generation rate is considerably below the average value, and the wall-to-coolant temperature difference would be less than 200 R. Therefore, the calculation procedure employed underestimates the helium temperature attainable for a given material temperature.

In order to obtain a large temperature rise in the coolant fluid passing through a given moderator region, it is necessary to employ a length-to-diameter ratio of the coolant passages on the order of 500. Since the thickness of each moderator region is fixed at either 3.5 or 8.7 in. (see Table I), the allowable diameters for straight-through radial holes would be on the order of 0.01 in. In order to use a larger cooling hole diameter, the coolant passage must be lengthened. The variations in the required slope of the cooling holes with hole diameter and coolant volume fraction are shown in Figs. 12 and 16, respectively. The design points selected require slopes of 3 and 4.5, which would correspond to an angle of entrance of 13 deg and 19 deg.

It is desirable to have the helium coolant inlets and cavity propellant inlets pass through the solid moderator in a radial direction. However, a moderator configuration having a sloped cooling hole pattern would be difficult to fit around these inlets. Therefore, a study was undertaken to determine the feasibility of using spiral cooling holes in the solid moderator regions. One possible method of fabricating a moderator with spiral cooling holes is shown in Fig. 17. Spiral grooves are machined on the outer surface of a cylinder of moderator which is inserted into a circular hole. A series of rings with grooves would be used to approximate a square array of cooling holes as shown in Fig. 18. The square array of cooling holes with a distance, s , between holes is represented by the grid in Fig. 18. The cylinders which serve as a base for the spiral grooves were sized to approximate the grid, and their radius may be expressed by the equation

$$r_n = \sqrt{\left(\frac{s}{2}\right)^2 + \left\{\frac{s}{2} + (n-1)s\right\}^2} \quad (1)$$

where n is the ring number as shown in Fig. 18. The spiral grooves are equally spaced around the circumference of the cylinders and the total number of holes in a block is the same for the cylindrical and square arrays. The maximum number of rings was limited to four in order to limit the maximum distance between coolant

holes in adjacent hexagonal blocks to approximately twice the original square pitch, s. The moderator transition blocks could be single hexagonal-shaped blocks as shown in Fig. 17 or could be larger blocks with holes to receive the grooved cylinders.

A survey was made of existing information on the heat transfer and fluid flow characteristics of spiral holes; the results of this survey are described in detail in Appendix C. A summary of the design specifications for the cooling holes for both straight and equivalent spiral holes is shown in Tables VII and VIII. The spiral-hole configuration is assumed to have the same hole diameter and void fraction as the straight-hole configuration, and to operate with the same volumetric heating rate and the same temperature difference between the wall and the coolant as the straight-hole configuration. As noted in Appendix C, the Nusselt number in a curved hole is greater than that in a straight hole, thereby permitting a reduction in passage length, and a corresponding increase in passage angle (from 13 to 19 deg in the beryllium oxide and from 19 to 39 deg in the graphite). Since a decrease in passage length will lead to more holes (for a given void fraction), the velocities and dynamic pressures in the holes are reduced. It can be seen from Tables VII and VIII that the dynamic pressures and frictional pressure losses are reduced substantially in a spiral-hole configuration relative to those in a straight-hole configuration.

The pressure difference between the inlet to the beryllium oxide and the outlet of the graphite, which is approximately 8.7 atm, forces the moderator pieces against a graphite support grid which is located inside the beryllium wall at the inside edge of the heavy-water region. A positive seal between the different pieces would be achieved by stepped or tapered regions at the interfaces between the beryllium oxide and graphite and between the graphite and the support grid as shown in Figs. 19 and 20. The support grid would contain ducts to allow passage of the helium to the outlets.

One of the factors which might limit the maximum temperature of helium coolant passing through the moderator is the resultant loss of graphite by vaporization. Vapor pressure data for carbon from Ref. 56 are presented in Fig. 21 as a function of temperature. The average molecular weight of the carbon vapor for the mixture of the different carbon molecules is approximately 29.5, substantially independent of temperature. Results of calculations of the weight loss of graphite for an operating time of 1000 sec are shown in Fig. 22. This information was determined for a helium flow of 1325 lb/sec and a helium pressure of 1000 atm. It can be seen from Fig. 22 that the graphite lost by vaporization at the maximum helium temperature of 4500 R employed in preceding sections would be only 0.004 lb.

The graphite vaporized into the helium stream would be taken primarily from the downstream end of the graphite portion of the moderator. The volume represented by the coolant passages in the downstream 10 percent of the graphite

moderator is approximately 0.34 ft^3 , and the graphite represented by this volume would weigh 34 lb. The volume loss of graphite at a helium temperature of 4500 R therefore represents only 0.01 percent of the volume in the downstream 10 percent of the coolant holes. Since the heat deposition rate at the downstream end of the graphite region is much less than in the upstream end, such a change in the diameter of the holes would have little effect on engine performance.

The loss of graphite due to vaporization for a helium temperature of 4500 R is negligible. Therefore, it should be possible to raise the helium temperature leaving the moderator to a somewhat higher value. If it is assumed that an increase of hole diameter in the downstream 10 percent of the coolant passages of 50 percent is permissible, then it would be permissible to lose 43 lb of graphite during an engine operating period. This loss of graphite, according to Fig. 22, would correspond to a helium exit temperature of approximately 6000 R.

Heavy-Water Moderator Region

The heavy water is contained by two concentric beryllium shells as shown in Fig. 23. The external surfaces of the heavy-water containment walls are insulated with pyrolitic graphite in order to minimize heat transfer into the heavy water and maintain a reasonable temperature in the beryllium.

The heavy water is circulated through the helium-to-heavy water heat exchangers at a rate of 1900 lb/sec. The inlet and outlet temperatures for the heavy water passing through the heat exchangers are 1000 R and 500 R, respectively. In order to maintain a relatively high velocity of flow in the D_2O region, the flow would be baffled (baffles not shown in Fig. 23) so that the 500 R fluid would pass upwards along the beryllium walls to the top of the reactor, and then flow downwards through the center region and exit to the heat exchangers at 1000 R. This configuration would result in D_2O velocities on the order of 3 ft/sec and an average temperature in the D_2O region on the order of 750 R.

The helium inlets, propellant inlets, and the helium outlets penetrate the D_2O region as shown in Fig. 23. The helium outlets consist of a beryllium tube lined with pyrolitic graphite. The propellant and helium inlets are as previously described.

CHARACTERISTICS OF EXTERNAL REGION

The external region is assumed to be composed of the following: external piping, heat exchangers, turbopumps, and pressure shell. Descriptions of each of these components are given in the following subsections.

External Piping

The 1100 propellant injection ducts are assumed to be arranged at 25 locations along the axial direction and at 44 locations around the peripheral wall of the configuration at each axial location. The piping region is divided into 44 regions for analysis. In each region there is a helium inlet pipe (stations 13 to 14 in Fig. 4), a helium outlet pipe (stations 20 to 21 in Fig. 4), and a propellant inlet pipe (stations 36 to 37 in Fig. 5), each of which has 25 branches along the axis of the reactor (see Figs. 3, 4, and 5). Each of these three pipes was sized and the pressure drop calculated on the basis of an average flow rate of one half of the total flow required for 25 individual inlets or outlets.

The bypass pipes (stations 22 to 23 in Fig. 4 and 34 to 35 in Fig. 5), which are continuous from the top to the bottom of the reactor, were sized based on 44 pipes for each system in order to minimize pipe diameter and wall thickness and to conform to the configuration required for inlets and outlets. The operating conditions, pipe sizes, insulation thicknesses and total weights of the piping are shown in Table IX. A typical section through the piping region with a cylindrical vessel is shown in Fig. 24. The 10 in. clearance which is shown is more than enough for the passage of the pipes but the excess space was allowed for manifolding and clearance between pipes necessary for assembly. The stagnant hydrogen gas surrounding the pipes in the piping region is assumed to be at a pressure of 980 atm and a temperature of 2300 R during operation in order to minimize piping wall thickness and insulation thickness.

Heat Exchangers

Each of the heat exchangers was designed as a straight-through, counterflow, shell-and-tube configuration. The weight and volume of the heat exchangers might be reduced by more design optimization studies. The heat exchanger dimensions were based on maintaining an equal pressure drop on the tube and shell sides. The details of the heat exchangers are listed in Table X. The location of the heat exchangers is shown schematically in Fig. 4, and calculations have been made to determine that sufficient space exists between the pressure vessel and the outer O_2O wall for the heat exchangers.

[REDACTED]

In the hydrogen-to-helium heat exchangers, the hydrogen, which is at a high pressure relative to ambient conditions, is on the tube side of the exchangers. The pressure differential across the shell of the exchangers would be on the order of 5 atm, and the heat exchanger shell would not be restricted to a cylindrical shape because of stress limitations. The helium-to-heavy water heat exchangers have helium on the tube side and, in this exchanger, the pressure levels are both approximately 20 atm above ambient (1000 atm) in both fluids. Since the D_2O heat exchanger is small, it may be made in a cylindrical form to provide sufficient containment. The high-temperature heat exchangers would be fabricated from tungsten since the operating temperatures are between 2200 R and 4500 R. The low-temperature heat exchanger and the heavy-water heat exchanger could be stainless steel. The required wall thickness in the tubes was determined by conventional equations for loop stress in a cylinder. In the calculation of heat exchanger weight and volume, the calculated area of the tube bundle was multiplied by 1.2 to allow for shell and header volume and weight.

Turbopumps

The results of a hydrogen turbopump design study which was performed under Corporate sponsorship at Pratt & Whitney Aircraft, Florida Research and Development Center, are summarized in Table XI. Although it might be possible to mount the entire turbopump system on a single shaft, it was decided to employ a configuration with four separate turbines and four separate pumps with each pump driven by its own turbine. The hydrogen flow would pass through each of the four pumps, would then be heated in the low-temperature heat exchanger shown in Fig. 5, and would then pass through each of the turbines. The advantages of using four separate turbopump units rather than a single unit are: 1) a reduction of shaft size which reduces the bearing problem and permits reasonable speed levels, and 2) the reduced number of stages per unit reduces the critical speed problem. The flow rate shown in Table XI of 414 lb/sec is equal to the sum of the bypass propellant flow (339 lb/sec) and the equivalent hydrogen content of the cavity propellant flow (75 lb/sec). However, the pump and turbine discharge pressures noted in Table XI are slightly less than those in Table VI (1000 vs 1086 atm).

The weight estimate of 11,300 lb shown in Table XI is based on the use of current fabrication techniques and a turbopump location external to the engine pressure shell. As indicated in Fig. 2, it is possible to install the turbine portion of the turbopump assembly within the pressure shell. The weight of 8000 lb in Table XI corresponds to installation of the turbine within the pressure shell and to the use of advanced materials.

No layout has been made of the pump required for helium recirculation (see Fig. 4 and Table V). However, a thermodynamic cycle analysis indicates that the temperature rise through the helium pump would be 5.4 R if its efficiency were 0.80.

[REDACTED]

The corresponding required pump power would be 12,700 hp. This power could be obtained from the hydrogen turbopump system since it represents only 3 percent of the power of the hydrogen turbopump. It could also be obtained from a turbine driven by the hot helium before the helium entered the low-temperature heat exchanger. Also, the helium pump power could be reduced by reducing the temperature at the pump inlet.

Although the mass flow of helium is relatively high, the size of the helium pump is within reason because of the high density of helium at a pressure of 1000 atm. If the Mach number averaged across the entire frontal area of an axial-flow helium compressor is assumed to be 0.3, and the compressibility correction for helium is neglected, the required diameter of the compressor would be only 4.4 in.

Pressure Vessel

The preliminary design investigation was based on the use of a cylindrical pressure vessel made of maraging steel. In order to maintain a high allowable stress in the material, it was specified that the maximum temperature in the pressure vessel would not exceed 800 R. In addition, the difference between the maximum and minimum temperatures in the pressure vessel was limited to 450 R in order to reduce thermal stresses. These criteria cannot be satisfied in a single-walled vessel with surface cooling.

An analysis of a double-walled pressure vessel was made assuming an exponential heat generation rate in the shells, helium cooling on the inner wall, and hydrogen cooling in the annulus between the two walls. The resulting thickness and the corresponding temperature distribution is shown in Fig. 25. The inner wall is 2.36 in. thick and the outer wall 3.6 in. thick. The helium coolant is the moderator coolant flow, and the hydrogen coolant is a portion of the hydrogen used for transpiration cooling of the nozzles. The total heat generation in the pressure vessel, according to Table IV, is 40,000 Btu/sec (30,000 Btu/sec in the inner shell, and 10,000 Btu/sec in the outer shell). The helium coolant on the inside of the inner shell removes 22,000 Btu/sec from the inner shell. The hydrogen coolant between the walls removes 8000 Btu/sec from the inner shell, and all of the heat generated in the outer shell.

The thickness of the cylindrical pressure vessel was chosen from standard equations for hoop stress in a cylinder using a design stress of 0.75 times the ultimate stress at operating temperature reduced by thermal stress resulting from the differential thermal growth in the vessel. The possible effects of hydrogen embrittlement on the vessel walls were not considered.

The cylindrical pressure vessel, if made of maraging steel, would weigh approximately 161,500 lb, and would represent the major portion of the total engine weight.

SECRET

A number of alternate configurations and materials were considered in an effort to reduce the size and weight of the vessel. One alternate configuration was a spherical maraging steel pressure vessel which had a thinner wall than the cylindrical configuration (the stress in a spherical shell is half that of a cylindrical shell of the same radius and wall thickness). However, the volume enclosed by the spherical pressure vessel is larger (see Fig. 2). A comparison of cylindrical and spherical vessels of maraging steel, and the estimated characteristics of filament-wound cylindrical vessels is shown in Table XII. A review of available metallic alloys was made by Pratt & Whitney Aircraft Engine Design Group, and one possible substitute for the maraging steel is AMS 4971 Titanium alloy. A comparison of the strength-to-weight ratio of maraging steel and AMS 4971 Titanium alloy is shown in Fig. 26. The data shown in Fig. 26 was taken from information published by the International Nickel Company and the Titanium Metals Corporation. The titanium alloy would be better only if the shell temperature could be held below 650 R. The thermal conductivity of the titanium alloy is about one third that of maraging steel and this would probably require a three- or four-walled vessel with internal cooling between each wall. The filament-wound vessels would also have relatively low thermal conductivity and might require multiple-wall configurations.


The information in Table XII for filament-wound pressure vessels is given for two different values of strength-to-weight ratio of the filament material: 2.5×10^6 in. and 5.0×10^6 in. The lower value was used in most of the studies in Ref. 36 and represents current technology, while the higher value represents advanced technology according to Ref. 57. In all calculations involving filament-wound pressure vessels, a structural efficiency of 50 percent was employed on the basis of the recommendations of Ref. 57 to allow for, among other factors, ducts passing through the pressure shell. However, studies made at Pratt & Whitney Aircraft indicate that the structural efficiency of filament-wound pressure vessels may be substantially less than 50 percent for many configurations which require a number of breaks in the pressure vessel for nozzle and duct passages. It should be pointed out that no designs have been made of filament-wound pressure vessels for the rocket engine being considered. Therefore, a considerable amount of additional work is required to determine the accuracy of the weights for the filament-wound pressure vessels indicated in Table XII.

Three different volumes are indicated for the filament-wound pressure vessels in Table XII. The smallest volume, 785 ft³, represents the volume of the cavity and moderator employed in the studies of Ref. 36. This volume makes no allowance for the volume required for the external piping and heat exchangers. The volume of 1385 ft³ was taken to be equal to that for the cylindrical pressure vessel made from maraging steel. This total volume of 1385 ft³ allows 600 ft³ for heat exchangers and piping. Because of the large weight associated with this volume, it would be very desirable to reduce this quantity. Therefore, a third volume of 1000 ft³ was chosen for analysis and might represent the volume between the moderator and pressure shell required for a relatively crowded piping arrangement, and also might

SECRET

represent a minimum practical volume.

On the basis of the preceding discussions, the probable range of weight of the pressure vessel was taken as between 30,600 and 125,100 lb. The weight of the cylindrical maraging steel pressure vessel of 161,500 lb was discarded because the spherical pressure vessel made of the same material was lighter. The weight of the filament-wound vessel of 23,950 lb was discarded because it did not leave room for the piping and heat exchangers.



ENGINE WEIGHT

The four major components of the engine in the studies of Ref. 36 were: the moderator; the pressure vessel; the turbopumps and plumbing; and the heat exchangers. A breakdown of the weight of each of these components as determined from the present study is given in Tables IX through XIII, and a comparison is given in Table XIV of these weights as determined from the present analysis and as calculated in Ref. 36. The weights from the present analysis are in general agreement with those from Ref. 36 with the exception of the weight due to the pressure vessel. The weights given for the pressure vessel in Table XIV range from 30,600 lb (calculated for a filament-wound pressure vessel with an enclosed volume of 1000 ft³ and a material strength-to-weight ratio of 5.0×10^6 in.) to 125,100 lb (calculated for a spherical pressure vessel having an enclosed volume of 1855 ft³ and made from maraging steel). A discussion of why this range of weights is less than that shown in Table XII is given in the preceding section. As noted in the discussion in the text concerning Table XII, the weight of a filament-wound pressure vessel is highly dependent on the details of the openings required in the structure and on the ability to fabricate a multi-wall pressure vessel with internal cooling between the walls. Additional effort is required to obtain a more accurate estimate of pressure vessel weight than that indicated by the range given in Table XIV.

As noted in Table XIV, the weight summary shown on the table excludes the weight of certain components. A number of these components are expected to add very little to the over-all structural weight. These components include the fuel injection system, the system for diluting the propellant before it is injected into the cavity, the heavy-water recirculating pump, and the helium recirculating pump. (As noted in preceding sections, the required inlet diameter of this helium pump is on the order of only 4.4 in.)

As noted in a preceding section, it is desirable to employ a magnetic field within the cavity in order to minimize heating of the cavity wall by beta particles. It was estimated in Ref. 20 that the weight of the required components to create the magnetic field would be on the order of 1000 lb. A helium accumulator and/or storage tank would also be required as part of the system necessary to equalize the pressure in the helium and hydrogen portions of the engine. Design of this equipment will require additional studies of the transients to be expected during off-design engine operation.

The two components which are most likely to cause a substantial increase in engine weight over that shown in Table XIV are the exhaust nozzle and the engine mounting structure. The weight of the engine mounting structure can be minimized if some form of shock control, such as fluid injection into the nozzle, is employed to provide side forces in the nozzle rather than requiring the use of gimbaling to obtain side forces. The exhaust nozzle required is fairly large in size, but the

pressure difference across most of the length of the nozzle wall is small. It is expected that the local static pressure in the nozzle will have dropped by more than an order of magnitude by the time the flow passes the outer boundary of the pressure shell.

ENGINE PERFORMANCE

A chart showing the various factors which have been considered in calculating specific impulse and thrust is given in Table XV. As noted in Table III, a total of 575 lb/sec of flow passes through the nozzle entrance. This flow has an enthalpy of 150,400 Btu/lb, a temperature of approximately 23,000 R, and a molecular weight equal to 1.39 times that of hydrogen at the same temperature and pressure. As noted in Table XV, expansion of this flow to zero pressure (resulting in conversion of all thermal energy to kinetic energy) would provide a specific impulse of 2695 sec. The specific impulse shown in line 2 in Table XV for a nozzle area ratio of 500 was determined from the tables of Ref. 41 for hydrogen, and was corrected downward by the square root of the molecular weight of the exhaust flow relative to that of hydrogen.

The flow entering the nozzle is completely dissociated and approximately one percent ionized. It was determined from the tables of Ref. 41 that freezing of the composition of both the dissociated and ionized species will result in a loss in specific impulse of approximately 18 percent. However, theoretical calculations indicate that the recombination of the ionized species will be almost instantaneous and that the dissociated species will be in equilibrium to an area ratio of approximately 90. If the flow is assumed to be frozen at an area ratio of 90, a loss in specific impulse of approximately 0.5 percent will result, leading to the performance indicated on line 3 of Table XV.

Two additional corrections were applied to the calculated value of specific impulse. The first of these is due to wall friction and flow nonuniformity in the nozzle. As noted in line 4 of Table XV, this correction was assumed to be equal to one percent. The second additional correction is that due to the requirement for transpiration coolant flow in the nozzle. It was determined from Ref. 54 that approximately 15 percent transpiration coolant flow would be required and that this would result in a loss in specific impulse of approximately 8 percent. The final calculated specific impulse is 2186 sec.

Specific impulse in Ref. 36 was calculated on the basis of a 20-percent reduction in the ideal vacuum specific impulse to allow for all contributions to nozzle inefficiency. According to Table XV, this loss in specific impulse is equal to 19 percent for the present calculations. The thrust in Ref. 36 was obtained by multiplying the flow upstream of the nozzle (575 lb/sec) by the specific impulse. The resulting thrust is less than that shown in Table XV primarily because no allowance was made in Ref. 36 for the thrust due to the transpiration coolant flow.

The engine performance parameter which is most uncertain at the present time is the rate of loss of nuclear fuel from the cavity. An experimental program is

now being conducted under Contract NASw-847 to determine the dimensionless time constants governing the containment of a heavy gas in a light-gas vortex at Reynolds numbers up to approximately 500,000. This Reynolds number, according to Table II, is approximately equal to the axial Reynolds number based on conditions at Station 6 for the engine considered in the present report. A nominal goal for the fluid mechanics tests is the achievement of a dimensionless time constant of 0.01 at a Reynolds number of 500,000 and a fuel density ratio of 5.0. If such a dimensionless time constant can be obtained, then the true time constant (obtained by multiplying the dimensionless time constant by the fuel time constant parameter of 1195 sec in Table II) would be 11.95 sec. Since the assumed critical fuel mass is 18.1 lb, the corresponding required fuel flow rate would be $18.1/11.95$ or 1.52 lb/sec. Thus, the ratio of nozzle entrance flow to fuel flow would be 380, and the ratio of total exhaust flow to fuel flow would be 438.

LIMITATIONS OF DESIGN STUDY

As noted in the Introduction, the design study described in this report is preliminary in nature and is meant primarily to provide better estimates of engine weight and to provide a configuration which can be employed to provide better estimates of required critical mass (see Ref. 40). No consideration has been given in this study to the following:

- (1) Off-design engine operation
- (2) Problems of joining of dissimilar materials (such as tungsten to beryllium and graphite to beryllium)
- (3) Thermal stresses due to differential growth of materials (except in pressure vessel)
- (4) Pressure vessel closure, including cooling of flanged joints or heat treating of welded joints without affecting internal parts
- (5) Details of the connectors between the various pipes and components
- (6) Dynamic or vibration loadings
- (7) Production facilities for large structures made from beryllium or tungsten
- (8) Manufacturing techniques required for joining a large number of tubes in close proximity without affecting previously jointed parts
- (9) A system for assembling moderator blocks around supply tubes and enclosing them within the beryllium vessels

EFFECT OF SELECTED DESIGN MODIFICATIONS ON ENGINE CHARACTERISTICS

Elimination of Helium Circuit

It would obviously be desirable to eliminate the need for the separate helium circuit which has been employed in the engine design. This separate helium circuit was chosen on the basis of studies of Ref. 20 as a means of eliminating hydrogen attack on the moderator material and as a means of eliminating the pressure differences in the moderator which would be caused if the pump-exit flow in a topping-cycle configuration were heated by being passed through the moderator. For the design considered in the present report, this pressure difference would be approximately 500 atm, and would require the introduction of a considerable quantity of neutron-absorbing structural material in the moderator. Although no study has been made of such a structure in the present study, the general effect of using such a structure can be determined by examining the engine design of Ref. 58.

The engine considered in Ref. 58 was assumed to have two different moderator regions which were separated by a tungsten-184 barrier having a thickness of 0.5 in., a radius of 22 in., and an operating temperature of 4000 R. The pressure difference across this barrier in the design of Ref. 58 was approximately 240 atm, and would result in a hoop stress in the tungsten barrier of 155,000 psi. Such a hoop stress is much greater than the allowable stress in tungsten at a temperature of 4000 R. In addition, the neutron absorption in the tungsten-184 barrier would result in a considerable increase in critical mass. For the engine described in the present report, the studies of Ref. 40 indicate that the addition of 0.5 in. of tungsten-184 would raise the critical mass by a factor of approximately 30. On the basis of this analysis, it does not appear to be desirable to employ direct cooling of the moderator by the pump-exit flow in a gaseous nuclear rocket engine employing a topping cycle if reliance must be placed on tungsten-184 as a pressure barrier material.

Use of Bleed Turbopump Cycle

In a bleed turbopump cycle, the power to run the turbine is obtained by expansion of a fraction of the flow heated in the moderator through a turbine to ambient conditions outside the engine. According to the studies of Ref. 35, approximately 15 percent of the flow would be required in a bleed turbine to obtain a cavity pressure of 1000 atm. The discharge pressure from this bleed turbine would be very low, which would probably preclude the possibility of using this flow for direct cooling of anything but the downstream end of the nozzle. If this flow were discharged to ambient conditions at a very low temperature, the fractional loss in specific impulse would be equal to the bleed flow fraction of 15 percent.

SECRET

If this flow could be heated to a temperature on the order of 2000 R by passing through a steel heat exchanger receiving energy from the recirculating helium flow, the loss in specific impulse would be reduced to approximately 11 percent. Although such a loss in specific impulse is not prohibitive, it is undesirable.

One of the biggest advantages to the use of a bleed turbine is that it might permit elimination of the helium coolant system, since the pump-exit pressure would then be much closer to the cavity pressure than in a topping cycle. However, the configuration described in the present report requires a cavity injection total pressure approximately 86 atm greater than the static pressure in the cavity. This pressure difference, plus the pressure difference due to moderator cooling, would have to be withstood by some structural barrier (possibly the beryllium liner). As noted in the discussion under the section entitled "Cavity Conditions," an arbitrary assumption was made in the present report as to the required ratio of tangential to axial velocity in the cavity. It may be possible to reduce this ratio, thereby reducing the required injection dynamic pressure. However, even if the injection dynamic pressure were reduced to zero, the structural barrier would still be required to withstand the pressure differences due to the friction drop in the various moderator and structural walls. In addition, the absorption of neutrons in the moderator would be increased by the required addition of the niobium-carbide coatings necessary to prevent hydrogen attack on the graphite moderator material.

Increase in Helium Temperature

As noted in the discussion of the characteristics of the graphite moderator region, the maximum helium temperature of 4500 R would result in vaporization of only 0.004 lb of graphite during a typical operating period. It was also noted in this section that the helium exit temperature can be raised to approximately 6000 R if it were permissible to allow the coolant hole diameter in the downstream ten percent of the graphite region to increase by approximately 50 percent during a single operating period. This 33 percent potential increase in helium temperature would also result in a potential increase in propellant injection temperature of approximately 33 percent. According to Ref. 36, such an increase in propellant injection temperature would lead to an increase in specific impulse of approximately 13 percent, or an increase from 2186 sec to 2472 sec for the present configuration (see Table XV).

Although the temperature in the helium circuit can be raised without disastrous effects on the graphite structure, the resulting effects on the ducts containing hydrogen would be more severe. For instance, the high-temperature heat exchanger made from natural tungsten would be forced to operate at a 33 percent higher temperature. The passage employed to duct the cavity propellant through the moderator region would also suffer more severe operational conditions. These conditions might be so severe as to preclude the possibility of using niobium-carbide-coated graphite in this region. The most severe problem area, however, would probably be the tungsten

CONFIDENTIAL

nozzle employed to inject the propellant into the cavity, since the pressure difference across this nozzle would be approximately 86 atm.

It should also be noted that an increase in the moderator coolant outlet temperature would require a complete revision of the moderator configuration since it would increase the maximum temperatures of the beryllium and beryllium oxide regions beyond the allowable temperature levels. Any changes in the thickness of the moderator materials would change the volumetric heat deposition rates and the nuclear characteristics of the entire region.

Increase in Critical Mass of Nuclear Fuel

The studies of Ref. 40 have indicated that the required critical mass of nuclear fuel would probably be somewhat greater than the 18.1 lb employed in the analysis described in preceding sections. However, the absolute increase in critical mass required is uncertain because insufficient studies have been completed to determine the effect of a number of variables on this critical mass. These variables include the amount of tungsten-184 (or niobium-carbide coating on graphite) required in the structure and the volume of the nozzle approach section.

Although the exact increase in critical mass required is not known, a generalized study of the effect of required critical mass on engine characteristics is given in Appendix B. According to this analysis, an increase in critical mass by a factor of two will result in a decrease in specific impulse of approximately 14 percent. Such a reduction in specific impulse would reduce the specific impulse shown in Table XV from 2186 sec to 1879 sec.

[REDACTED]

REFERENCES

1. Anderson, O.: Theoretical Solutions for the Secondary Flow on the End Wall of a Vortex Tube. UAC Research Laboratories Report R-2494-1 prepared under Contract AF 04(611)-7448, November 1961. (report unclassified)
 2. Owen, F. S., R. W. Hale, B. V. Johnson, and A. Travers: Experimental Investigation of Characteristics of Confined Jet-Driven Vortex Flows (U). UAC Research Laboratories Report R-2494-2 prepared under Contract AF 04(611)-7448, November 1961. (report classified Confidential)
 3. Owen, F. S., and A. E. Mensing: Heat Transfer to Confined Vortex Flows by Means of a Radio-Frequency Gas Discharge (U). UAC Research Laboratories Report R-2494-3 prepared under Contract AF 04(611)-7448, November 1961. (report classified Confidential)
 4. McLafferty, G. H.: Investigations of a Unique Gaseous-Core Nuclear Rocket Concept - Summary Report (U). UAC Research Laboratories Report R-2494-4 prepared under Contract AF 04(611)-7448, November 1961. (report classified Confidential)
 5. Patch, R. W.: Methods for Calculating Radiant Heat Transfer in High-Temperature Hydrogen Gas. UAC Research Laboratories Report M-1492-1 prepared under Contract AF 04(611)-7448, November 1961 (report unclassified)
 6. Mensing, A. E., and J. S. Kendall: Experimental Investigation of Containment of Gaseous Iodine in a Jet-Driven Vortex (U). Air Force Systems Command Report RTD-TDR-63-1093 prepared by UAC Research Laboratories under Contract AF 04(611)-8189, November 1963. (report classified Confidential)
 7. Johnson, B. V., A. Travers, and R. W. Hale: Measurements of Flow Patterns in a Jet-Driven Vortex (U). Air Force Systems Command Report RTD-TDR-63-1094 prepared by UAC Research Laboratories under Contract AF 04(611)-8189, November 1963. (report classified Confidential)
 8. McLafferty, G. H., and G. E. Anderson: Analytical Investigation of Diffusive Loss Rates of Gaseous Iodine from a Helium Vortex (U). Air Force Systems Command Report RTD-TDR-63-1095 prepared by UAC Research Laboratories under Contract AF 04(611)-8189, November 1963. (report classified Confidential)
 9. Saunders, A. R.: Theoretical Investigation of Radiant Heat Transfer in a Vortex-Stabilized Gaseous Nuclear Rocket (U). Air Force Systems Command Report RTD-TDR-63-1096 prepared by UAC Research Laboratories under Contract AF 04(611)-8189, November 1963. (report classified Confidential)
- [REDACTED]

- CONFIDENTIAL
10. McLafferty, G. H.: Summary of Investigations of a Vortex-Stabilized Gaseous Nuclear Rocket Concept (U). Air Force Systems Command Report RTD-TDR-63-1097 prepared by UAC Research Laboratories under Contract AF 04(611)-8189, November 1963. (report classified Confidential)
 11. Anderson, O. L.: Theoretical Effect of Mach Number and Temperature Gradient on Primary and Secondary Flow in a Jet-Driven Vortex. Air Force Systems Command Report RTD-TDR-63-1098 prepared by UAC Research Laboratories under Contract AF 04(611)-8189, November 1963. (report unclassified)
 12. Bisshopp, F. E.: Theoretical Investigation of the Hydromagnetic Stability of a Free Boundary Layer. Air Force Systems Command Report RTD-TDR-63-1099 prepared by UAC Research Laboratories under Contract AF 04(611)-8189, November 1963. (report unclassified)
 13. Carta, F. O.: The Effects of Body Force and Finite Electrical Conductivity on the Hydromagnetic Stability of a Discontinuous Shear Flow. Air Force Systems Command Report RTD-TDR-63-1100 prepared by UAC Research Laboratories under Contract AF 04(611)-8189, November 1963. (report unclassified)
 14. Krascella, N. L.: Theoretical Investigation of Spectral Opacities of Hydrogen and Nuclear Fuel. Air Force Systems Command Report RTD-TDR-63-1101 prepared by UAC Research Laboratories under Contract AF 04(611)-8189, November 1963. (report unclassified)
 15. Marteney, P. J., and N. L. Krascella: Theoretical and Experimental Investigations of Spectral Opacities of Mixtures of Hydrogen and Diatomic Gases. Air Force Systems Command Report RTD-TDR-63-1102 prepared by UAC Research Laboratories under Contract AF 04(611)-8189, November 1963. (report unclassified)
 16. Krascella, N. L.: Theoretical Investigation of the Absorption and Scattering Characteristics of Small Particles. UAC Research Laboratories Report C-910092-1 prepared under Contract NASw-847, September 1964. Also issued as NASA CR-210 (report unclassified)
 17. Marteney, P. J.: Experimental Investigation of the Opacity of Small Particles. UAC Research Laboratories Report C-910092-2 prepared under Contract NASw-847, September 1964. Also issued as NASA CR-211. (report unclassified)
 18. Roback, R.: Thermodynamic Properties of Coolant Fluids and Particle Seeds for Gaseous Nuclear Rockets. UAC Research Laboratories Report C-910092-3 prepared under Contract NASw-847, September 1964. Also issued as NASA CR-212. (report unclassified)

SECRET

19. Schneiderman, S. B.: Theoretical Viscosities and Diffusivities in High-Temperature Mixtures of Hydrogen and Uranium. UAC Research Laboratories Report C-910099-1 prepared under Contract NASw-847, September 1964. Also issued as NASA CR-213. (report unclassified)
20. McLafferty, G. H.: Analytical Study of Moderator Wall Cooling of Gaseous Nuclear Rocket Engines. UAC Research Laboratories Report C-910093-9 prepared under Contract NASw-847, September 1964. Also issued as NASA CR-214. (report unclassified)
21. Johnson, B. V.: Analysis of Secondary-Flow-Control Methods for Confined Vortex Flows (U). UAC Research Laboratories Report C-910091-1 prepared under Contract NASw-847, September 1964. (report classified Confidential)
22. Travers, A., and B. V. Johnson: Measurements of Flow Characteristics in a Basic Vortex Tube (U). UAC Research Laboratories Report C-910091-2 prepared under Contract NASw-847, September 1964. (report classified Confidential)
23. Travers, A., and B. V. Johnson: Measurements of Flow Characteristics in an Axial-Flow Vortex Tube (U). UAC Research Laboratories Report C-910091-3 prepared under Contract NASw-847, September 1964. (report classified Confidential)
24. McLafferty, G. H., and W. G. Burwell: Theoretical Investigation of the Temperature Distribution in the Propellant Region of a Vortex-Stabilized Gaseous Nuclear Rocket (U). UAC Research Laboratories Report C-910093-10 prepared under Contract NASw-847, September 1964. (report classified Confidential)
25. Mensing, A. E., and J. S. Kendall: Experimental Investigation of Containment of a Heavy Gas in a Jet-Driven Light-Gas Vortex (U). UAC Research Laboratories Report D-910091-4 prepared under Contract NASw-847, March 1965. (report classified Confidential)
26. McFarlin, D. J.: Experimental Investigation of the Effect of Peripheral Wall Injection Technique on Turbulence in an Air Vortex Tube. UAC Research Laboratories Report D-910091-5 prepared under Contract NASw-847, September 1965. (report unclassified)
27. Johnson, B. V.: Analytical Study of Propellant Flow Requirements for Reducing Heat Transfer to the End Walls of Vortex-Stabilized Gaseous Nuclear Rocket Engines (U). UAC Research Laboratories Report D-910091-6 prepared under Contract NASw-847, September 1965. (report classified Confidential)
28. Travers, A.: Experimental Investigation of Peripheral Wall Injection Techniques in a Water Vortex Tube. UAC Research Laboratories Report D-910091-7 prepared under Contract NASw-847, September 1965. (report unclassified)

SECRET

- [REDACTED]
29. Johnson, B. V., and A. Travers: Analytical and Experimental Investigation of Flow Control in a Vortex Tube by End-Wall Suction and Injection (U). UAC Research Laboratories Report D-910091-8 prepared under Contract NASw-847, September 1965 (report classified Confidential)
 30. Mensing, A. E., and J. S. Kendall: Experimental Investigation of the Effect of Heavy-to-Light-Gas Density Ratio on Two-Component Vortex Tube Containment Characteristics (U). UAC Research Laboratories Report D-910091-9 prepared under Contract NASw-847, September 1965. (report classified Confidential)
 31. Krascella, N. L.: Theoretical Investigation of the Opacity of Heavy-Atom Gases. UAC Research Laboratories Report D-910092-4 prepared under Contract NASw-847, September 1965. (report unclassified)
 32. Kesten, A. S., and R. B. Kinney: Theoretical Effect of Changes in Constituent Opacities on Radiant Heat Transfer in a Vortex-Stabilized Gaseous Nuclear Rocket (U). UAC Research Laboratories Report D-910092-5 prepared under Contract NASw-847, September 1965. (report classified Confidential)
 33. Marteney, P. J., N. L. Krascella, and W. G. Burwell: Experimental Refractive Indices and Theoretical Small-Particle Spectral Properties of Selected Metals. UAC Research Laboratories Report D-910092-6 prepared under Contract NASw-847, September 1965. (report unclassified)
 34. Williamson, H. A., H. H. Michels, and S. B. Schneiderman: Theoretical Investigation of the Lowest Five Ionization Potentials of Uranium. UAC Research Laboratories Report D-910099-2 prepared under Contract NASw-847, September 1965. (report unclassified)
 35. McLafferty, G. H., H. H. Michels, T. S. Latham, and R. Roback: Analytical Study of Hydrogen Turbopump Cycles for Advanced Nuclear Rockets. UAC Research Laboratories Report D-910093-19 prepared under Contract NASw-847, September 1965. (report unclassified)
 36. McLafferty, G. H.: Analytical Study of the Performance Characteristics of Vortex-Stabilized Gaseous Nuclear Rocket Engines (U). UAC Research Laboratories Report D-910093-20 prepared under Contract NASw-847, September 1965. (report classified Confidential)
 37. Krascella, N. L.: Theoretical Investigation of the Absorptive Properties of Small Particles and Heavy-Atom Gases. NASA CR-693, 1967. (report unclassified)

- SECRET
38. Kinney, R. B.: Theoretical Effect of Seed Opacity and Turbulence on Temperature Distributions in the Propellant Region of a Vortex-Stabilized Gaseous Nuclear Rocket (U). NASA CR-694, 1967. (report classified Confidential)
 39. Kesten, A. S., and N. L. Krascella: Theoretical Investigation of Radiant Heat Transfer in the Fuel Region of a Gaseous Nuclear Rocket Engine. NASA CR-695, 1967. (report unclassified)
 40. Latham, Thomas S.: Nuclear Criticality Study of a Specific Vortex-Stabilized Gaseous Nuclear Rocket Engine (U). NASA CR-697, 1967. (report classified Confidential)
 41. Roback, R.: Theoretical Performance of Rocket Engines Using Gaseous Hydrogen in the Ideal State at Stagnation Temperatures up to 200,000 R. NASA CR-696, 1967. (report unclassified)
 42. Ragsdale, Robert G., Herbert Weinstein, and Chester Lanzo: Correlation of a Turbulent Air-Bromine Coaxial-Flow Experiment. NASA TN D-2121, February 1964.
 43. Weinstein, H., and R. Ragsdale: A Coaxial Flow Reactor--A Gaseous Nuclear-Rocket Concept. ARS Preprint 1518-60, presented at the ARS 15th Annual Meeting, Washinton, D. C., December 1960.
 44. Weinstein, Herbert, and Carroll A. Todd: A Numerical Solution of the Problem of Mixing of Laminar Coaxial Streams of Greatly Different Densities - Isothermal Case. NASA TN D-1534, February 1963. (report unclassified)
 45. Ragsdale, Robert G.: Effects of Momentum Buffer Region on Coaxial Flow of Dissimilar Fluids. NASA TM X-52098, Technical preprint prepared for AIAA Propulsion Joint Specialist Conference, Colorado Springs, Colorado, June 14-18, 1965. (report unclassified)
 46. Ragsdale, Robert G., and Oliver J. Edwards: Turbulent Coaxial Mixing of Dissimilar Gases at Nearly Equal Stream Velocities. NASA TM X-52082, 1965. (report unclassified)
 47. Weinstein, H., and Carroll A. Todd: Analysis of Mixing of Coaxial Streams of Dissimilar Fluids Including Energy-Generation Terms. NASA TN D-2123, March 1964. (report unclassified)

48. Lanzo, Chester D., and Robert G. Ragsdale: Heat Transfer to a Seeded Flowing Gas from an Arc Enclosed by a Quartz Tube. NASA TM X-52005, prepared for Heat Transfer and Fluid Mechanics Institute, June 10-12, 1964. (report unclassified)
49. Ragsdale, Robert G., and Oliver J. Edwards: Data Comparisons and Photographic Observations of Coaxial Mixing of Dissimilar Gases at Nearly Equal Stream Velocities. NASA TN D-3131, December 1965. (report unclassified)
50. Ragsdale, Robert G.: Effects of a Momentum Buffer Region on the Coaxial Flow of Dissimilar Gases. NASA TN D-3138, December 1965. (report unclassified)
51. Rom, Frank E., and Robert G. Ragsdale: Advanced Concepts for Nuclear Rocket Propulsion. Nuclear Rocket Propulsion, NASA SP-20, December 1962, pp. 3-15.
52. Lanzo, Chester D., and Robert G. Ragsdale: Experimental Determination of Spectral and Total Transmissivities of Clouds of Small Particles. NASA TN D-1405, September 1962. (report unclassified)
53. Paul, D. J.: Effect of Fission Product Residence Time on Fraction of Fission Energy Deposited in Walls of a Gaseous Nuclear Rocket. UAC Research Laboratories Report UAR-BL39, September 4, 1963. (report unclassified)
54. McLafferty, George H.: Approximate Limitations on the Specific Impulse of Gaseous Nuclear Rocket Engines Due to Nozzle Coolant Requirements. UAC Research Laboratories Report D-110224-1, April 1965. (report unclassified)
55. Sparrow, E. M.: Temperature Distribution and Heat Transfer Results for an Internally Cooled, Heat Generating Solid. Journal of Heat Transfer, November 1960, pp. 389-393.
56. Stull, D. R., et al: JANAF Thermal Chemical Tables. Dow Chemical Company, Midland, Michigan, 1961.
57. Schuerch, H. U. and O. R. Burggraf: Analytical Design for Optimum Filamentary Pressure Vessels. AIAA Journal, Vol. 2, No. 5, May 1964, pp. 809-820.
58. Duke, Edward E., and William J. Houghton: Gaseous Fueled Nuclear Rocket Engine. AIAA Paper No. 66-621 presented at AIAA Second Propulsion Joint Specialist Conference, Colorado Springs, Colorado, June 13-17, 1966.
59. Ito, H.: Friction Factors for Turbulent Flow in Curved Pipes. ASME Journal of Basic Engineering, Vol. 81, Series D, pp. 123-124 (1959).
60. Seban, R. A. and E. F. McLaughlin: Heat Transfer in Tube Coils with Laminar and Turbulent Flow. International Journal of Heat and Mass Transfer, Vol. 6, pp. 387-395 (1963).

LIST OF SYMBOLS

(Excludes Symbols Employed Only in Appendix C)

A_T	Throat area of exhaust nozzle, ft^2
d	Diameter of moderator cooling passage, in.
d_T	Diameter of throat of exhaust nozzle, ft or in.
D	Diameter of helix for spiral cooling holes, in.
D_c	Cavity diameter, ft
H	Average enthalpy of cavity propellant, Btu/lb
I_{sp}	Specific impulse, sec
K_p	Ratio of density of cavity propellant to density of hydrogen at same temperature and pressure
L	Length of engine cavity or length of coolant passage, ft or in.
M_E	Engine weight, lb
P	Pressure, atm
q	Dynamic pressure, atm
Q_v	Volumetric heat deposition rate, Btu/sec-ft ³
Q_T	Total heat generated in engine, Btu/sec or megw
q_{z_1}	Axial-flow dynamic pressure, atm
r	Distance from centerline of engine or distance from centerline of spiral-hole configuration, in. or ft
Re_d	Reynolds number based on diameter of coolant hole
Re_z	Axial-flow Reynolds number

s	Spacing between moderator coolant holes in slanted configuration, in.
T	Temperature, deg R
T_C	Local coolant temperature in moderator, deg R
T_W	Local moderator wall surface temperature, deg R
T_0	Stagnation temperature at entrance to exhaust nozzle, deg R
T_6	Temperature at edge of fuel-containment region, deg R
V_P	Coolant or void volume fraction
W	Weight flow, lb/sec
W_C	Cavity propellant flow, lb/sec
W_F	Fuel or heavy-gas flow, lb/sec
W_T	Total propellant flow, lb/sec
X	Distance from inner wall in pressure vessel, in.
Z	Weight parameter for pressure vessel, lb/ft ³ -atm
α	Helix angle for spiral hole configuration
ΔP_f	Frictional pressure loss
ΔP_{TOTAL}	Total pressure loss
$\Delta l / \Delta X$	Slope of cooling holes in straight hole configuration
μ	Propellant viscosity, lb/sec-ft
ρ	Density, lb/ft ³
$\bar{\rho}_{F_i}$	Average critical fuel density, lb/ft ³
ρ_P	Propellant density, lb/ft ³

τ_{F_1} Dimensionless fuel or heavy-gas time constant

σ Filament strength, lb/in.²

Subscripts

1 Outside radius of vortex tube

6 Outside radius of fuel-containment region

8 Centerline of engine

11-24 Stations in helium circuit - see Table V

31-39 Stations in hydrogen circuit - see Table VI

STAND. Standard value

APPROXIMATE CONDITIONS DURING ENGINE START-UP

A series of calculations have been made to determine the approximate conditions which might exist in the fixed-geometry vortex-stabilized gaseous nuclear rocket engine described in the text as a function of the nozzle inlet total temperature. This information, together with information on criticality and off-design-operation turbopump characteristics, will permit determination of engine characteristics during the start-up process.

The object of using a cavity propellant having a density greater than that of hydrogen during design-point operation is to reduce the ratio of the average density of the nuclear fuel to the propellant density at the edge of the fuel to a value of 5.0. Since the loss of specific impulse due to the use of a cavity propellant having a density greater than hydrogen is relatively unimportant during the start-up process, it would probably be desirable to employ a more dense propellant in the cavity during start-up than during normal engine operation in order to minimize cavity pressure. It is also possible to change the ratio of cavity propellant flow to total propellant flow during start-up. However, in the following calculations it is assumed that the ratio of cavity propellant flow to total propellant flow and the ratio of the density of cavity propellant to that of hydrogen at the same temperature and pressure are both held constant.

The procedure followed in calculating start-up characteristics was to assume a temperature at the entrance to the exhaust nozzle and calculate the weight flow passing through the nozzle as a function of nozzle total pressure for the nozzle throat area of 0.27 ft^2 required for design-point operation. In calculating this flow, it was assumed that the static density at the throat of the nozzle was 0.64 times the stagnation density at the nozzle entrance and that the velocity at the throat of the nozzle was 0.45 times that which would result by conversion to velocity of all of the thermal energy associated with the stagnation enthalpy of the nozzle entrance flow. (For comparison, the ratio of throat static density to stagnation density is 0.65 and 0.63 for perfect gases having ratios of specific heats of 1.67 and 1.40, respectively, and the ratio of throat velocity to maximum exit velocity is 0.50 and 0.40 for perfect gases having ratios of specific heats of 1.67 and 1.40, respectively.) This simplified procedure was followed rather than using the tables of Ref. 41 because these tables were not available before the following analysis was completed. The nozzle flow thus determined was multiplied by the nozzle entrance stagnation enthalpy to obtain the total engine power. This power was then divided by the cavity length of 6 ft to obtain the heat flux per unit length required from

SECRET

the fuel region and was divided by the fuel surface area of 84.8 ft² to obtain the heat flux per unit area at the edge of the fuel. The assumed pressure and heat transfer rates then determined the required temperature at the edge of the fuel-containment region (see following paragraph) and the corresponding density of the cavity propellant flow at this location.

The density of the cavity propellant flow at the edge of the fuel-containment region, ρ_6 , was then plotted as a function of the assumed pressure within the engine. The specific density of interest is that which provides a fuel density ratio of 5.0. Since the required fuel density, ρ_F , employed in Ref. 36 is 0.107 lb/ft³, the cavity propellant density of interest at Station 6 is 0.107/5.0 or 0.0214 lb/ft³. This density was then employed in a curve showing the variation of ρ_6 with pressure to determine the required engine operating pressure.

Two different procedures were employed to determine the temperature at the edge of the fuel-containment region, T_6 , necessary to provide the energy required to heat the propellant flow. At low temperatures, hydrogen is sufficiently transparent so that there should be little trouble depositing the radiant energy from the fuel region at a relatively uniform rate across the propellant region in the cavity (assuming that the cavity propellant employed is also relatively transparent at low temperatures). Therefore, at low temperatures it should be possible to set the edge-of-fuel temperature, T_6 , at a value equal to the black-body radiating temperature corresponding to the required radiant heat flux at this station. However, at high temperatures, hydrogen is sufficiently opaque that the required edge-of-fuel temperature is substantially greater than the equivalent black-body radiating temperature. For instance, at the design power the temperature at the edge of the fuel-containment region for the configuration of preceding paragraphs is equal to 102,000 R, while the black-body radiating temperature is only 38,000 R. Therefore, the curves of Refs. 9 and 10 which indicate the magnitude of the required temperature at Station 6 were employed for high pressures within the engine.

The results of the calculation are shown in Fig. 27. The data plotted on each curve for temperatures lower than that indicated by the dashed lines represents information calculated assuming that the temperature at the edge of the fuel-containment region is equal to the equivalent black-body radiating temperature at this station. The information shown for temperatures greater than that indicated by the dashed line were determined from Refs. 9 and 10. The exact temperature at which the transition between the two curves occurs was chosen arbitrarily, but fits the general requirement that the edge-of-fuel temperature can be low for low propellant temperatures, but must be high at high propellant temperatures. It can be seen from Fig. 27 that all engine characteristics change rapidly with changes in nozzle inlet temperature in the region indicated by the dashed line, indicating the need for more detailed calculations of engine characteristics in this region. The propellant flow stays relatively constant at low temperatures. The magnitude of

SECRET

the required pressures and weight flows for low values of nozzle-entrance temperature could be substantially reduced by employing higher values of seed fractions in the cavity, as noted in preceding sections.

SECRET

EFFECT OF CHANGES IN CRITICAL MASS AND AVERAGE CAVITY
PROPELLANT ENTHALPY ON ENGINE CHARACTERISTICS

A series of calculations was made using the procedures of Ref. 36 to investigate the effect on engine performance of changes in two of the parameters which were specified in all of the calculations in Ref. 36: the criteria for critical fuel density (see Fig. 10 of Ref. 36) and the criteria for the average enthalpy of the cavity propellant flow (see Figs. 4 and 5 of Ref. 36). Unless otherwise specified, all calculations were made using the same assumptions and the same values of input parameters noted in Table I of Ref. 36. The parameters which were varied in Ref. 36 but which are held constant in the following calculations are:

1. The pressure in the cavity is 1000 atm.
2. The temperature of both the bypass and cavity flows injected into the engine is 5300 R on the basis of 10 percent energy release in the wall. (As noted in the main text, this also corresponds to a wall temperature of 4300 R and 7.6 percent of the energy deposited in the wall.)
3. The dimensionless time constant, τ_{F_1} , is equal to 0.01.
4. The shell strength parameter, σ/ρ , is equal to 2.5×10^6 in.
5. No space radiator is employed
6. The engine thrust-to-weight ratio is equal to 20. (The engine discussed in the text is assumed to have a nominal thrust-to-weight ratio of 10.)

The results of calculations to determine the effect of a change in the criteria for critical fuel density are given in Figs. 28 through 34 (following the same pattern employed in Ref. 36 - see Figs. 25 through 32, for example). The calculations shown in Figs. 28 through 34 were carried out for critical fuel densities equal to 0.1, 0.3, 1.0, 3.0, and 10.0 times the critical fuel densities specified in Fig. 10 of Ref. 36. The variable of greatest interest, specific impulse, is shown in Fig. 29. For an engine weight of 150,000 lb, an increase of required fuel density by a factor of 3 relative to the standard value results in a reduction in specific impulse from 2100 to 1640 sec, while a decrease in critical fuel density to three-tenths of the standard value results in an increase in specific impulse from 2100 sec to 2500 sec.

The second new variable investigated which was not considered in Ref. 36 is the average enthalpy of the cavity propellant. The values of enthalpy employed in Ref. 36 were determined from propellant temperature distributions determined in the 1963 Air Force study (Ref. 10). Since this original determination of propellant temperature distribution, a large amount of information has become available on

SECRET

seed materials, etc., which will result in changes in propellant temperature distribution. Although no generalized determination of temperature distribution as a function of seed material and seed density has been made, it is of interest to determine the influence of changes in the average cavity propellant enthalpy on engine characteristics. Therefore, the standard conditions employed in Ref. 36 were used along with average cavity propellant enthalpies equal to 0.25, 0.5, 1.0 and 2.0 times the standard enthalpies from Figs. 4 and 5 of Ref. 36. The results of the calculations are given in Figs. 35 through 41. It is shown in Fig. 41 that the primary effect of a reduction in average cavity propellant enthalpy is an increase in the fraction of the flow which passes through the cavity. Since the cavity propellant flow is of higher molecular weight than the bypass flow, a decrease in specific impulse results, as is shown in Fig. 36.

MODERATOR CONFIGURATION WITH SPIRAL HOLES

List of Symbols Employed in Appendix C

A	Cross sectional area of individual coolant passage, in. ² or ft ²
C _p	Specific heat of coolant fluid, Btu/lb
d	Diameter of coolant passage, in. or ft
f	Friction coefficient
f _s	Friction coefficient in straight duct
m	Exponent governing variation of viscosity with temperature (see Eq. (C-9))
n	Exponent governing variation of friction coefficient with Reynolds number (see Eq. (C-8))
Nu	Nusselt number
Nu _s	Nusselt number in straight duct
P	Pressure, lb/ft ² or atm
Pr	Prandtl number
Q	Heat removed by coolant fluid in single passage, Btu/sec
R	Radius of curvature of coolant passage, in. or ft
Re _d	Reynolds number based on diameter of coolant passage
T ₀	Temperature of coolant fluid at entrance to heat exchanger, deg R
T _e	Temperature of coolant fluid at exit of heat exchanger, deg R
\bar{T}	Average temperature of coolant fluid in heat exchanger, deg R
\bar{V}	Average velocity of coolant fluid in heat exchanger, ft/sec

[REDACTED]

W Weight flow passing through single coolant passage, lb/sec

$\bar{\mu}$ Viscosity corresponding to \bar{T} , lb/sec-ft

$\bar{\rho}$ Average density of coolant fluid in heat exchanger, lb/ft³

A problem associated with the geometry of the moderator coolant passages was encountered in choosing the moderator cooling configuration for the reference engine design. This problem was evident in both the beryllium oxide and graphite portions of the moderator, although it is illustrated in the following paragraphs only for the beryllium oxide portion of the moderator. In this reference engine design, heat balance considerations have led to the desirability of employing a thickness of beryllium oxide moderator of 3.5 in. and a length-to-diameter ratio in the coolant passages in this portion of the moderator of approximately 500. If the coolant holes were drilled normal to the surface of the moderator, the resulting required hole diameter would be approximately 0.007 in., which would be difficult to fabricate and would lead to problems of laminar flow instability. These problems were avoided in the studies of Ref. 20 by assuming that the coolant passages would be slanted and intersect the inside surface of the moderator at an angle substantially less than 90 deg. However, the use of straight slanted holes in a moderator leads to the requirement that either the primary flow-distribution ducts passing through the moderator have centerlines slanted relative to the radial direction or that the primary ducts cut through the slanted moderator configuration in an awkward manner (both requirements are due to the desirability of minimizing the void fraction in the moderator).

An alternate solution to this moderator design problem has been evolved and is illustrated in Fig. 17. In this alternate solution, the slanted-hole effect is obtained by employing spiral grooves. These grooves are formed on the outside of either an inner rod or one or more surrounding cylinders such that spiral passages are obtained when the various pieces of the moderator configuration are assembled. The outside element in the configuration has a hexagonal outer shape to permit stacking with other similar configurations. Although not shown in Fig. 17, the leakage between the various portions of the unit hexagonal block could be minimized by reducing the clearance between different parts by tapering the contacting surfaces. Sealing between the beryllium oxide and graphite, and between the graphite and the support structure is achieved by stepped or tapered contacting surfaces as shown in Figs. 19 and 20.

Besides easing the problem of passing primary ducts through the moderator, the spiral hole configuration shown in Fig. 17 has two additional advantages relative to the straight configuration. The first of these advantages is that the curved passages provide higher heat transfer rates (and, concurrently, higher friction coefficients) than the corresponding straight passage. The second advantage is that

the curvature of the passages will minimize the possibility of laminar flow instabilities during low power operation. Information from Refs. 59 and 60 on the friction coefficient in curved ducts is given in Fig. 42 (the definition of friction coefficient for this figure is taken from Ref. 59). According to Ref. 60, the ratio of friction coefficient in a curved duct to that in a straight duct at high Reynolds numbers is

$$\frac{f}{f_s} = Re_d^{0.05} \left(\frac{d}{2R} \right)^{0.10} \quad (C-1)$$

Also, from Ref. 60, the Nusselt number in a curved duct at high Reynolds numbers is

$$Nu = 0.023 Pr^{0.4} Re_d^{0.85} \left(\frac{d}{2R} \right)^{0.10} \quad (C-2)$$

For a straight duct,

$$Nu_s = 0.023 Pr^{1/3} Re_d^{0.8} \quad (C-3)$$

Therefore, the ratio of heat transfer in a curved duct to that in a straight duct is

$$\frac{Nu}{Nu_s} = Pr^{0.0667} Re_d^{0.05} \left(\frac{d}{2R} \right)^{0.10} \quad (C-4)$$

In making use of these equations, it is tacitly assumed that the holes having the noncircular shape provided by the configuration in Fig. 17 would have the same characteristics as round holes. For hydrogen, the Prandtl number is approximately 0.65, and Prandtl number to the 0.0667 power is 0.997. Therefore, Eqs. (C-1) and (C-4) are substantially identical and, hence, the effect of curvature on heat transfer is substantially identical to the effect on friction coefficient (i.e., Reynolds analogy holds approximately for flow in curved ducts).

Determination of the effect of duct curvature on the onset of laminar flow instability requires a detailed examination of the cause of such instabilities. Laminar flow instability occurs when a decrease in the flow in a single passage in a heat exchanger results in an increase in the pressure drop in that passage and, hence, a further reduction in flow. In the following simplified analysis, it is assumed that the total heat which must be removed by the coolant fluid passing through a single passage is fixed, and that the exit temperature of the coolant fluid must adjust with a change in weight flow to permit removal of this heat. The

total heat absorbed by the flow passing through a single passage is

$$Q = W C_p (T_e - T_0) \quad (C-5)$$

Let the average temperature in the passage be defined such that

$$\bar{T} = \frac{T_e + T_0}{2} \quad (C-6)$$

Therefore, from Eqs. (C-5) and (C-6), assuming that specific heat is independent of temperature,

$$W \sim \frac{1}{\bar{T} - T_0} \quad (C-7)$$

Also assume that

$$f \sim (Re_d)^n \quad (C-8)$$

$$\bar{\mu} \sim \bar{T}^m \quad (C-9)$$

$$\bar{\rho} \sim \frac{1}{\bar{T}} \quad (C-10)$$

$$\bar{V} = \frac{W}{\bar{\rho} A} \sim W \bar{T} \quad (C-11)$$

The pressure drop in a single passage due to friction is

$$\Delta P \sim f \bar{\rho} \bar{V}^2 \quad (C-12)$$

In order to determine the criteria for laminar flow instability, it is necessary to substitute Eqs. (C-7) through (C-11) into Eq. (C-12) in order to obtain an expression for the variation of pressure drop with weight flow. When this resulting expression is differentiated and set equal to zero, the following criterion is established under which a small change in weight flow results in no change in pressure drop (i.e., the criterion for neutral laminar flow stability):

$$n = - \frac{1 + \frac{T_0}{\bar{T}}}{1+m \left(1 - \frac{T_0}{\bar{T}}\right)} \quad (C-13)$$

This criterion is plotted in Fig. 43 as a function of the ratio of the temperature of the gas entering the heat exchanger to the average temperature of the gases in the heat exchanger, T_0/\bar{T} , for two different variations of viscosity with temperature ($m = 0.5$ and 0.75). It can be seen from Fig. 43 that turbulent flow is always stable, while laminar flow leads to instabilities when the ratio T_0/\bar{T} is less than a value between approximately 0.33 and 0.42, depending on the variation of viscosity with temperature.

The approximate criterion for laminar flow instability given in Fig. 43 can now be employed with the information on the variation of friction coefficient with Reynolds number in curved ducts given in Fig. 42 to obtain a criterion for the onset of laminar flow instabilities in curved ducts. For a ratio of radius of curvature to duct diameter of 8.5, the exponent n is approximately equal to -0.72 for Reynolds numbers between 100 and 1000. It can be seen from Fig. 43 that such an exponent will lead to laminar flow instabilities only for values of the ratio T_0/\bar{T} less than 0.05 for $m = 0.5$ and for values of T_0/\bar{T} less than 0.17 for $m = 0.75$. For the reference gaseous nuclear rocket engine being analyzed under the contract, the temperature at the entrance to the beryllium oxide portion of the moderator is 1356 R at the design point, while the average temperature in the beryllium oxide and graphite portions of the moderator is approximately 2900 R (considering that the cooling passages in the two materials are continuous). For this design point temperature distribution, the parameter T_0/\bar{T} is therefore equal to 0.47. It can be seen from Fig. 43 that such a value of T_0/\bar{T} is out of the range of laminar flow instabilities for a duct curvature which leads to a value of n of -0.72 . Thus, for the same temperature distribution at low power operation as at design-point operation, the possibility of laminar flow instability is avoided for Reynolds number above

approximately 100.

A comparison of the flow characteristics of the design configuration with straight slanted holes and spiral holes is given in Tables VII and VIII. It can be seen that the use of spiral holes results in a shortening of the passage length (and, hence, an increase in the number of holes to maintain the same void fraction), and an increase in the angle of the hole. Because of the increase in number of holes, the velocity of the flow in the passages and the Reynolds number corresponding to this velocity are both decreased. Although the Reynolds number is decreased by approximately 30 percent, the Reynolds number for the onset of laminar flow instability is reduced by a factor of approximately 20. This decrease in velocity also corresponds to a decrease in dynamic pressure and a decrease in pressure drop.

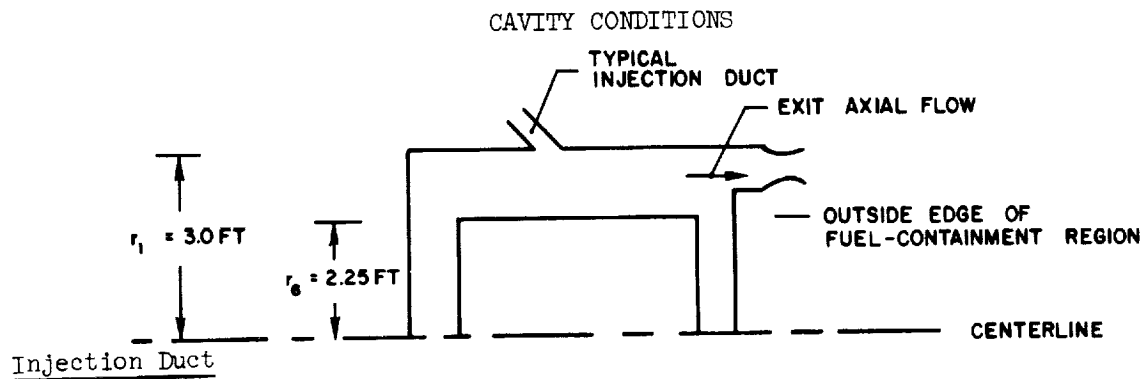
It is also possible that the advantages to be gained by using spiral holes could be applied to solid-core nuclear rockets, particularly in small-size configurations where the minimum length is determined by some minimum desirable coolant passage diameter.

TABLE I
RADIAL DIMENSIONS, VOID FRACTIONS AND MATERIAL VOLUMES
OF REGIONS WITHIN PRESSURE SHELL

Region	Radial Thickness of region, in.	Radius at Outside edge of region, in.	Volume of region, ft ³	Material volume, ft ³	Void fraction	Summation of volumes
Cavity	36.0	36.0	170	0	1.0	170
Tungsten tubes	0.63 ⁽¹⁾	36.63	9.0	0.47	0.948	179
Beryllium liner	0.30	36.93	4.5	3.9	0.133	183.5
Plenum	0.30	37.23	4.5	0	1.0	188.0
Beryllium Oxide	3.50	40.73	59	50.5	0.144	247
Plenum	0.10	40.83	1.8	0	1.0	248.8
Graphite	8.70	49.53	194	170.2	0.123	442.8
Plenum	0.30	49.83	8.0	0	1.0	450.8
Beryllium wall	0.30	50.13	8.2	8.2	0	459.6
Heavy water	9.95	60.08	330.3	297.3	0.100	789.6
Beryllium wall	0.30	60.38	10.46	10.46	0	800
Heat exchanger & piping	10.0	70.38	585	31.7	0.945	1385

(1) 0.185 in. O D tubes plus 0.445 in. space between tubes and liner

TABLE II



Static pressure	1000 atm
Stagnation pressure	1086 atm
Temperature	4300 R

Outside Edge of Fuel-Containment Region (Station 6)

Temperature	102,000 R
Density	0.0215 lb/ft^3
Viscosity	$6.85 \times 10^{-5} \text{ lb/sec-ft}$

Exit Axial Flow

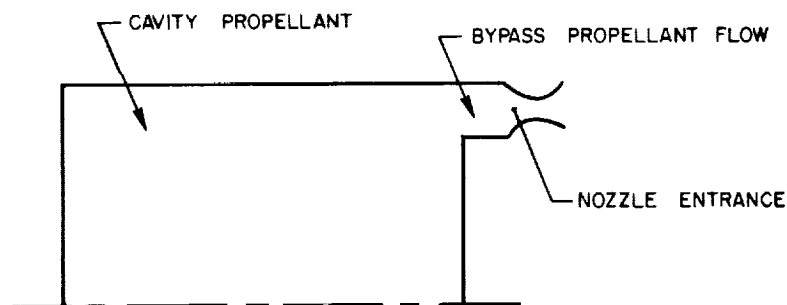
Axial velocity	508 ft/sec
Axial dynamic pressure (using density for $T = 4300 \text{ R}$)	3.82 atm
Axial dynamic pressure (using density for $T = 102,000 \text{ R}$)	0.041 atm
Axial Reynolds number (based on conditions at Station 6)	4.8×10^5

Centerline

Temperature, T_8	136,000 R
Density of cavity propellant at centerline condition, ρ_{P8}	0.0158 lb/ft^3
Viscosity, μ_8	$11.9 \times 10^{-5} \text{ lb/sec-ft}$
Fuel time constant parameter, $\rho_{P8} r_1^2 / \mu_8$	1195 sec

TABLE III

OVER-ALL HEAT BALANCE

Injection Conditions at Wall

	Cavity Propellant Flow	Bypass Propellant Flow	Total
Flow, lb/sec	236*	339	575
Molecular weight	6.32	2.0	-
Temperature, deg R	4300	4300	-
Enthalpy, Btu/lb.	5320	16,800	-
Energy absorbed before injection, Btu/sec . .	1.26×10^6	5.70×10^6	$6.96 \times 10^{6**}$

Nozzle Entrance Conditions

Weight flow	575 lb/sec
Temperature	23,000 R
Enthalpy	150,400 Btu/lb
Energy flow	86.5×10^6 Btu/sec

* Composed of 75 lb/sec of hydrogen and 161 lb/sec of high-molecular-weight diluent.

** 6.56×10^6 Btu/sec due to deposition of heat within wall due to neutrons and gamma rays and 0.4×10^6 Btu/sec due to heat deposition on surface of wall due to convection and thermal radiation.

TABLE IV
HEAT DEPOSITION IN DIFFERENT REGIONS OF ENGINE

Region	Internal Heat Deposition Due to Neutrons & Gamma Rays, Btu/sec	Radiant and Convective Heat Deposition on Cavity Surface, Btu/sec
Tungsten liner tubes	0.05×10^6	0.40×10^6
Beryllium liner	0.30×10^6	
Beryllium oxide	2.5×10^6	
Graphite	2.7×10^6	
D ₂ O	0.95×10^6	
Piping	0.02×10^6	
Pressure Vessel	0.04×10^6	
	6.56×10^6	0.40×10^6
Total Heat Generation	6.96×10^6	

TABLE V

OPERATING TEMPERATURES AND PRESSURES IN HELIUM CIRCUIT

Note: See Figures 3 and 4 for schematic diagrams showing station locations

Station Number	Location	Operating Conditions	
		Temperature, deg R	Pressure, atm
11	Pump Outlet (1)	300	1010.0
12	D ₂ O Heat Exchanger Inlet	324	1002.7
13	D ₂ O Heat Exchanger Outlet	898	1002.2
14	Entrance to Inlet Ducts	898	1001.4
15	Liner Tube Entrance	903	1000.1
16	Liner Tube Outlet	1175	1000.1
17	Entrance to BeO Moderator	1356	1000.0
18	Entrance to Graphite Moderator	2866	994.0
19	Exit from Graphite Moderator	4500	991.3
20	Exit from Outlet Duct	4500	990.1
21	High-Temperature Heat Exchanger Inlet	4500	988.0
22	High-Temperature Heat Exchanger Outlet	2400	981.7
23	Low-Temperature Heat Exchanger Inlet	2400	975.5
24	Low-Temperature Heat Exchanger Outlet	300	975.0
Total System Pressure Loss = 35 atm Total Helium Flow = 1325 lb/sec			

(1) Temperature difference across pump is not included.

TABLE VI

OPERATING TEMPERATURES AND PRESSURES
IN HYDROGEN CIRCUIT

Note: See Figures 3 and 5 for schematic
diagrams showing station locations

Station Number	Location	Operating Conditions	
		Temperature, deg R	Pressure, atm
31	Pump Inlet ⁽¹⁾	36	1.0
32	Low-Temperature Heat Exchanger Inlet	100	1616.4
33	Low-Temperature Heat Exchanger Outlet	2200	1608.9
34	Turbine Outlet ⁽¹⁾	2200	1108.9
35	High-Temperature Heat Exchanger Inlet	2200	1101.5
36	High-Temperature Heat Exchanger Outlet	4300	1095.2
37	Injection Duct Inlet	4300	1092.8
38	Cavity Injection Nozzle	4300	1086
39	Bypass Injection Nozzle	4300	1086 ⁽²⁾
Turbine Pressure Drop = 500 atm Total System Pressure Loss (excluding turbine) = 30 atm Total Hydrogen Flow Between Stations 31-36 = 414 lb/sec			

(1) Temperature difference across pump and turbine is not included.

(2) Requires throttling from 1095.2 atm.

COOLANT HOLE CONFIGURATION IN
BERYLLIUM OXIDE MODERATOR55

CONFIDENTIAL

TABLE VIII

COOLANT HOLE CONFIGURATION IN GRAPHITE MODERATOR

Volumetric Heat Deposition Rate, Q_v	1.575×10^4 Btu/sec-ft ³
Wall to Coolant Temperature Difference, $T_w - T_c$	200 R
Design Conditions for Straight Holes	
Hole Diameter, d	0.05 in.
Coolant Volume Fraction, V_p	0.02
Pressure Loss, ΔP_f	1.95 atm
Dynamic Pressure, q	3.4 atm
Reynolds Number, Re_d	4.5×10^4
Slope, $\Delta l / \Delta x$	3.0
Passage Angle	19°
Hole Spacing for Square Pitch, s	0.216 in.

Spiral Cooling Configuration				
Ring Number ⁽¹⁾	Radius of Ring, in.	$\frac{D}{d}$	Calculated Helix Angle, α	Number of Holes in Ring
1	0.1529	6.1	46° 45'	4
2	0.342	13.7	39° 3'	8
Selected Value of Helix Angle, α			39 deg	
Dynamic Pressure, q			1.325 atm	
Pressure Loss, ΔP_f			0.706 atm	
Reynolds Number, Re_d			2.8×10^5	
$\Delta P_{TOTAL} = \Delta P_f + 1.5q$			2.70 atm	

(1) Only two rings used since hexagon size is limited by the beryllium oxide region dimensions.

CONFIDENTIAL

TABLE IX

EXTERNAL PIPING SPECIFICATIONS

Quantity	Units	Helium Inlets	Helium Outlets	Helium Connecting Pipes	Pressure Vessel Coolant Shell	Hydrogen Connecting Pipes	Propellant Inlets	Total
ID	in.	2.0	2.5	2.25	144.0	1.5	1.0	
OD	in.	2.2	2.6	2.45	144.0	2.0	1.35	
Length	ft	10	10	10	10	10	10	
Number		44	44	44	1	44	44	
Flow Rate	lb/sec	15.1	15.1	30.1	1325	9.38	2.69	
Fluid Density	lb/ft ³	8.46	1.37	2.72	15	1.25	2.18	
Dynamic Pressure	atm	0.416	1.05	3.21	1.715 ⁶	3.44	0.871	
Re _d		7.8x10 ⁶	1.51x10 ⁶	5.77x10 ⁶	8.25x10 ⁶	6.18x10 ⁶	1.82x10 ⁶	
($\Delta P/q$) Friction		0.462	0.511	0.435	2.74	2.21	1.235	
($\Delta P/q$) Turns		1.5	115	1.5	1.5	1.5	1.5	
ΔP Total	atm	0.8	2.11	6.21	7.26	7.36	2.38	
Inlet Pressure	atm	1002.2	990.1	981.7	1010	1108.9	1095.2	
Inlet Temperature	deg R	898	4500	2400	300	2200	4300	
Inlet Station No.		13	20	22	11	35	36	
Volume	ft ³	2.02	1.62	2.26	1.79	4.20	1.96	13.85
Material Density	lb/ft ³	115.4	1204	540	115.4	540	1204	
Insulation OD	in.	2.5	3.1	-	143.7	-	2.0	5.24
Insulation Volume	ft ³	3.36	5.55	-	2.13	-	4.20	
Insulation Density	lb/ft ³	124.8	124.8	-	124.8	-	124.8	
Insulation Wt	lb	420	692	-	266	-	524	1902
Material Wt	lb	233	1950	1359	207	2540	2370	8659
Total Wt	lb	653	2642	1359	473	2540	2894	10,561

TABLE X

HEAT EXCHANGER SPECIFICATIONS

All heat exchangers are shell & tube, counterflow type with ΔP tube = ΔP shell.
Helium is on shell side of all exchangers.

Material	<u>Helium to Hydrogen Heat Exchanger</u>		<u>Helium to D₂O</u>	Total
	High-Temperature	Low-Temperature	Heat Exchanger	
	Tungsten	Stainless Steel	Stainless Steel	
Tube ID, in.	0.03125	0.03125	0.10	
Tube OD, in.	0.0432	0.0432	0.106	
Length, ft	3.5	3.0	1.0	
Number of tubes	3.86×10^5	3.77×10^5	6.93×10^4	
Tube pitch, in.	0.069	0.069	0.117	
Tube bundle area, in. ²	2000	2000	730	
Shell OD, ft	4.5	4.5	2.7	
Pressure loss, atm	6.25	7.5	0.5	
Total heat trans., Btu/sec	3.48×10^6	3.48×10^6	0.95×10^6	
Maximum bursting pressure in tubes, atm	119.8	621.4	2.2	
Operating temp range, deg R	4500-2200	2400-100	320-1000	
Material volume, ft ³	6.55	5.6	0.466	12.61
Material density, lb/ft ³	1204	540	540	
Tube weight, lb	7930	3020	252	11,202
Total weight ⁽¹⁾ , lb	9510	3650	302	13,462
Total volume, ft ³	48.6	41.6	5.06	95.26

(1) Includes 1.2 factor for shell & header weight

TABLE XI

HYDROGEN TURBOPUMP

Data from study conducted at Pratt and Whitney Aircraft,
Florida Research and Development Center

General Characteristics

Flow rate = 414 lb/sec

Speed = 20,800 rpm

Power = 435,000 hp

Pump

Description: four centrifugal pumps with two stages in each pump

Pressure rise = 21,700 psi = 1476 atm

Pump efficiency = 0.85

Impeller tip speed = 1950 ft/sec

Impeller diameter = 21.4 in.

First stage inlet diameter = 13.5 in.

Blade height at discharge = 1.19 in.

Head coefficient, per stage = 0.525

Flow coefficient, per stage = 0.11

Number of blades = 24

Net positive suction head = 750 ft

Net positive suction pressure = 23 psi

(cont'd on next page)

TABLE XI - cont'd

Specific speed = 1000

First stage suction specific speed = 30,000

Turbine

Description: four axial-flow turbines with two stages in each turbine

Turbine inlet temperature = 2200 R

Turbine pressure ratio = 1.413

Turbine exit pressure = 1000 atm

Pressure ratio per stage = 1.044

Turbine efficiency = 0.80

Mean wheel speed = 1300 ft/sec

Mean blade diameter = 14.3 in.

Length of first stage blade = 1.0 in.

Stator exit angle = 18 deg

Weight

Using current technology = 11,300 lb

Projected weight = 8,000 lb

TABLE XII

COMPARISON OF PRESSURE VESSEL CONFIGURATIONS

Internal Pressure of All Configurations = 1000 atm

Shape of Vessel	Wall Construction	Density, lb/ft ³	Strength-to-Weight Ratio, σ / ρ , of Wall Material, in.	Total Volume Enclosed (see Text and Fig. 2), ft ³	Total Weight of Pressure Vessel, lb	Weight Parameter, $Z^{(1)}$, lb/ft ³ -atm
Cylindrical	Maraging Steel, see Fig. 1	485	0.575×10^6	1385	161,500	0.116
Spherical				1855	125,100 ⁽²⁾	0.0675
Cylindrical	Filament-Wound, see Refs. 36 and 57	-	2.5×10^6	785	47,900	0.0610
				1000	61,000	0.0610
				1385	84,500	0.0610
				785	23,950	0.0305
				1000	30,600 ⁽²⁾	0.0305
			5.0×10^6	1385	42,250	0.0305

$$(1) Z = \frac{\text{Total Weight (lb)}}{\text{Volume Enclosed (ft}^3\text{)} \times \text{Internal Pressure (atm)}}$$

(2) These values taken as probable upper and lower limits of weight (see text)

TABLE XIII

WEIGHT OF MODERATOR REGION COMPONENTS

Item	Volume - ft ³	Density, $\frac{\text{lb}}{\text{ft}}$	Weight - lb
Heavy Water	297.3	63.0	18,750
Graphite	170.2	100.1	17,100
Beryllium Oxide	50.5	188.5	9530
Beryllium Metal			
Inner liner	3.9	115.4	451
Containment walls for D ₂ O	18.66	115.4	2160
Helium inlet ducts	1.23	115.4	142
Helium outlet ducts	3.20	115.4	370
Pyrolytic Graphite Insulation	8.14	124.8	1015
Tungsten-184			
Inner liner tubes	0.47	1204	566
Cavity propellant nozzles	0.04	1204	50
Cavity propellant ducts	0.46	1204	555
Totals	554.10		50,689

TABLE XIV

SUMMARY OF WEIGHTS OF MAJOR COMPONENTS

Component weights from present analysis from Tables IX through XIII

Component	Weight Calculated in Ref. 36, lb	Weight Determined from Present Analysis, lb
Moderator region	57,200	50,689
Pressure vessel	47,900	30,600 to 125,100
Turbopump and piping	10,300	18,561 to 21,861
Heat exchangers	8,600	13,462
Total*	124,100	113,312 to 211,112

*Excludes certain components (see text)

TABLE XV
DETERMINATION OF ENGINE SPECIFIC IMPULSE AND THRUST

Calculation	Description	Specific Impulse, sec	Flow, lb/sec	Thrust, lb
①	Ideal nozzle; exhaust to vacuum; infinite area ratio (conversion of all thermal energy corresponding to stagnation enthalpy of 150,400 Btu/lb to kinetic energy)	2695	575	1.550×10^6
②	Like Calculation ①, but area ratio = 500	2412	575	1.387×10^6
③	Like Calculation ②, but flow frozen beyond area ratio of 90	2400	575	1.380×10^6
④	Like Calculation ③, but 1.0 percent loss allowed for friction and flow nonuniformities in nozzle	2376	575	1.366×10^6
⑤	Like Calculation ④, but allowance for 15 percent nozzle transpiration coolant flow with accompanying loss in specific impulse of 8 percent (see Ref. 54)	2186*	661	1.445×10^6 *

*Corresponding calculations using procedures of Ref. 36 yield specific impulse of 2155 sec and thrust of 1.24×10^6 lb

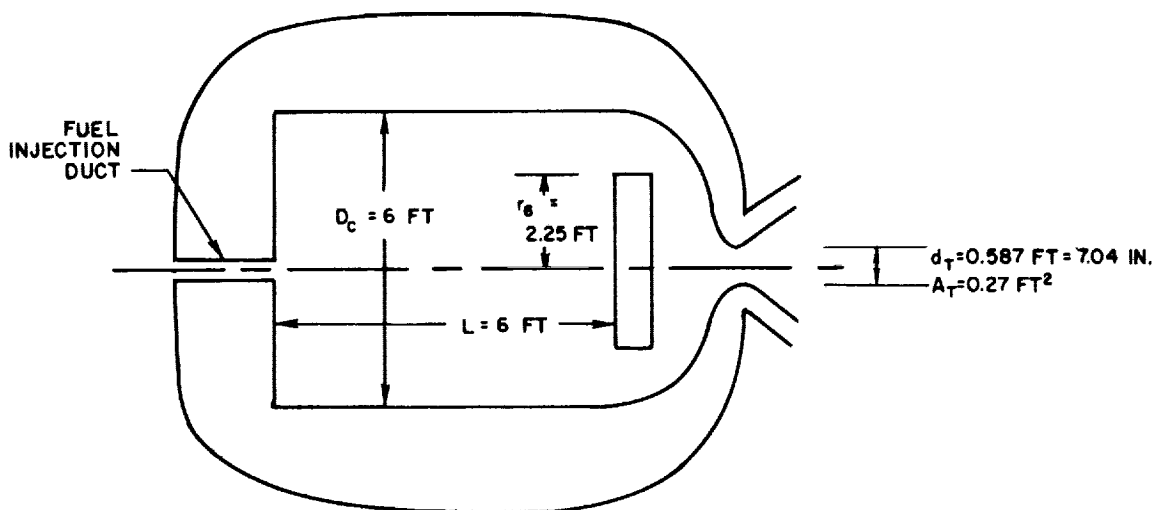
CONFIDENTIAL

FIG. 1

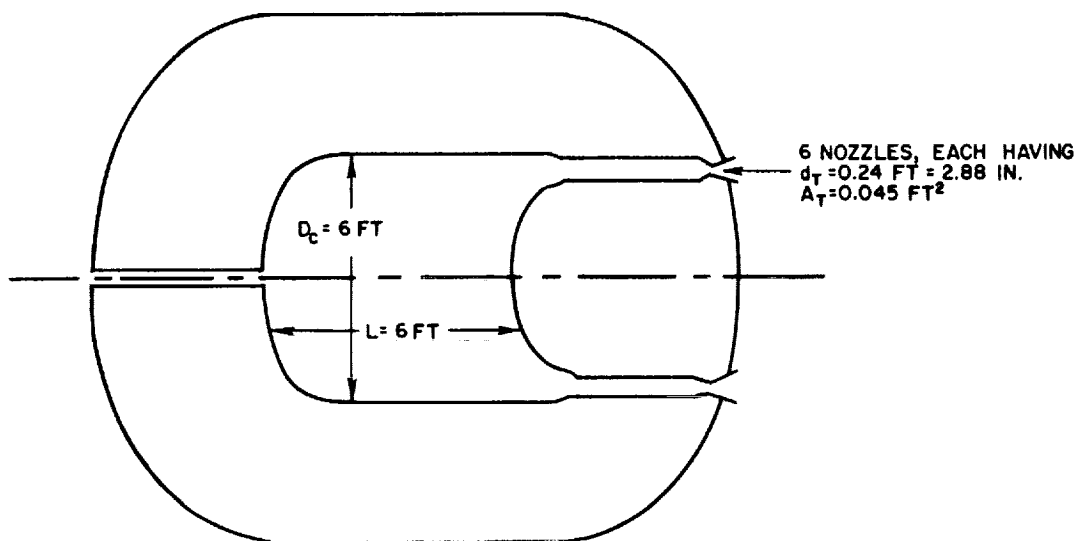
GEOMETRY OF VORTEX-STABILIZED GASEOUS NUCLEAR ROCKET ENGINE

FOR BOTH CONFIGURATIONS:
NOMINAL INSIDE SURFACE AREA = 170 FT²
CAVITY PRESSURE = 1000 ATM

GEOMETRY CONSIDERED IN REFS. 4, 10 AND 36



GEOMETRY CONSIDERED IN PRESENT STUDY



CONFIDENTIAL

LAYOUT DRAWING OF ENGINE DESIGN CONFIGURATION

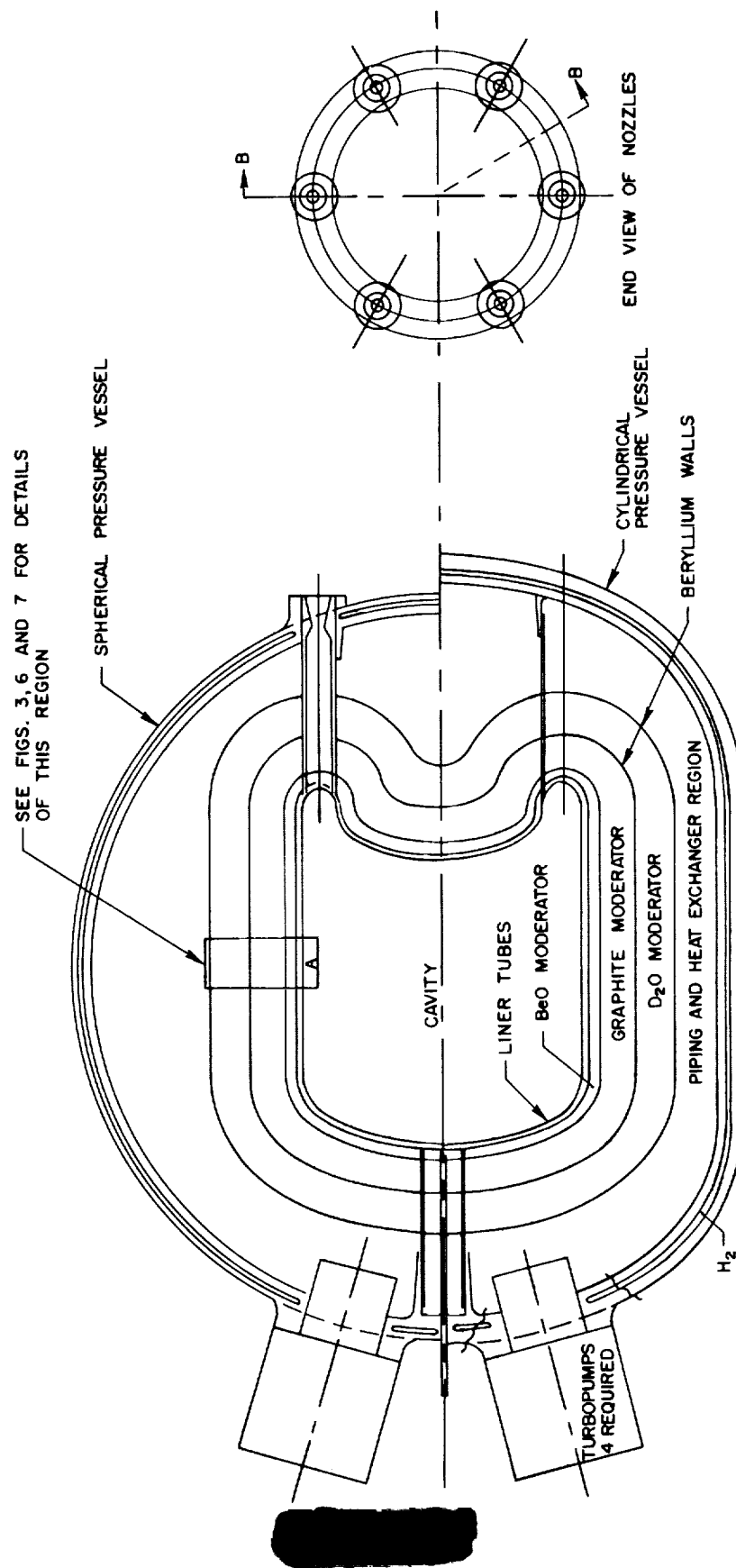
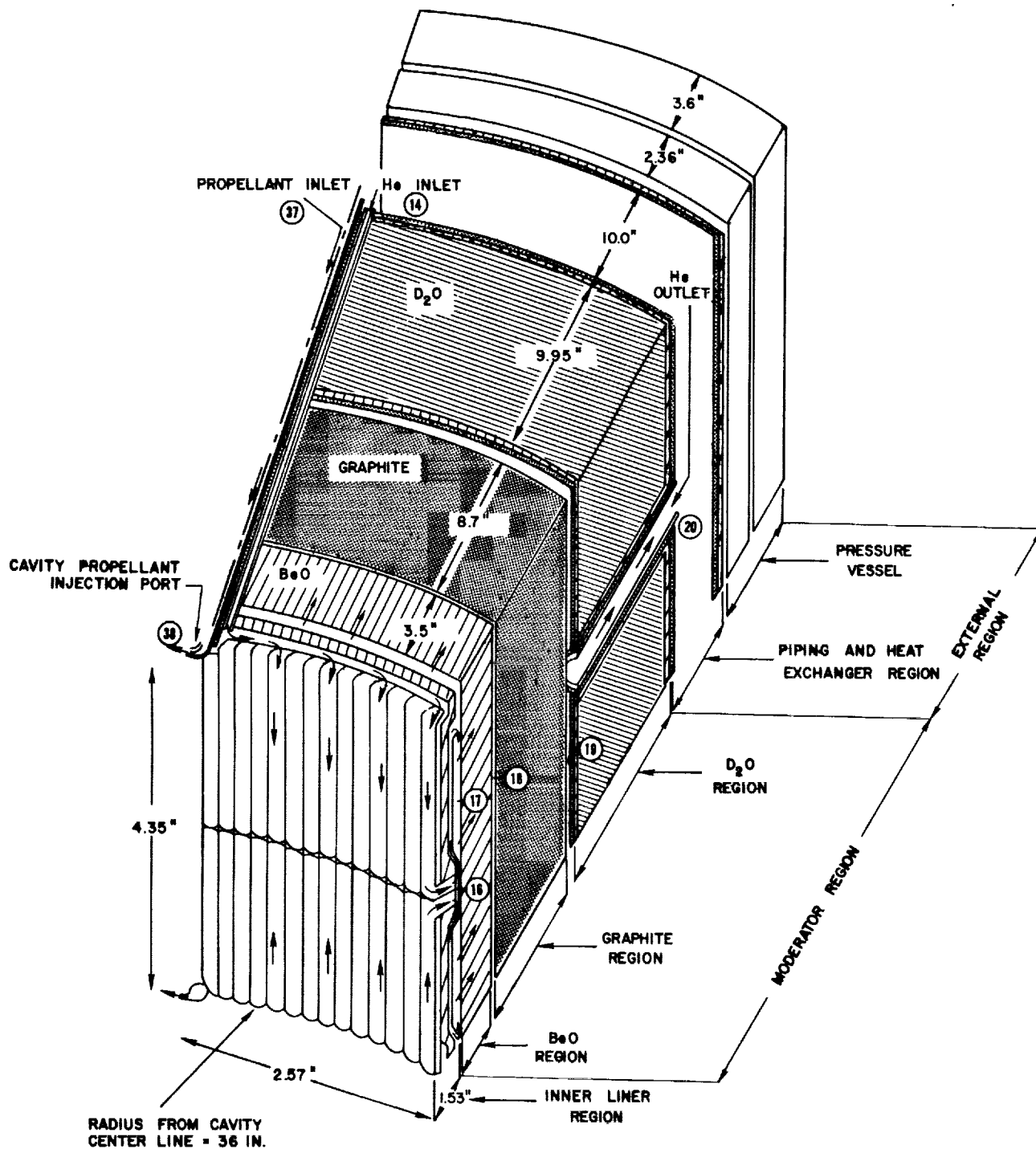


FIG. 3

OBLIQUE SKETCH OF TYPICAL SECTION THROUGH CYLINDRICAL REGION

NOT TO SCALE

NOTE: CIRCLED NUMBERS REPRESENT STATION NUMBERS REFERRED TO IN THE TEXT

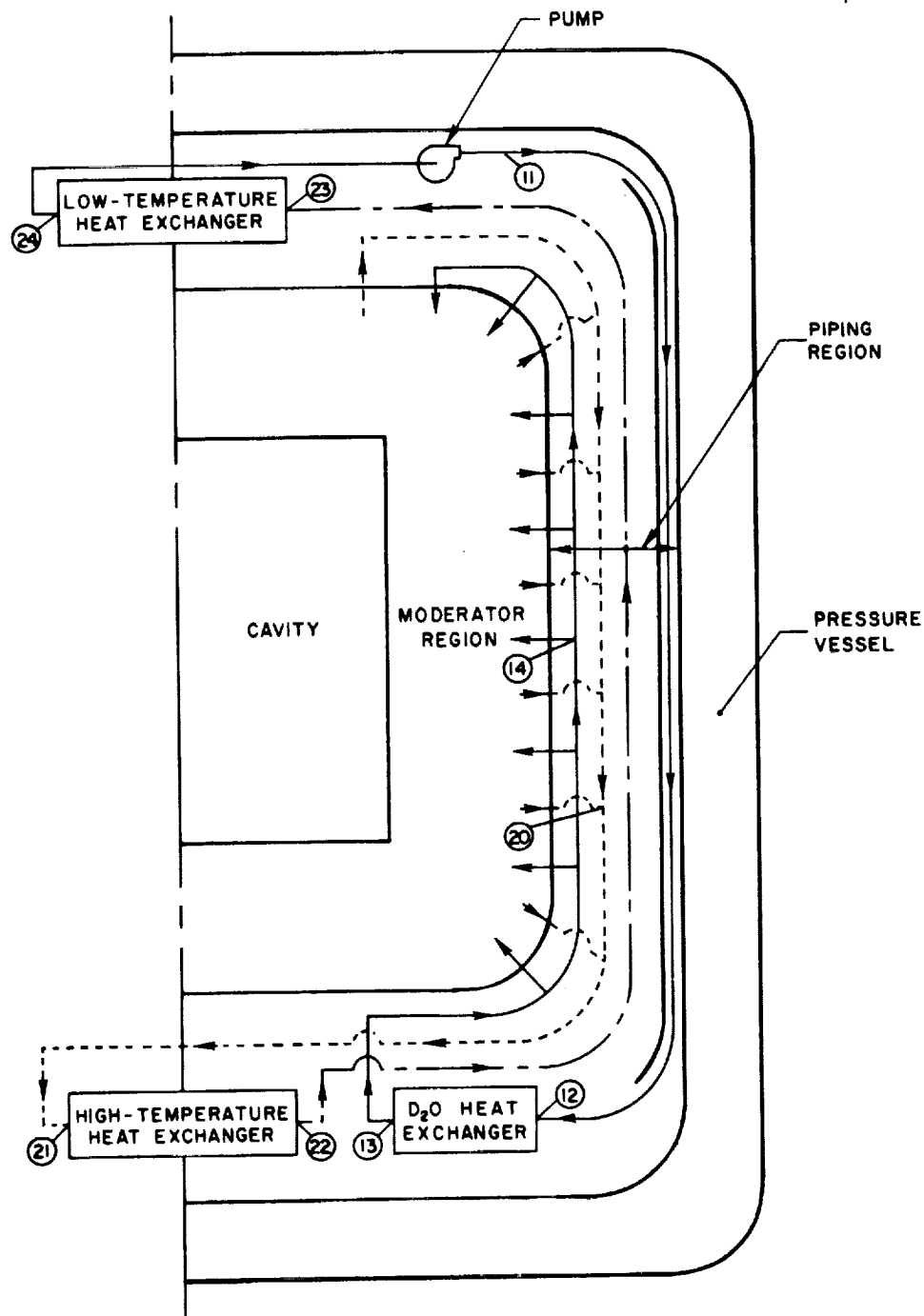


SCHEMATIC DIAGRAM OF HELIUM SYSTEM

FIG. 4

NOTE: SEE TABLE X FOR TEMPERATURE AND PRESSURE LEVELS AT EACH NUMBERED STATION
NOT TO SCALE

DUCT DESIGNATION	HELIUM TEMPERATURE, DEG R
—	300 - 900
- - -	~ 2400
- - - -	~ 4500



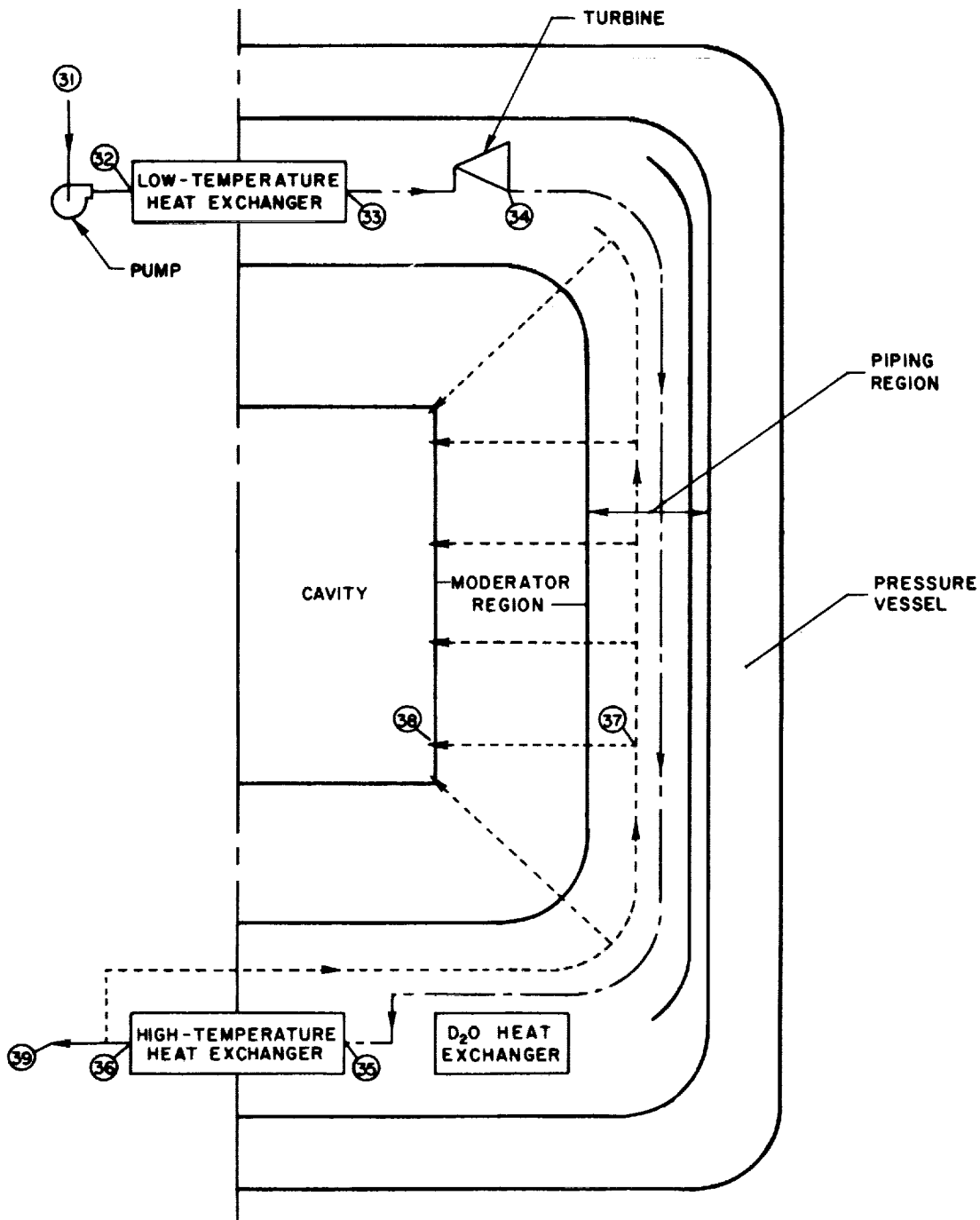
SCHEMATIC DIAGRAM OF HYDROGEN SYSTEM

FIG. 5

NOTE: SEE TABLE VI FOR TEMPERATURE AND PRESSURE LEVELS AT EACH NUMBERED STATION

NOT TO SCALE

DUCT DESIGNATION	HYDROGEN TEMPERATURE, DEG R
—	~ 100
- - -	~ 2200
- - - -	~ 4300



TEMPERATURE AND PRESSURE LEVELS IN INNER LINER REGION

NOT TO SCALE

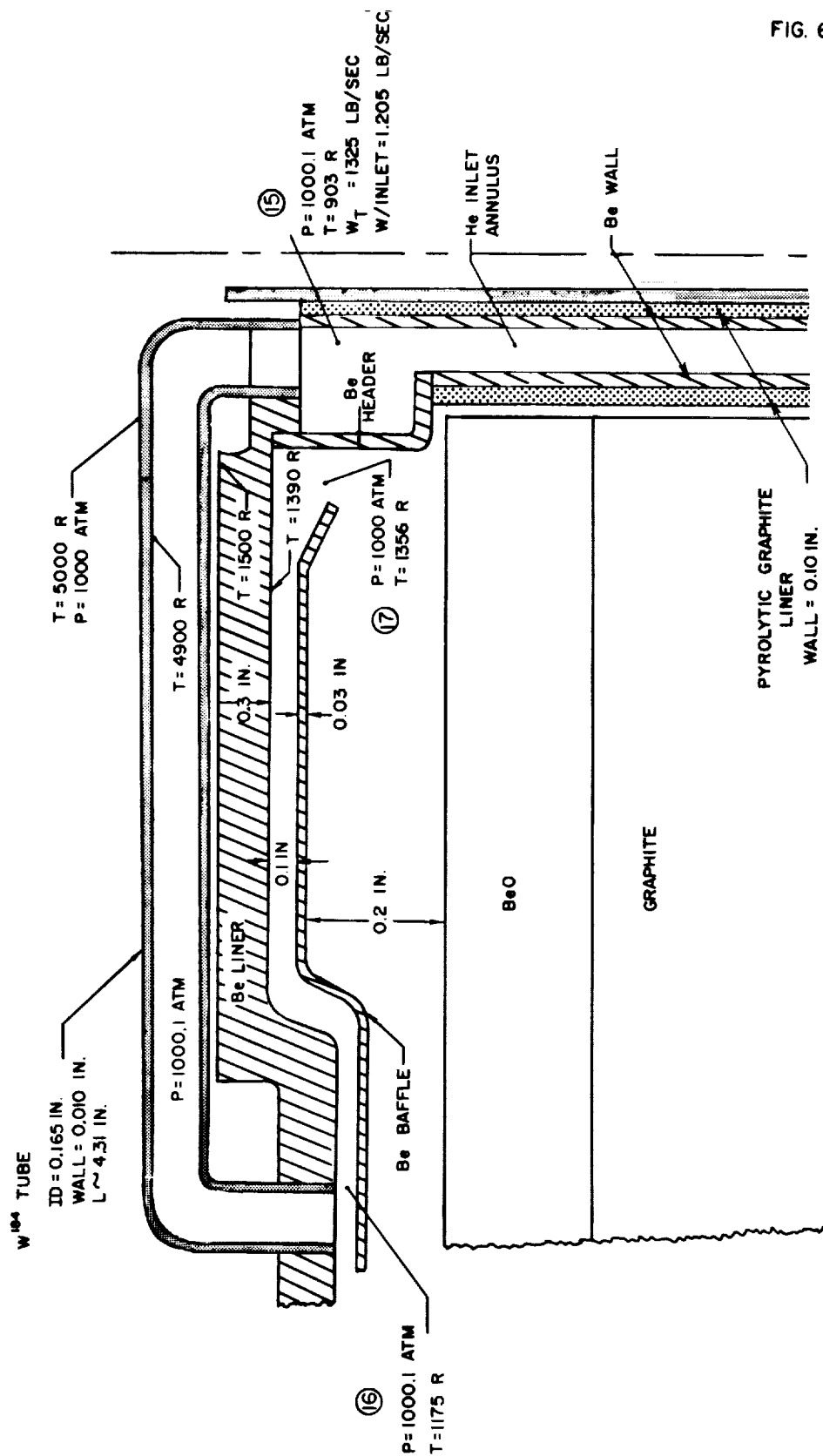
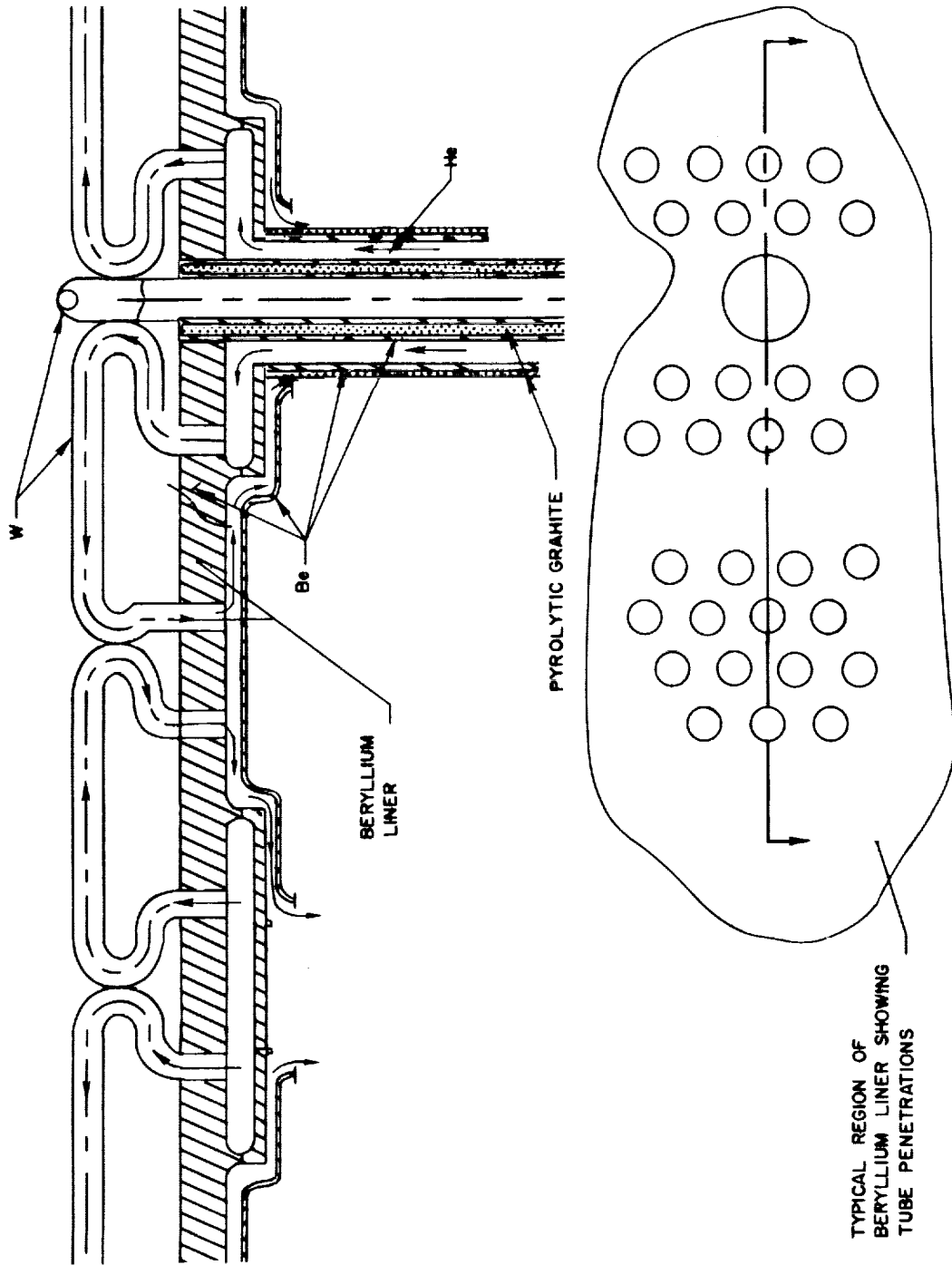


FIG. 6

DETAIL DRAWING OF INNER LINER REGION



TYPICAL REGION OF
BERYLLIUM LINER SHOWING
TUBE PENETRATIONS

FIG. 7

ALTERNATE METHOD OF CONSTRUCTING LINER TUBES

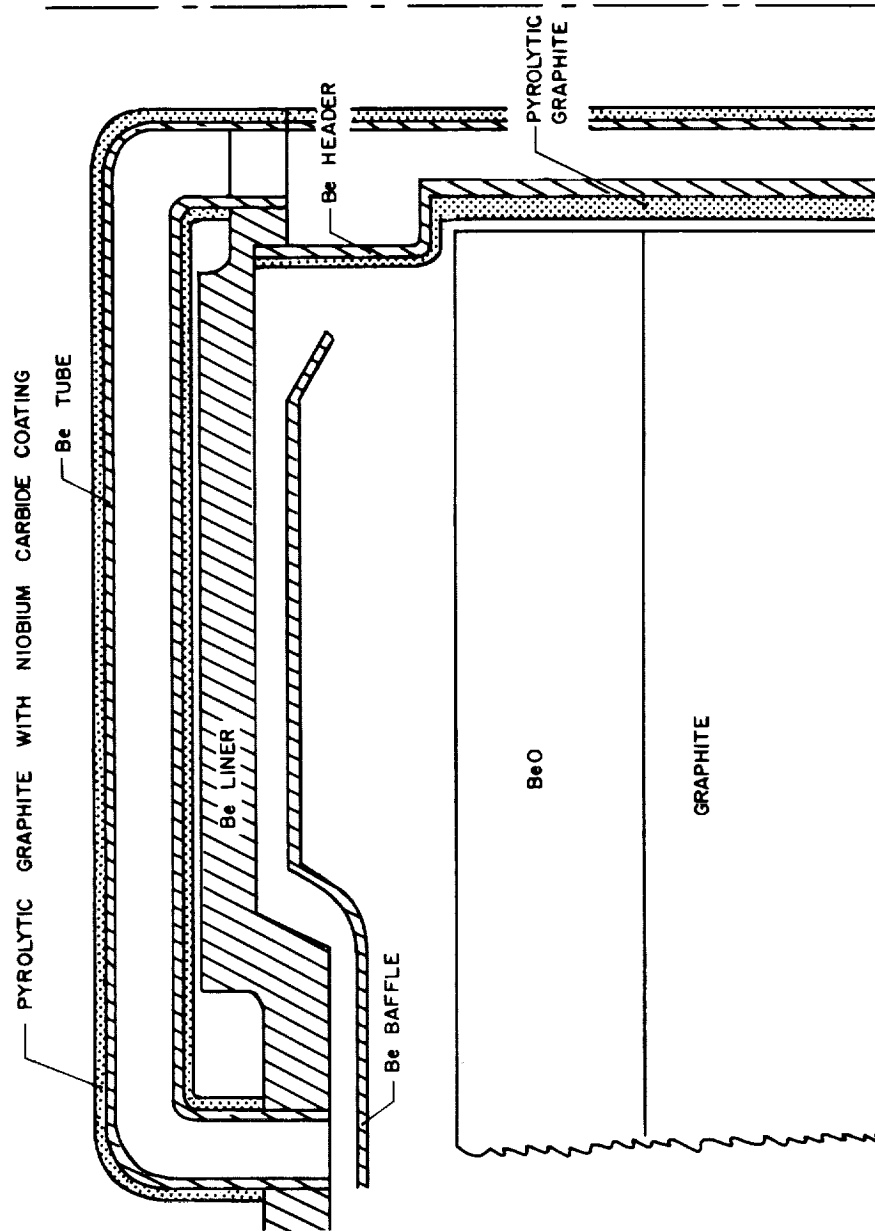
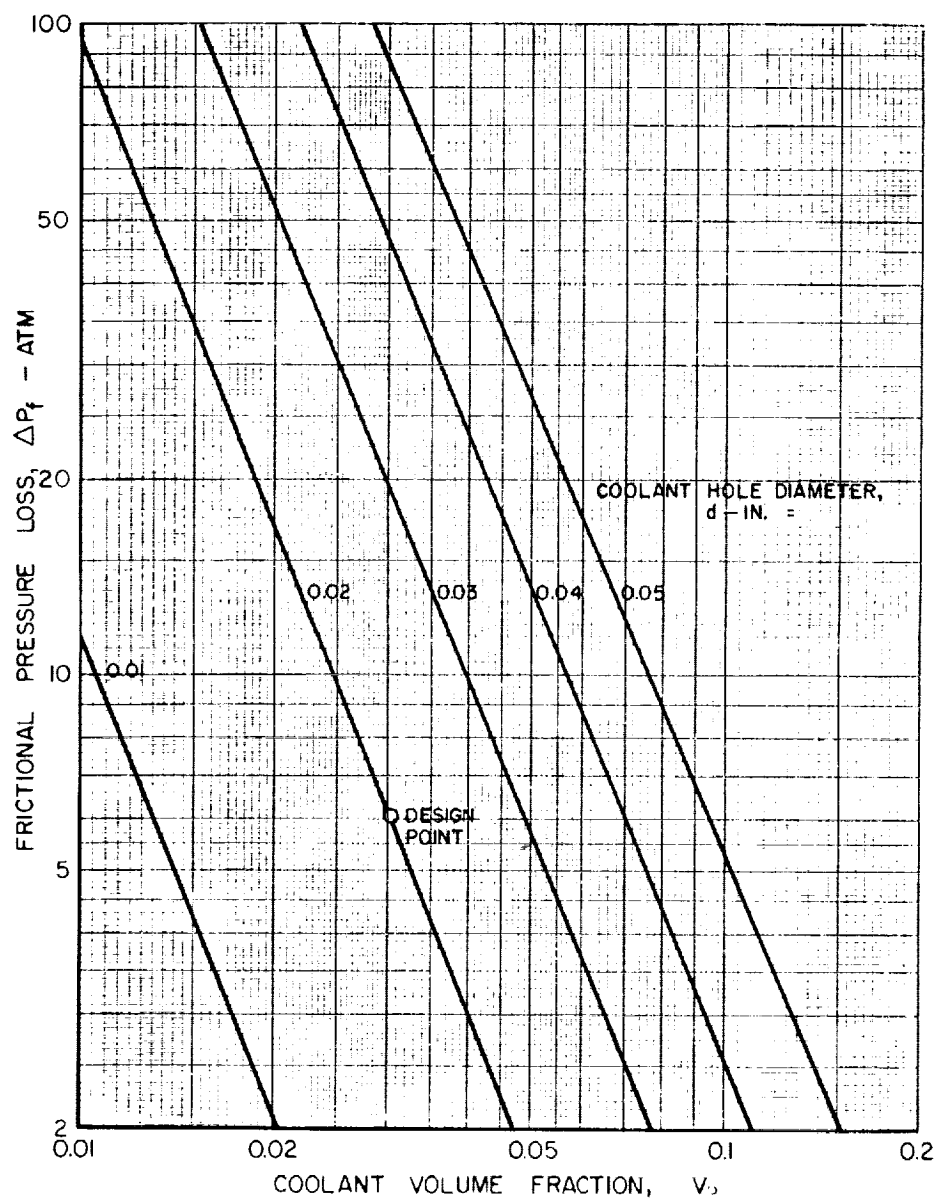


FIG. 8

FIG. 9

VARIATION OF PRESSURE LOSS WITH COOLANT VOLUME FRACTION AND COOLANT HOLE DIAMETER IN BERYLLIUM OXIDE MODERATOR REGION

$$\begin{aligned}\bar{P} &= 997 \text{ ATM} & \bar{T} &= 2100 \text{ R} \\ Q_v &= 4.55 \times 10^4 \text{ BTU/SEC-FT}^3 \\ (T_w - T_c) &= 200 \text{ R} \\ \Delta X &= 3.5 \text{ IN.} \\ \Delta P_f (\text{ATM}) &= 121 \frac{d^3 (\text{IN.})^3}{V_p^2} \end{aligned}$$



VARIATION OF DYNAMIC PRESSURE WITH COOLANT VOLUME FRACTION AND COOLANT HOLE DIAMETER IN BERYLLIUM OXIDE MODERATOR REGION

$$\begin{aligned}\bar{P} &= 997 \text{ ATM} & \bar{T} &= 2100 \text{ R} \\ Q_v &= 4.55 \times 10^4 \text{ BTU/SEC-FT}^3 \\ (T_w - T_c) &= 200 \text{ R} \\ q(\text{ATM}) &= 73 \frac{d^3(\text{IN.})^3}{V_p^{2.5}}\end{aligned}$$

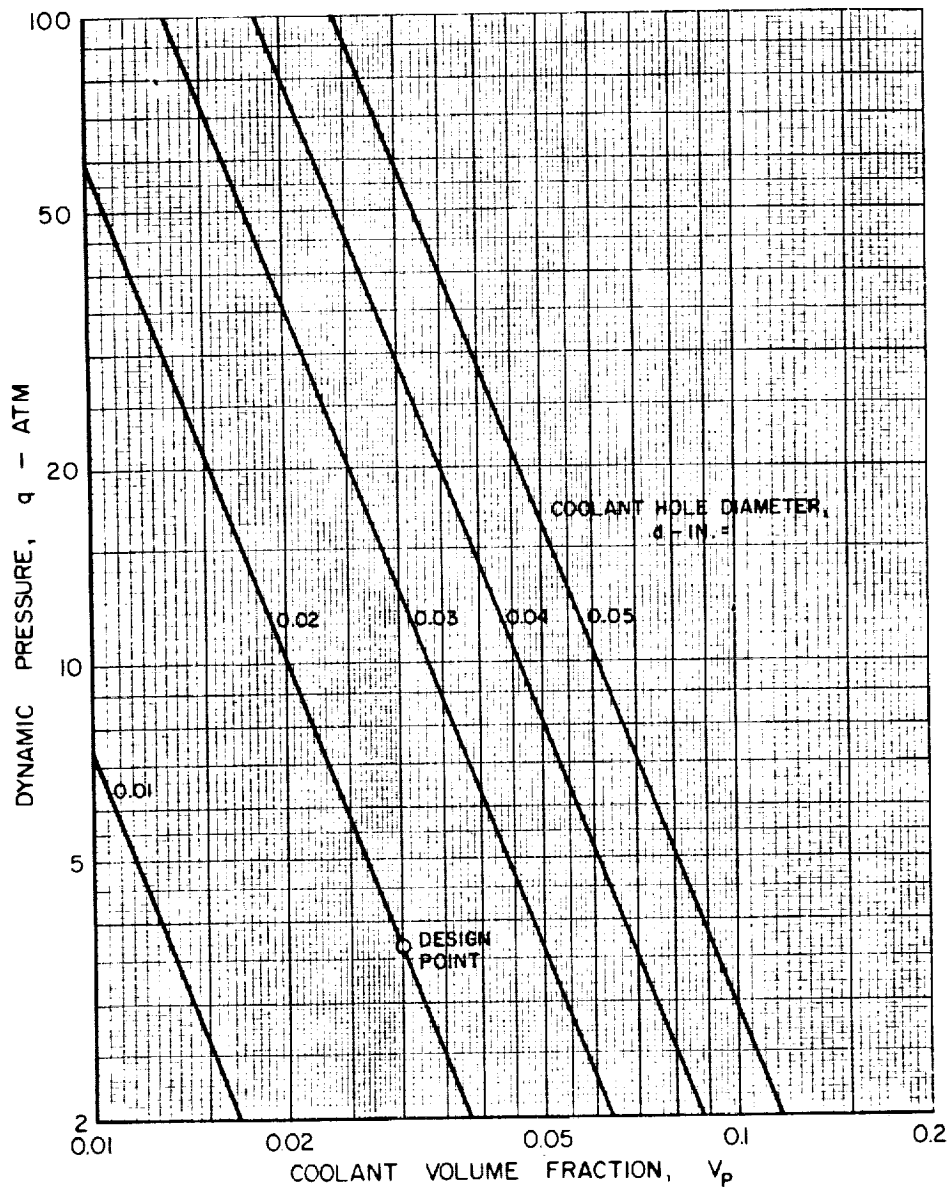


FIG. II

VARIATION OF REYNOLDS NUMBER WITH COOLANT VOLUME FRACTION
AND COOLANT HOLE DIAMETER
IN BERYLLIUM OXIDE MODERATOR REGION

$$\begin{aligned}\bar{P} &= 997 \text{ ATM} & \bar{T} &= 2100 \text{ R} \\ Q_v &= 4.55 \times 10^4 \text{ BTU/SEC-FT}^3 \\ (T_w - T_c) &= 200 \text{ R} \\ Re_d &= 954 \times 10^6 \frac{d^{2.5} (IN)^{2.5}}{V_p^{1.25}}\end{aligned}$$

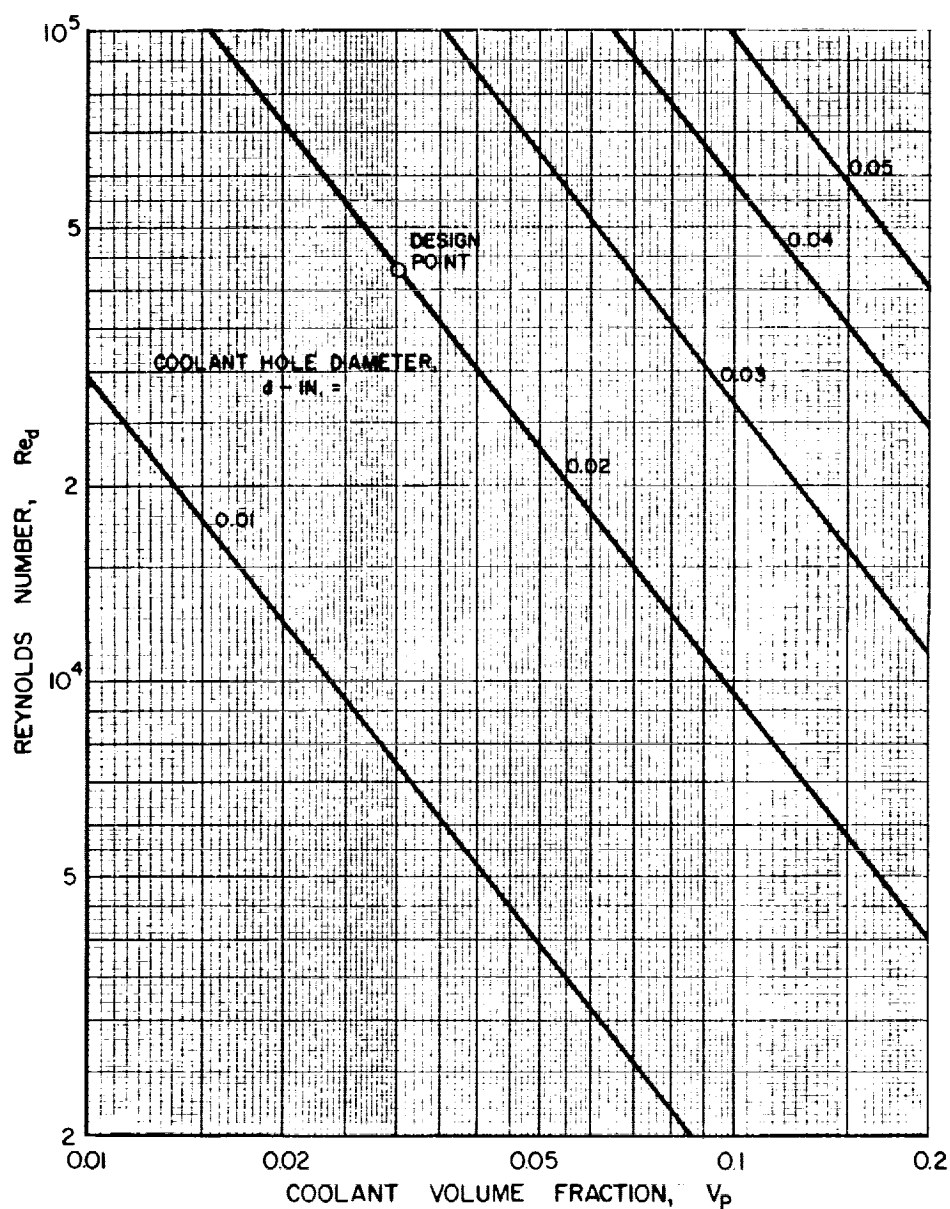


FIG. 12

VARIATION IN REQUIRED SLOPE OF COOLING PASSAGES
WITH COOLANT VOLUME FRACTION AND COOLANT HOLE DIAMETER
IN BERYLLIUM OXIDE MODERATOR REGION

$$\begin{aligned} \bar{P} &= 997 \text{ ATM} & \bar{T} &= 2100 \text{ R} \\ Q_v &= 4.55 \times 10^4 \text{ BTU/SEC-FT}^3 \\ (T_w - T_c) &= 200 \text{ R} \\ \Delta x &= 3.5 \text{ IN.} \\ \frac{\Delta \ell}{\Delta x} &= 650 \frac{d^{1.5} (\text{IN.})^{1.5}}{V_p^{0.25}} \end{aligned}$$

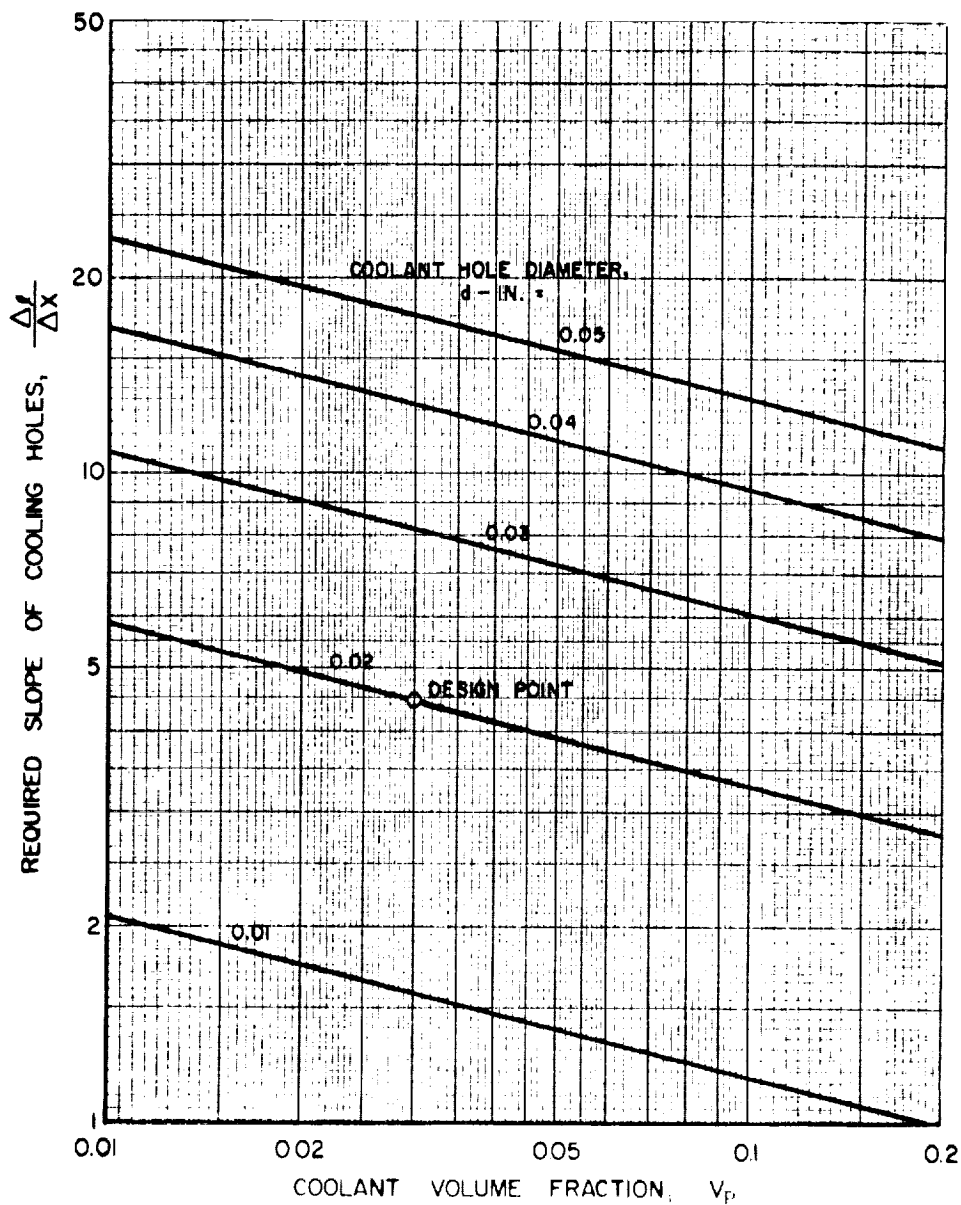


FIG. 13

VARIATION OF PRESSURE LOSS WITH COOLANT VOLUME FRACTION AND COOLANT HOLE DIAMETER IN GRAPHITE MODERATOR REGION

$$\begin{aligned} \bar{P} &= 992.5 \text{ ATM} & \bar{T} &= 3680 \text{ R} \\ Q_v &= 1.575 \times 10^4 \text{ BTU/SEC-FT}^3 \\ (T_w - T_c) &= 200 \text{ R} \\ \Delta X &= 8.7 \text{ IN.} \\ \Delta P \text{ (ATM)} &= 0.85 \frac{d^3 (\text{IN.})^3}{V_p^{2.5}} \end{aligned}$$

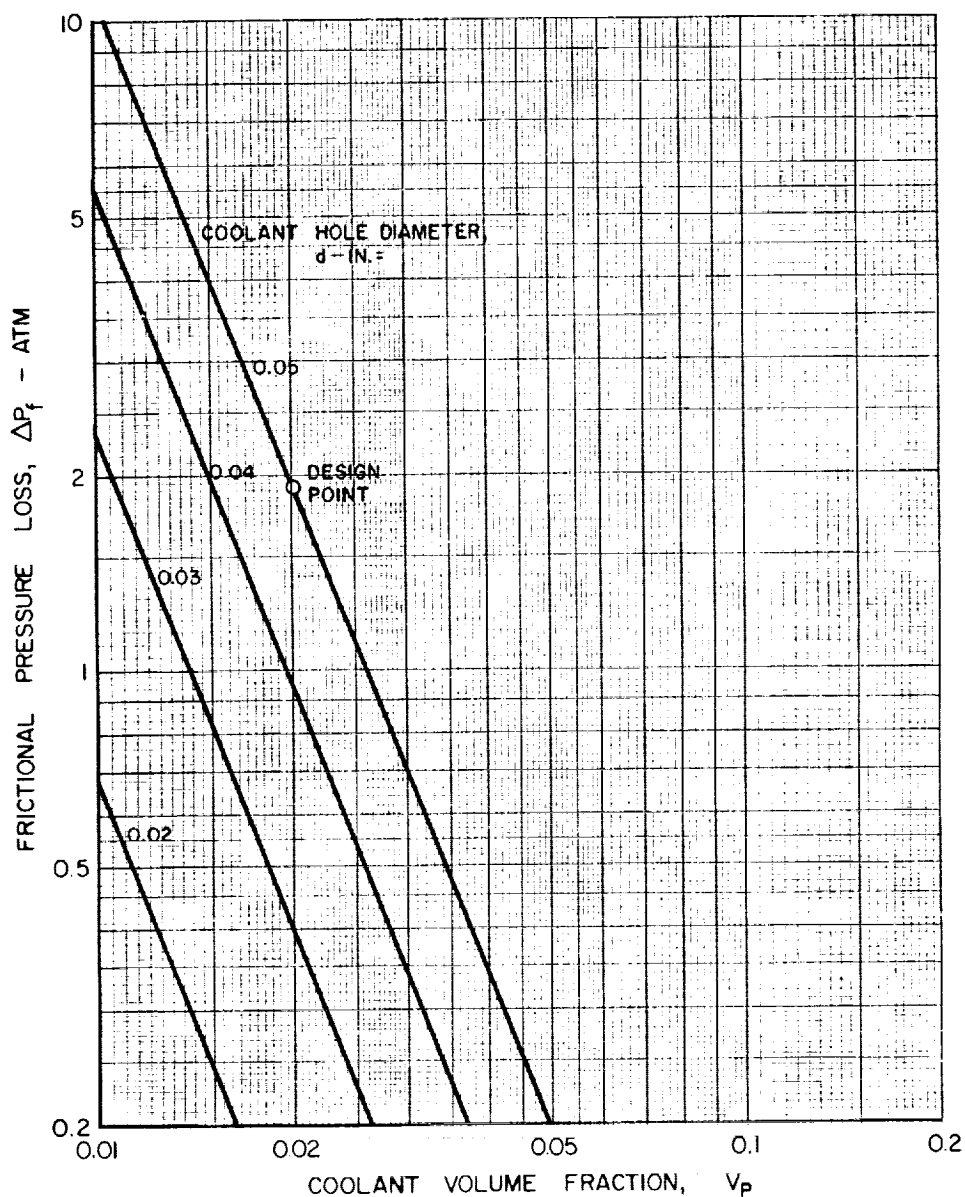
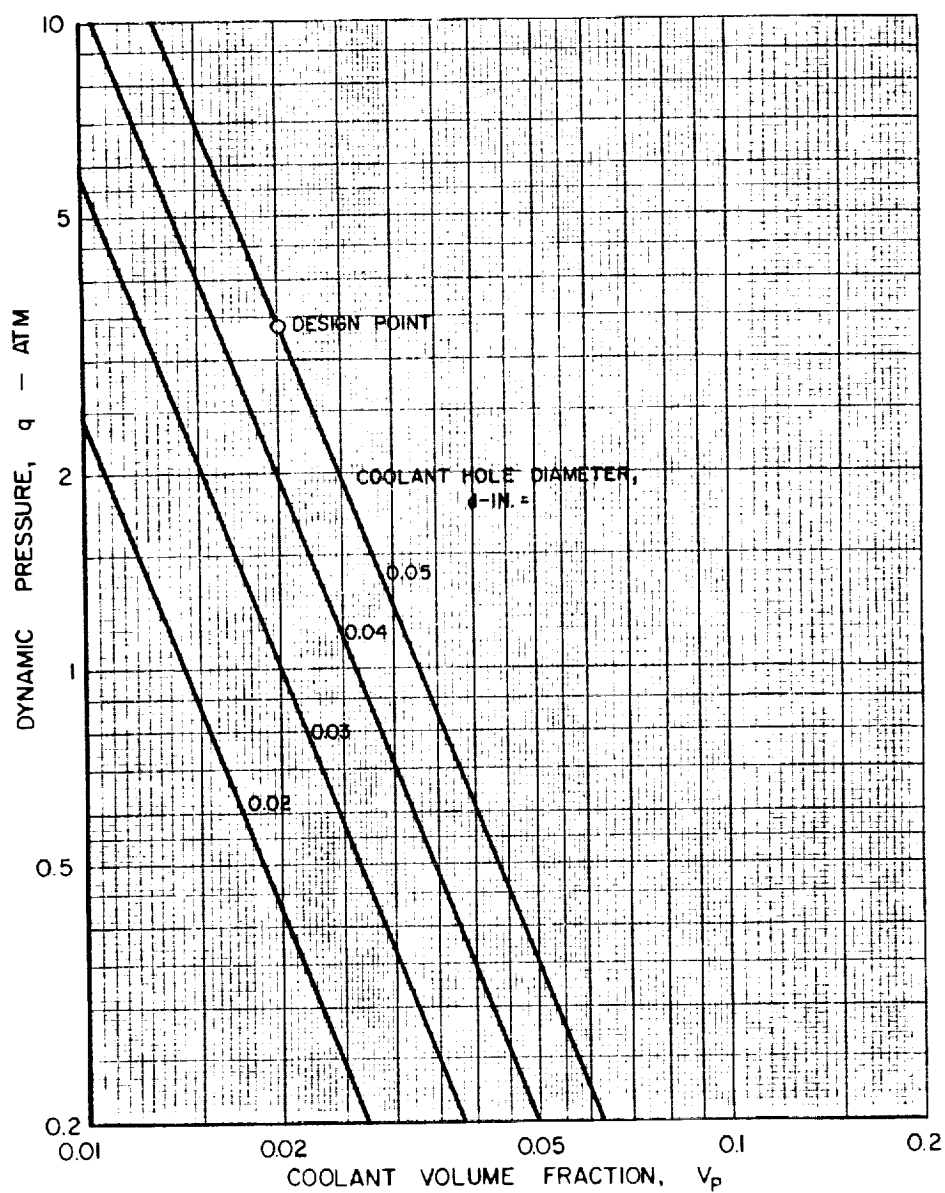


FIG. 14

VARIATION OF DYNAMIC PRESSURE WITH COOLANT VOLUME FRACTION AND COOLANT HOLE DIAMETER IN GRAPHITE MODERATOR REGION

$$\begin{aligned} \bar{P} &= 992.5 \text{ ATM} & \bar{T} &= 3680 \text{ R} \\ Q_v &= 1.575 \times 10^4 \text{ BTU/SEC-FT}^3 \\ (T_w - T_c) &= 200 \text{ R} \\ q(\text{ATM}) &= 0.9 \frac{d^3(\text{IN.})^3}{V_p^{2.5}} \end{aligned}$$

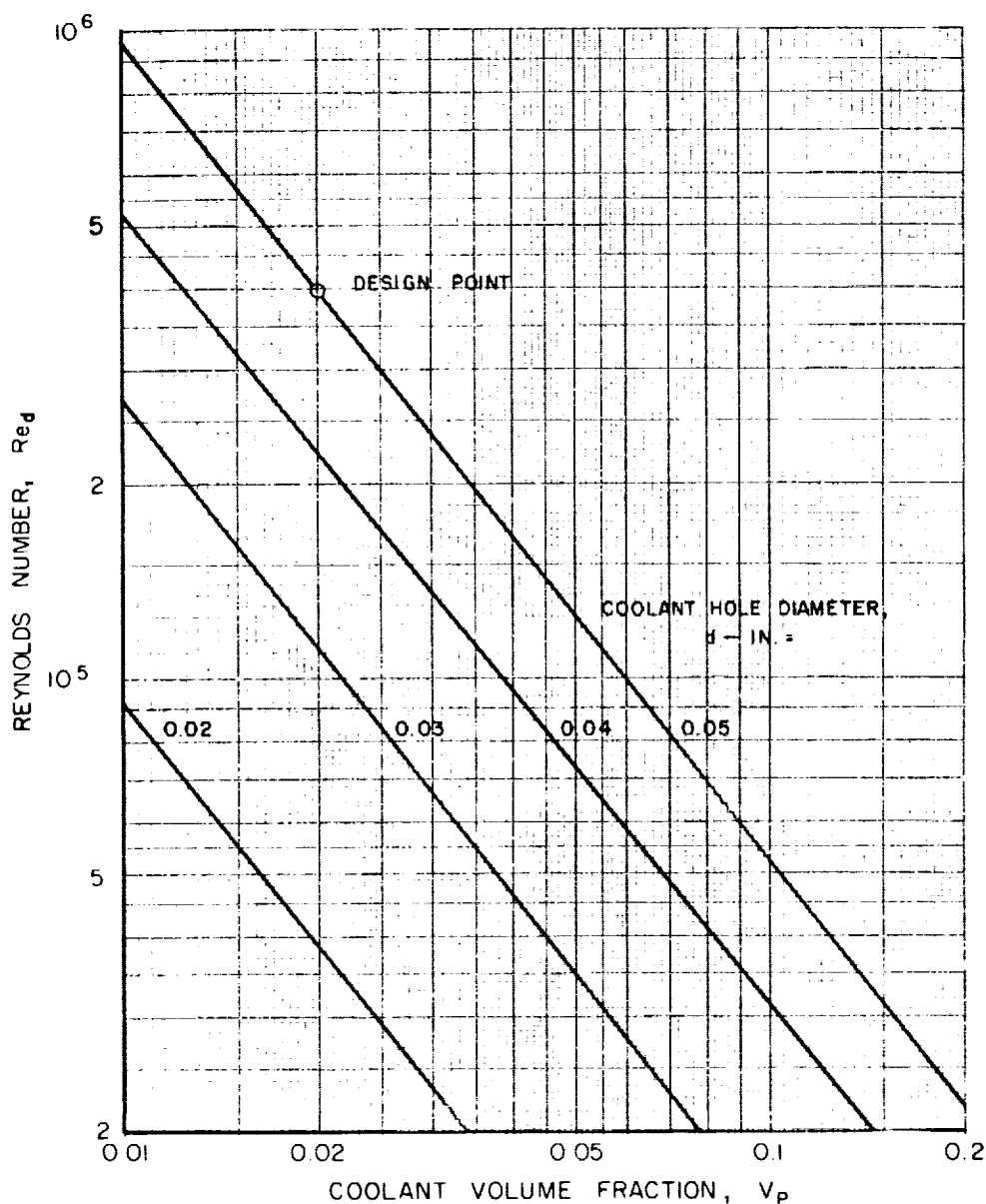


CONFIDENTIAL

FIG. 15

VARIATION OF REYNOLDS NUMBER WITH COOLANT VOLUME FRACTION AND COOLANT HOLE DIAMETER IN GRAPHITE MODERATOR REGION

$$\begin{aligned} \bar{P} &= 992.5 \text{ ATM} & \bar{T} &= 3680 \text{ R} \\ Q_v &= 1.575 \times 10^4 \text{ BTU/SEC-FT}^3 \\ (T_w - T_c) &= 200 \text{ R} \\ Re_d &= 5.12 \times 10^6 \frac{d^{2.5} (\text{IN})^{2.5}}{V_p^{1.25}} \end{aligned}$$

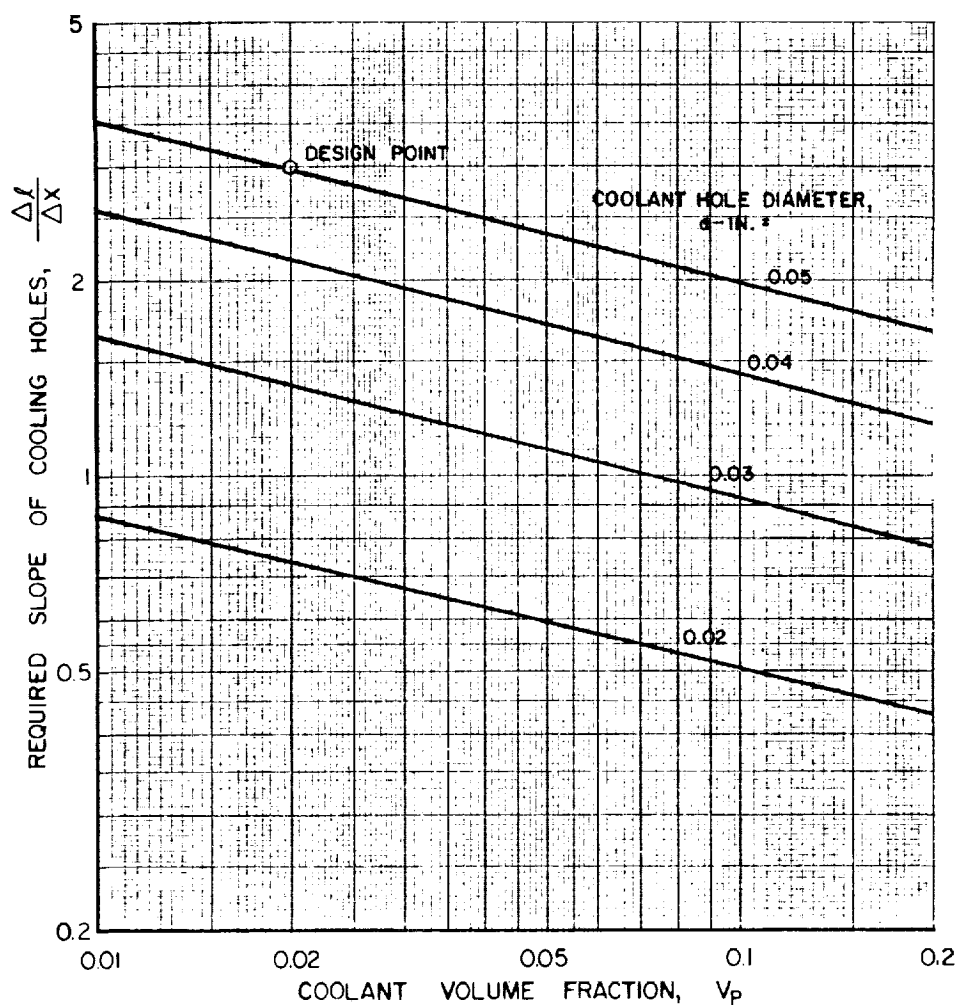


CONFIDENTIAL

FIG. 16

VARIATION IN REQUIRED SLOPE OF COOLING PASSAGES
WITH COOLANT VOLUME FRACTION AND COOLANT HOLE DIAMETER
IN GRAPHITE MODERATOR REGION

$$\begin{aligned}\bar{P} &= 992.5 \text{ ATM} & \bar{T} &= 3680 \text{ R} \\ Q_v &= 1.575 \times 10^4 \text{ BTU/SEC-FT}^3 \\ (T_w - T_c) &= 200 \text{ R} \\ \Delta X &= 8.7 \text{ IN.} \\ \frac{\Delta f}{\Delta X} &= 99.1 \frac{d^{1.5} (\text{IN})^{1.5}}{V_p^{0.25}}\end{aligned}$$



TYPICAL HEXAGONAL MODERATOR BLOCK WITH SPIRAL COOLING HOLES

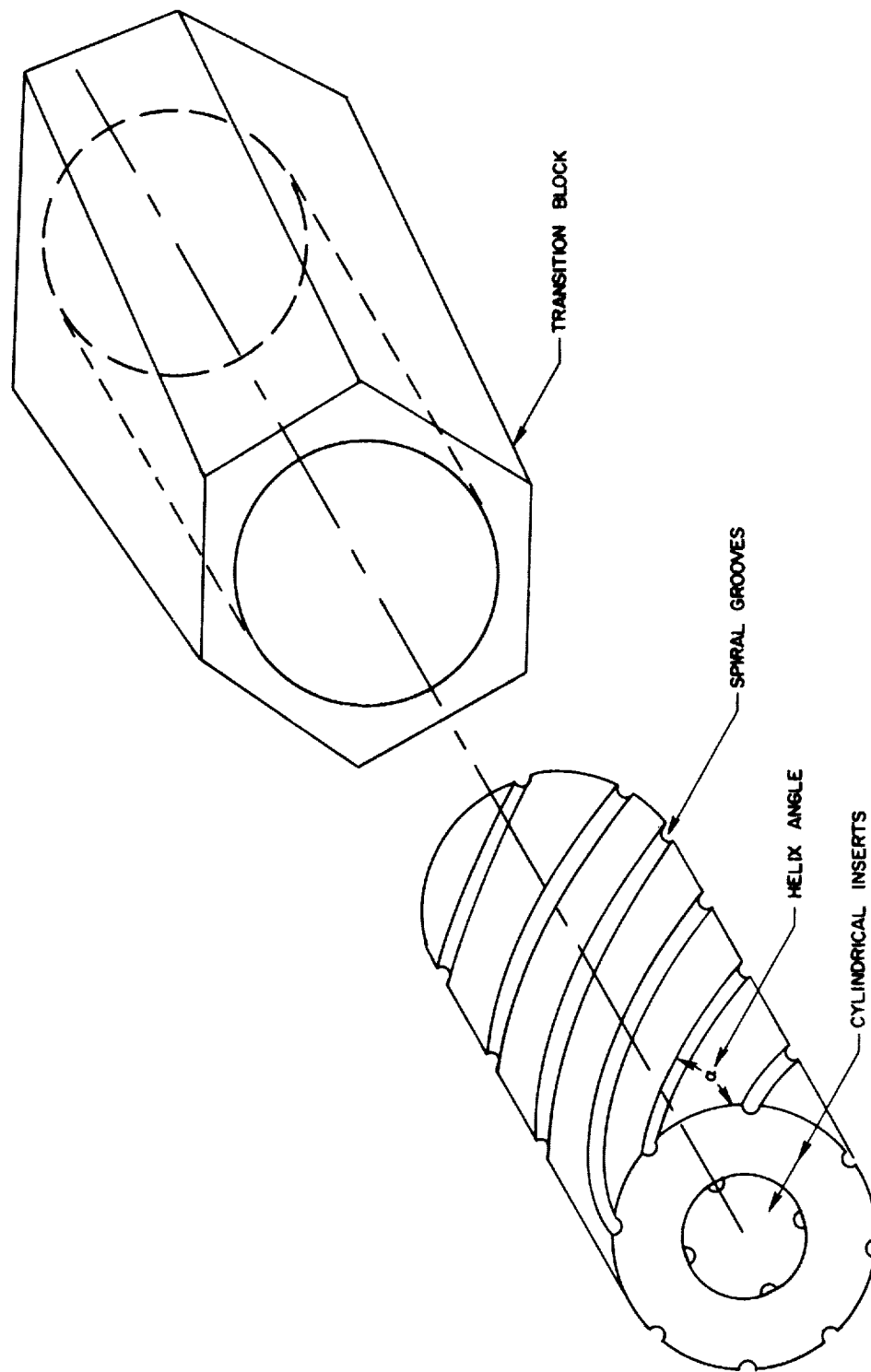


FIG. 17

FIG. 18

GENERALIZED CONVERSION FROM COOLING HOLES ON SQUARE PITCH TO CYLINDRICAL PATTERN

NOTE: GRID INTERSECTIONS REPRESENT CENTERLINES OF COOLING HOLES ON SQUARE PITCH

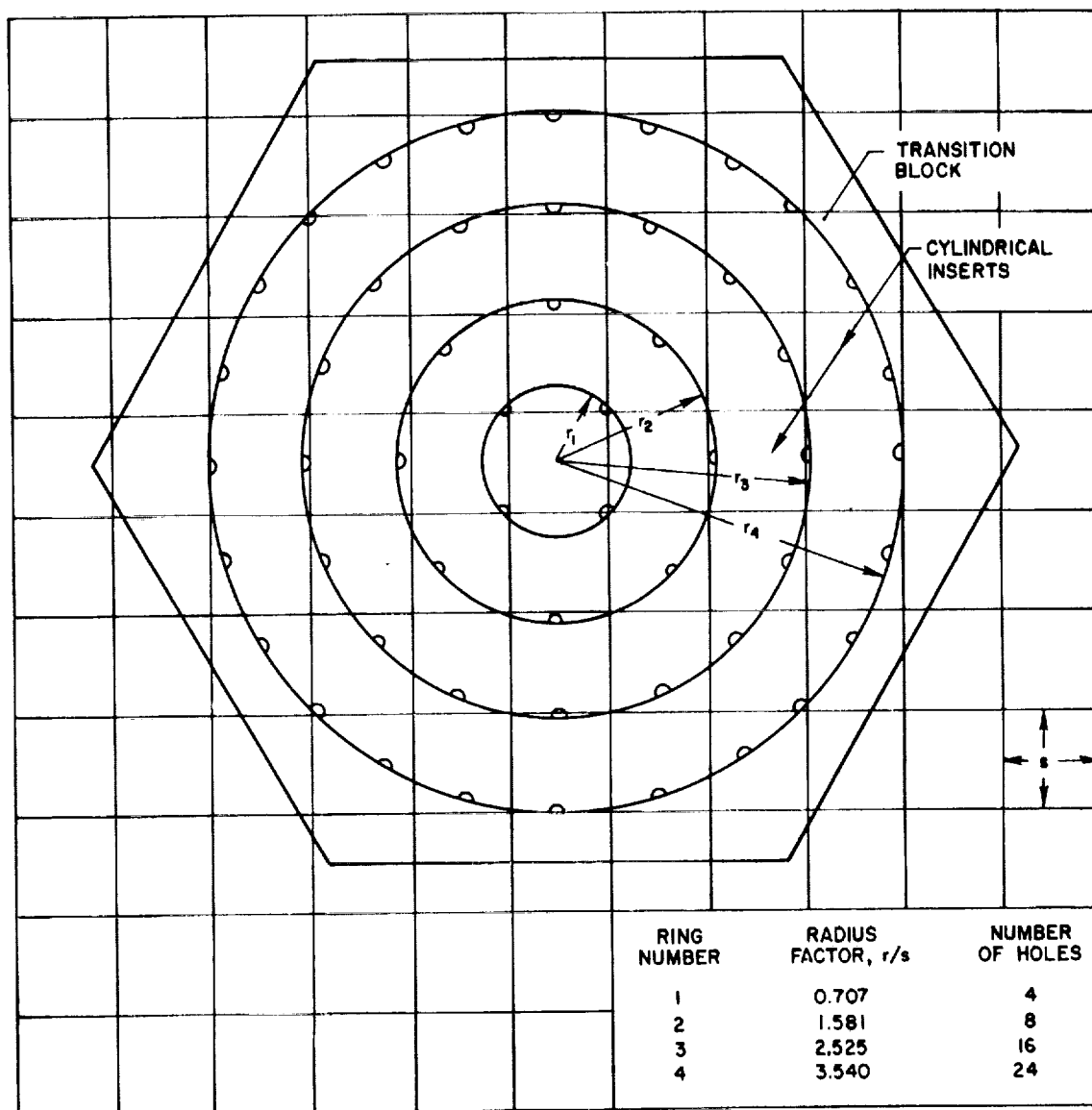
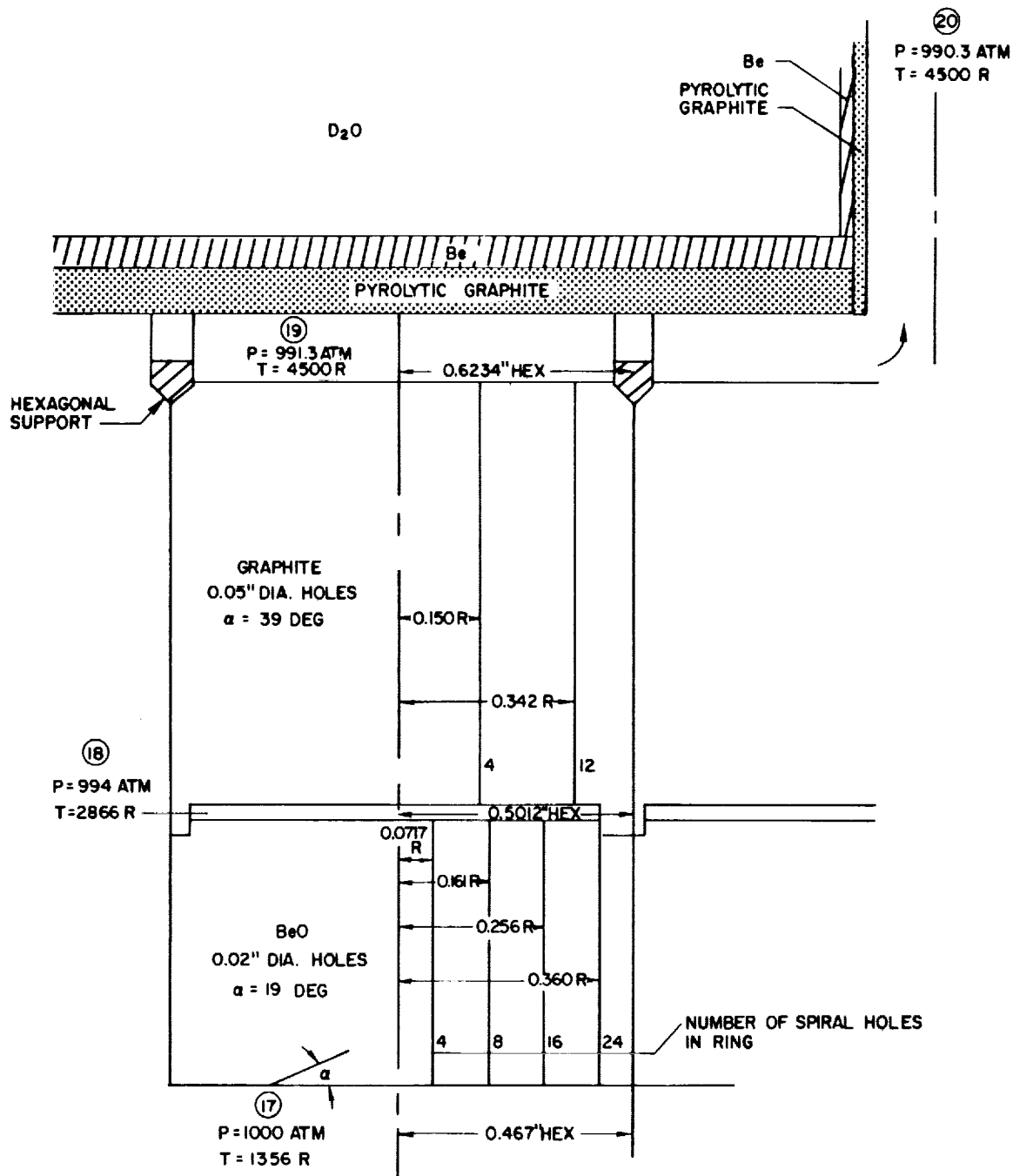


FIG 19

TEMPERATURE AND PRESSURE LEVELS IN BERYLLIUM OXIDE AND GRAPHITE MODERATOR

NOT TO SCALE

NOTE: SEE FIGURE 20 FOR OBLIQUE SKETCH OF MODERATOR ASSEMBLY



SKETCH OF SOLID MODERATOR BLOCKS AND SUPPORT GRID

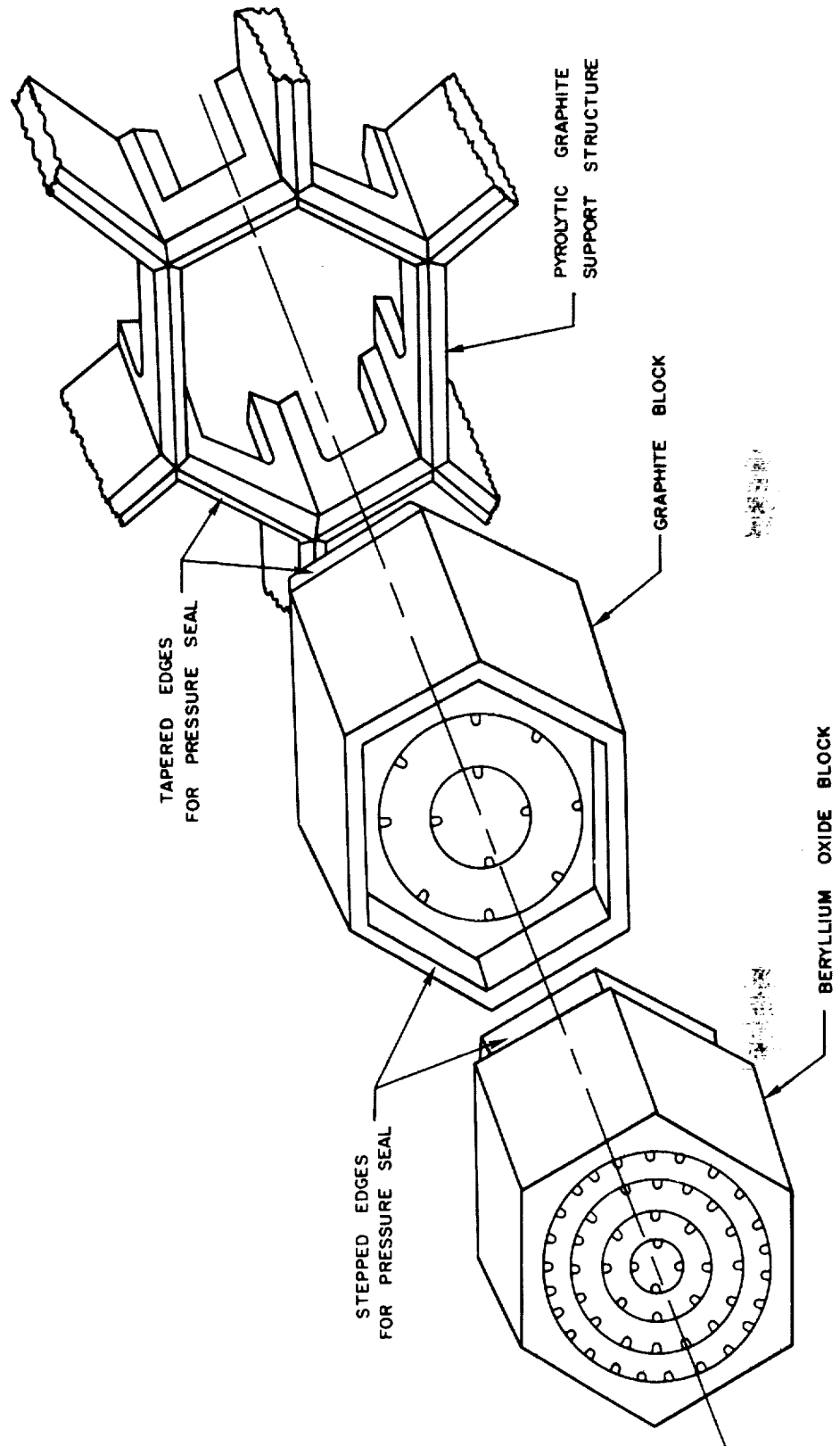


FIG. 20

FIG. 21

VAPOR PRESSURE OF GRAPHITE

DATA FROM REF. 56

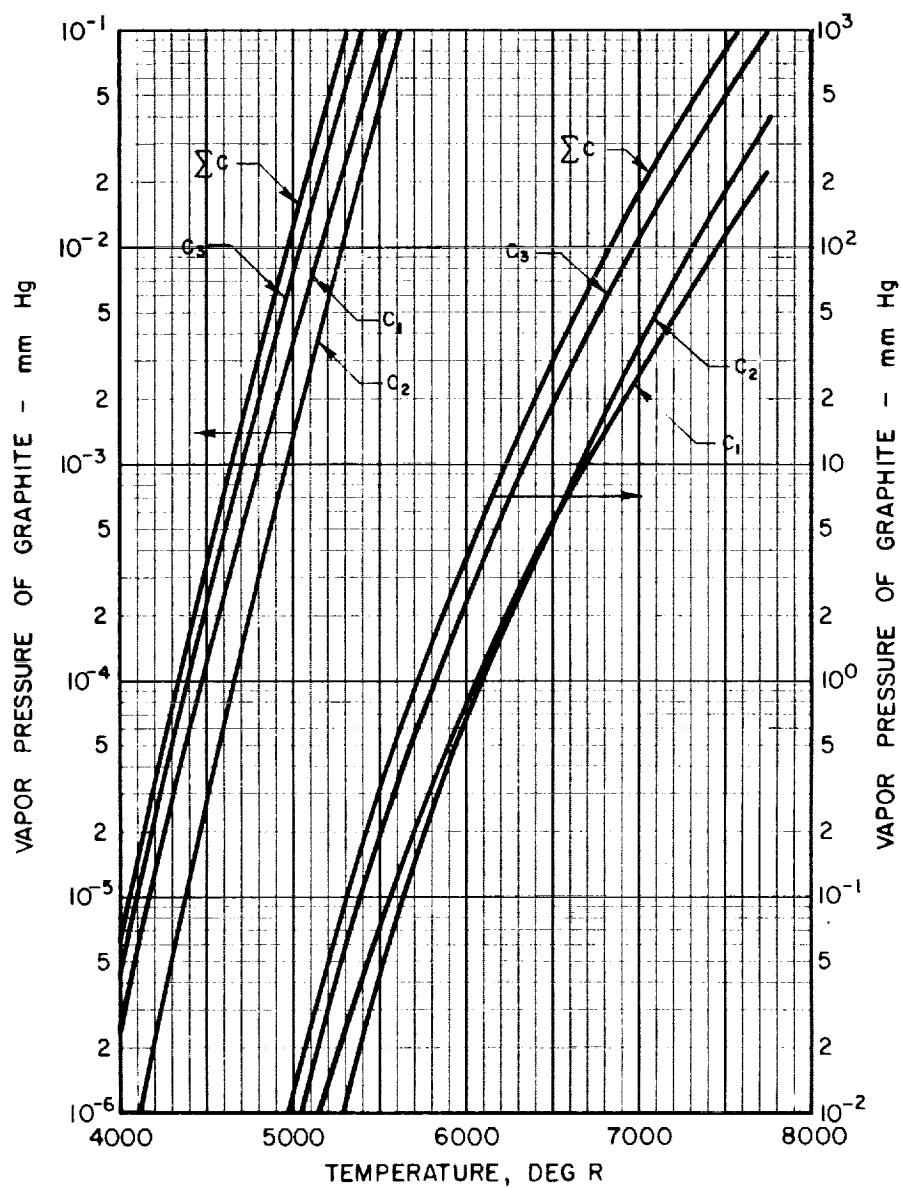
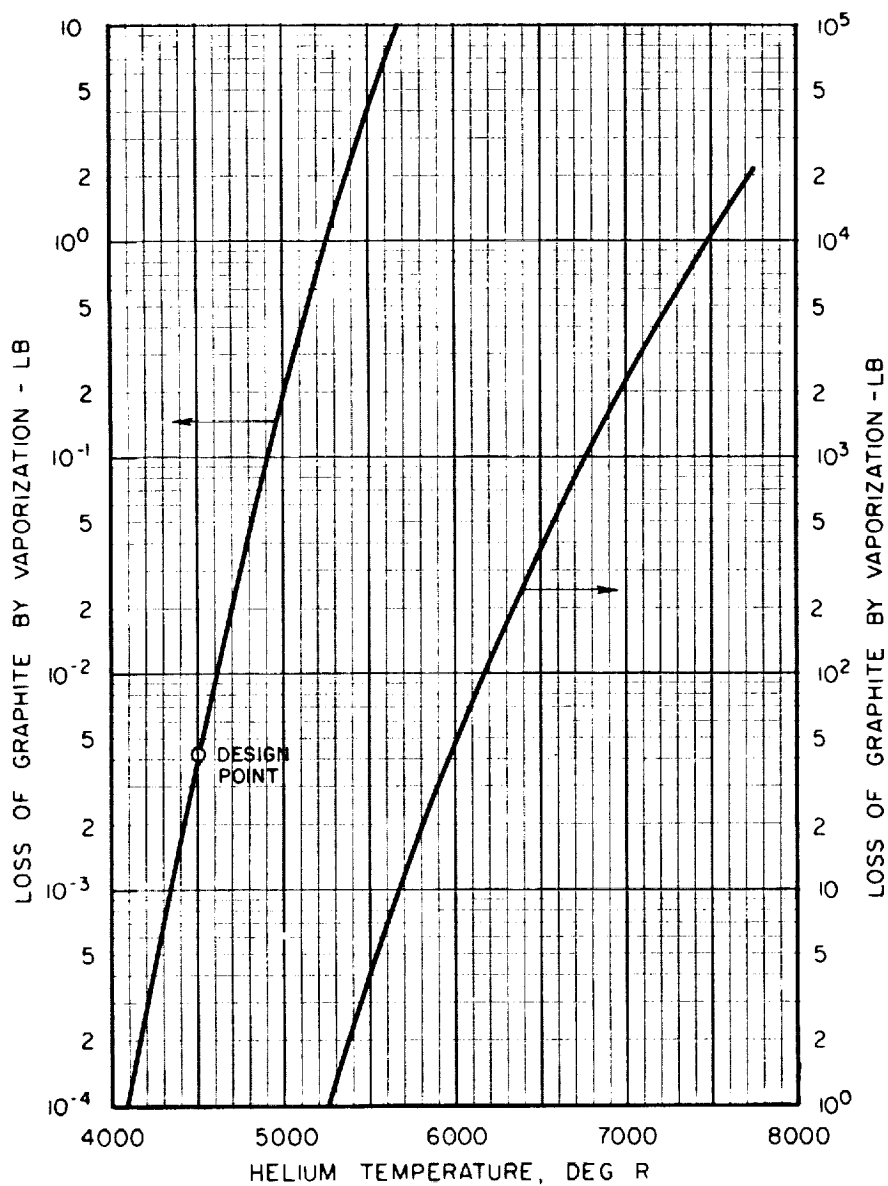


FIG. 22

LOSS OF GRAPHITE DUE TO VAPORIZATION

ENGINE OPERATING TIME = 10^3 SEC
 HELIUM FLOW = 1325 LB / SEC
 HELIUM PRESSURE = 1000 ATM = 7.6×10^5 mmHg
 GRAPHITE VAPOR PRESSURE FROM FIG. 21



DETAIL OF HEAVY WATER MODERATOR REGION

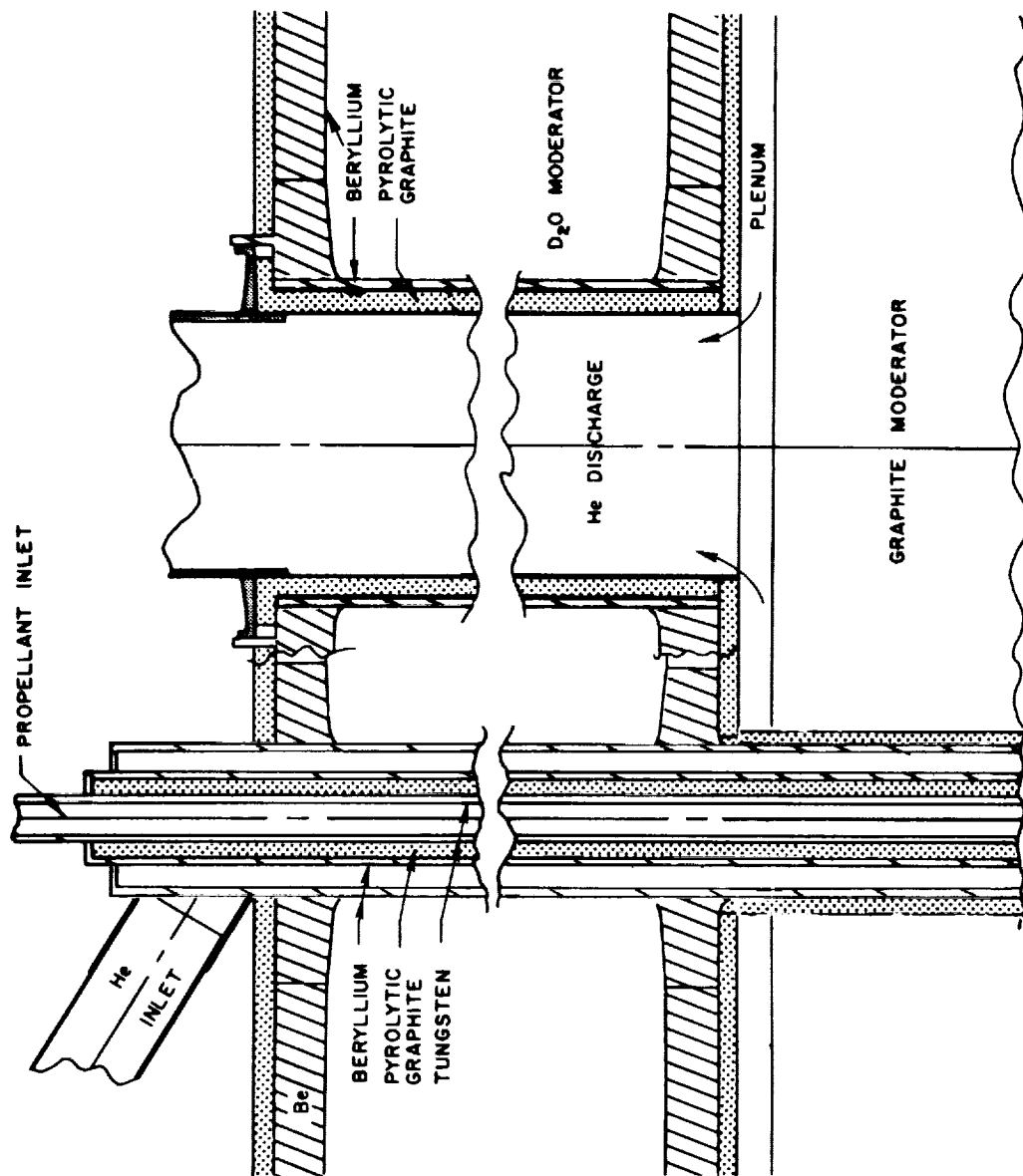


FIG. 23

FIG. 24

TYPICAL SECTION THROUGH PIPING REGION

NOTE: DETAILED PIPING AND INSULATION DIMENSIONS SHOWN IN TABLE IX

SCALE = $\frac{1}{2}$ SIZE

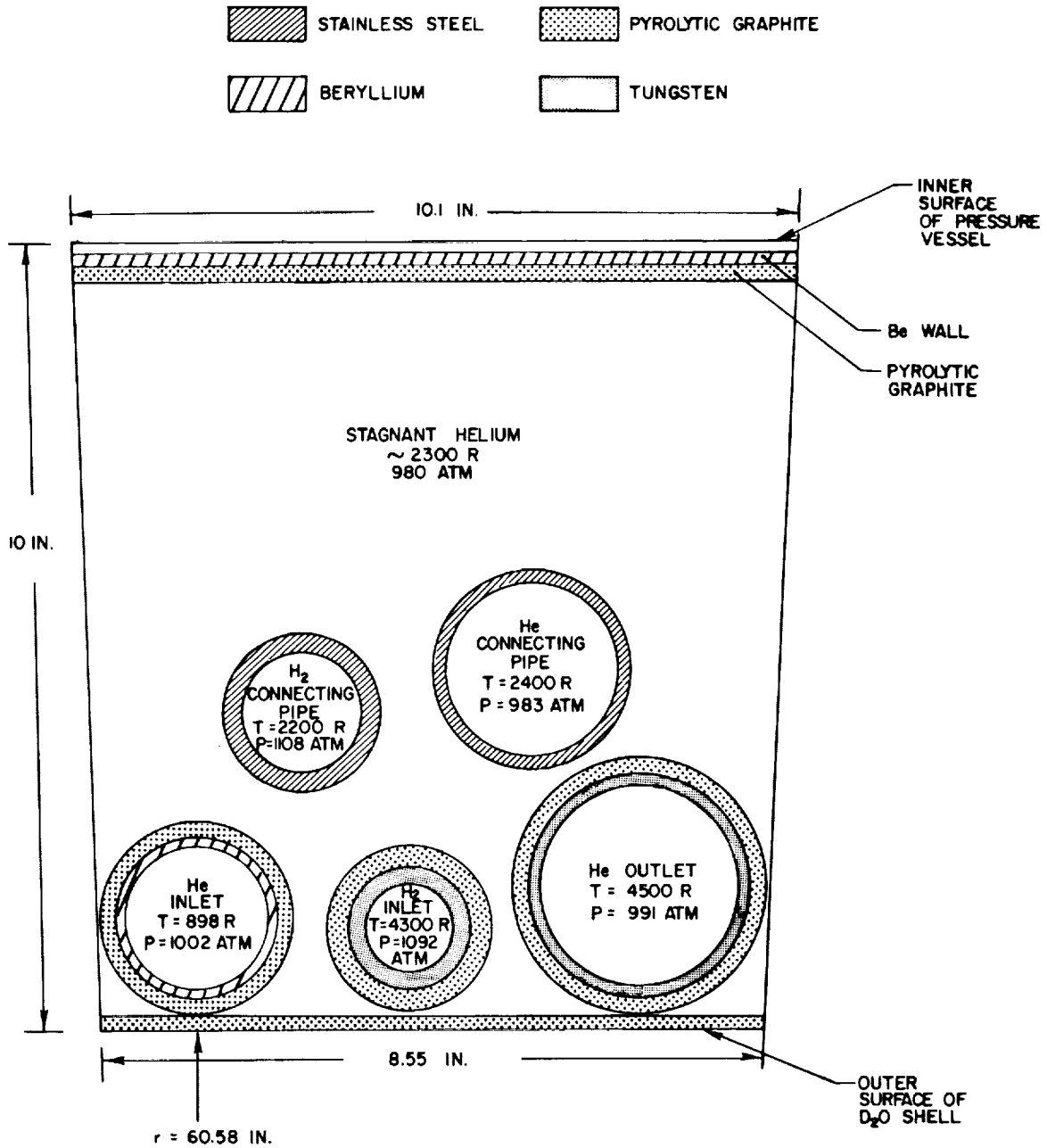


FIG. 25

PRESSURE VESSEL TEMPERATURE DISTRIBUTION FOR CYLINDRICAL VESSEL

MATERIAL: MARAGING STEEL

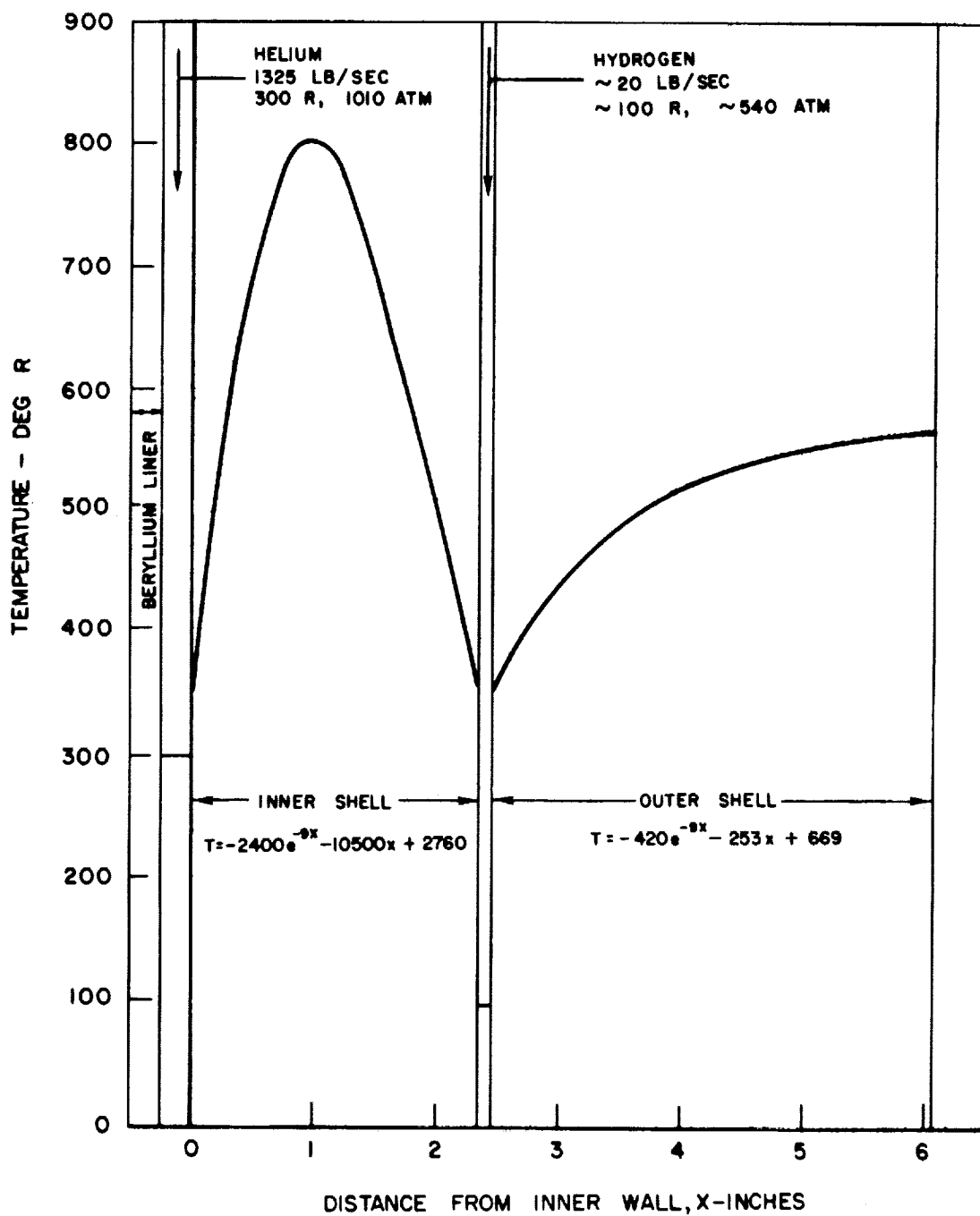
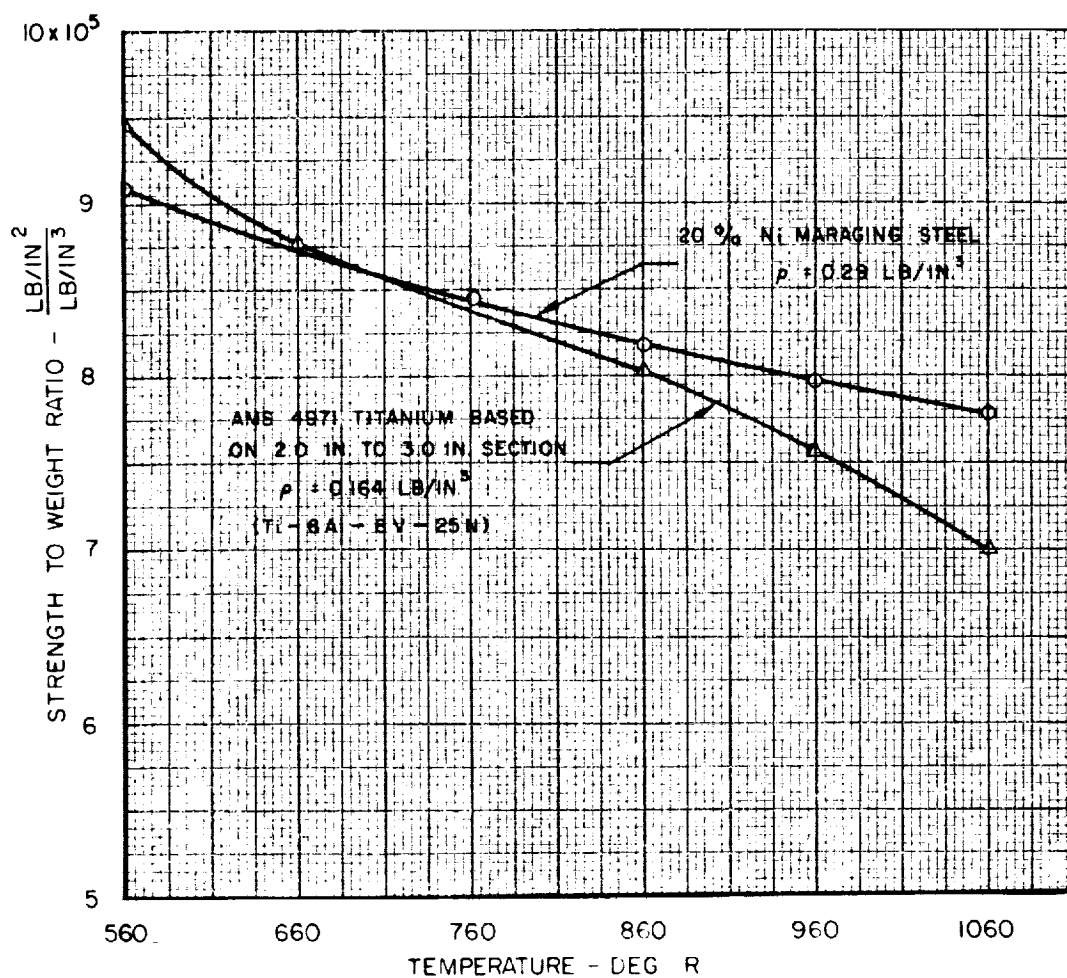


FIG. 26

STRENGTH TO WEIGHT RATIO OF MARAGING STEEL AND TITANIUM ALLOY

NOTE : MATERIAL IN FULLY HEAT TREATED CONDITION

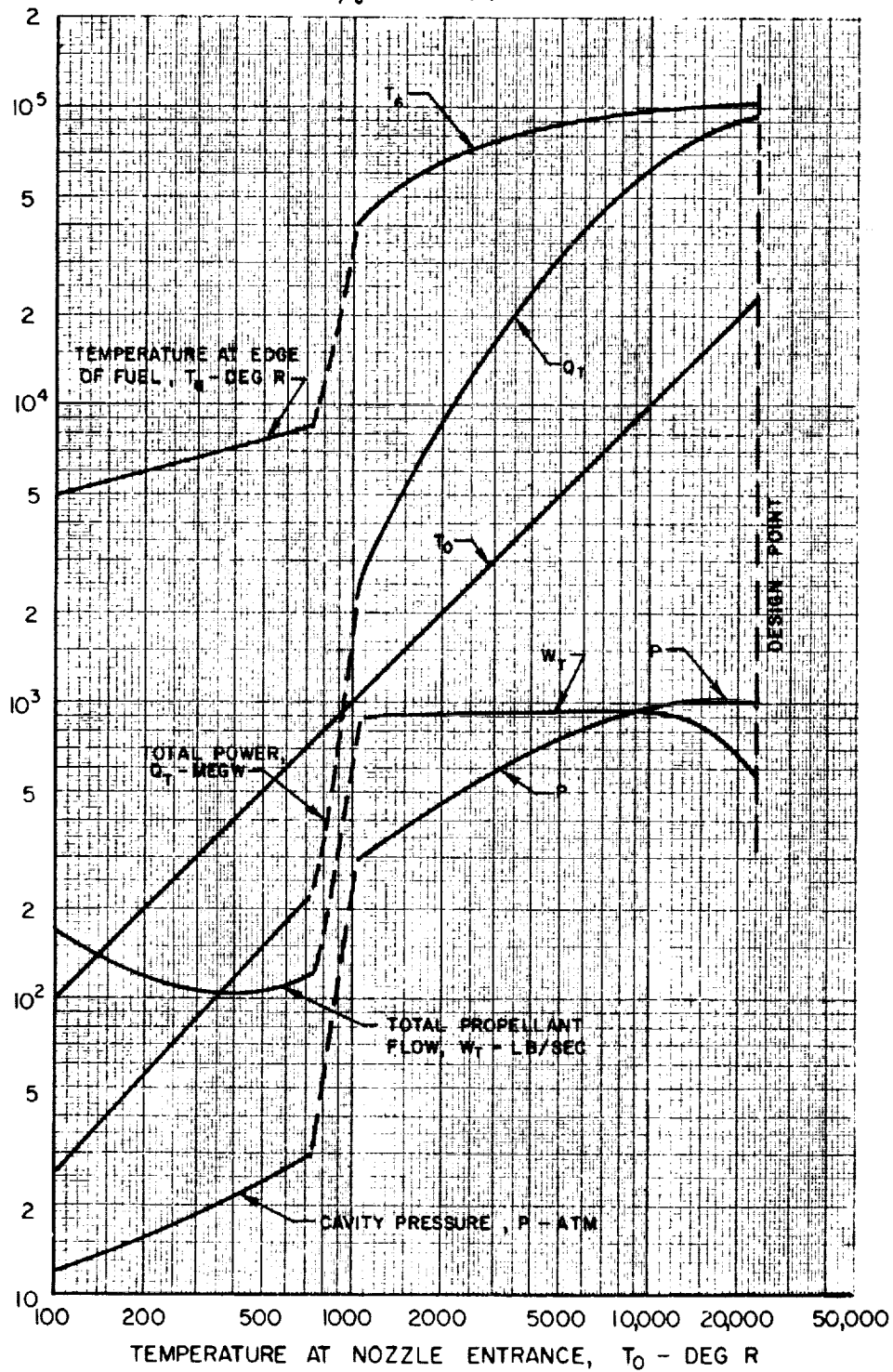


EFFECT OF NOZZLE-ENTRANCE TEMPERATURE ON CHARACTERISTICS OF FIXED-GEOMETRY GASEOUS NUCLEAR ROCKET ENGINE DURING ENGINE START-UP

FIG. 27

SEE APPENDIX A

$$\rho_0 = 0.0214 \text{ LB/FT}^3$$

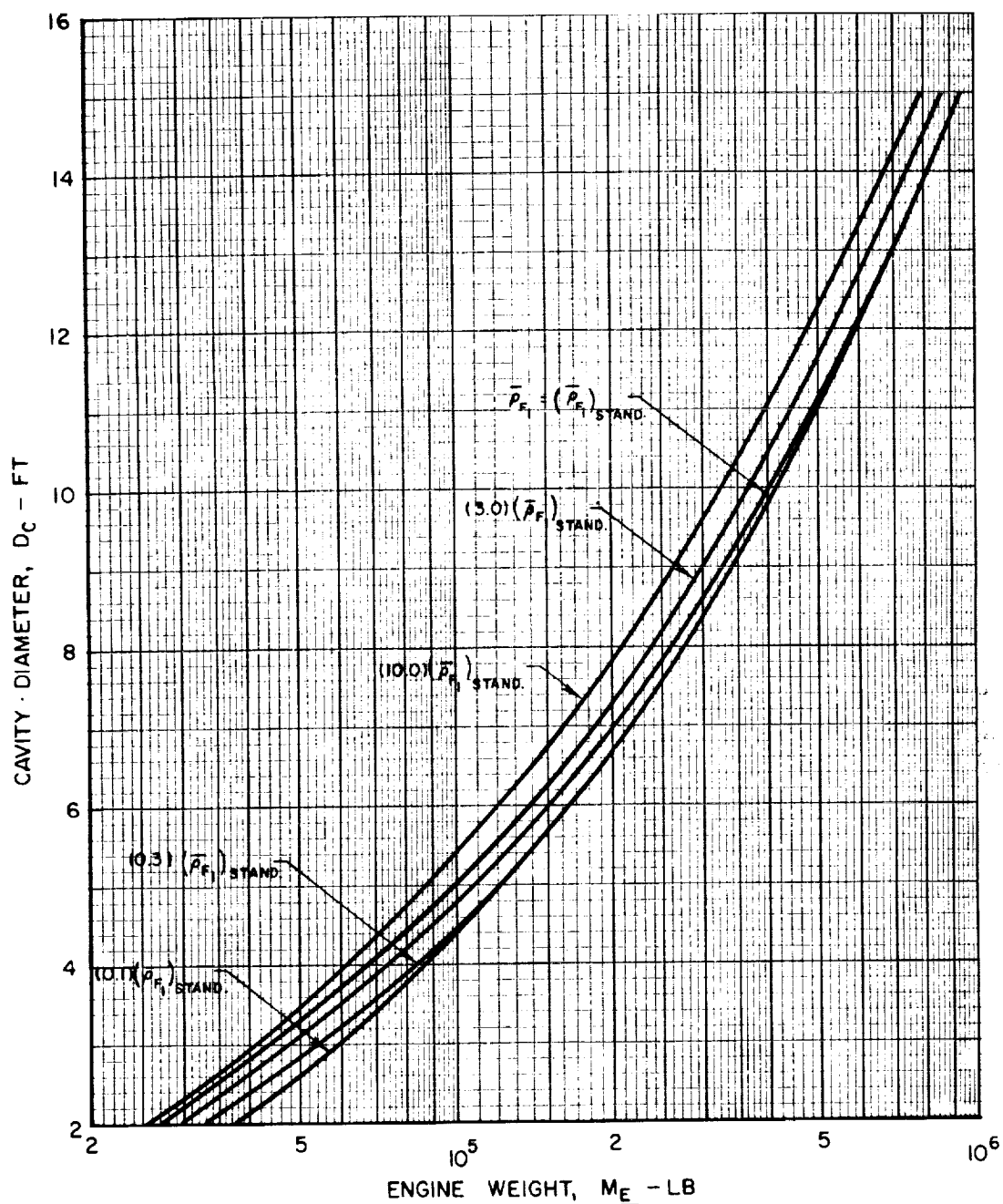


EFFECT OF ENGINE WEIGHT ON CAVITY DIAMETER FOR FIXED CRITERIA FOR CRITICAL FUEL DENSITY

SEE APPENDIX B

CURVES CALCULATED USING STANDARD VALUES OF PARAMETERS
EMPLOYED IN REF.36(SEE TEXT)

$(\bar{\rho}_F)_{\text{STAND.}}$ GIVEN IN FIG. 10 OF REF. 36

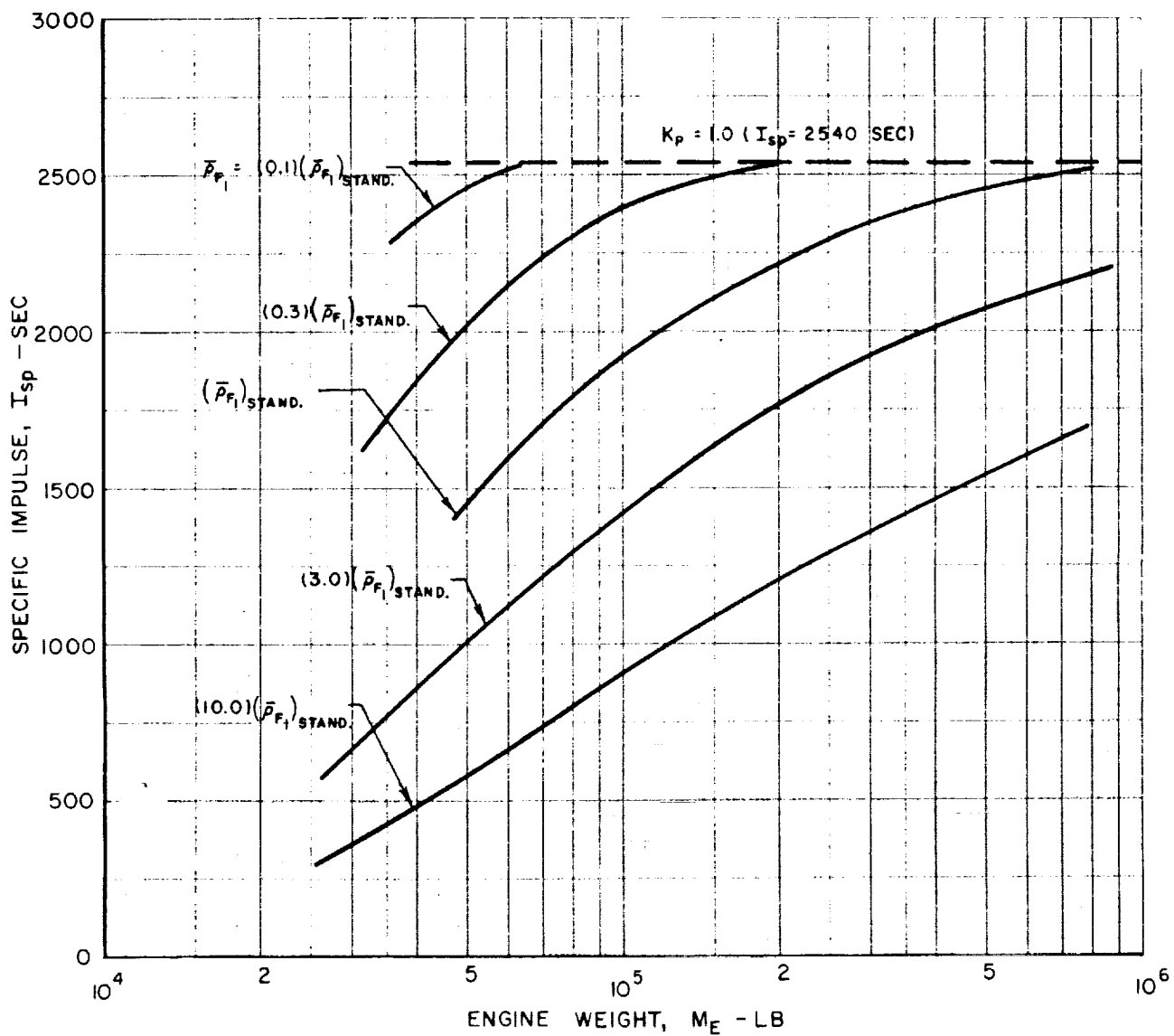


EFFECT OF ENGINE WEIGHT ON SPECIFIC IMPULSE FOR FIXED CRITERIA FOR CRITICAL FUEL DENSITY

SEE APPENDIX B

CURVES CALCULATED USING STANDARD VALUES OF PARAMETERS
EMPLOYED IN REF. 36 (SEE TEXT)

$(\bar{\rho}_{F_1})_{\text{STAND.}}$ GIVEN IN FIG. 10 OF REF. 36



EFFECT OF ENGINE WEIGHT ON RATIO OF CAVITY PROPELLANT DENSITY TO HYDROGEN DENSITY FOR FIXED CRITERIA FOR CRITICAL FUEL DENSITY

SEE APPENDIX B

CURVES CALCULATED USING STANDARD VALUES OF PARAMETERS
EMPLOYED IN REF.36(SEE TEXT)

$(\bar{\rho}_F)_\text{STAND.}$ GIVEN IN FIG. 10 OF REF. 36

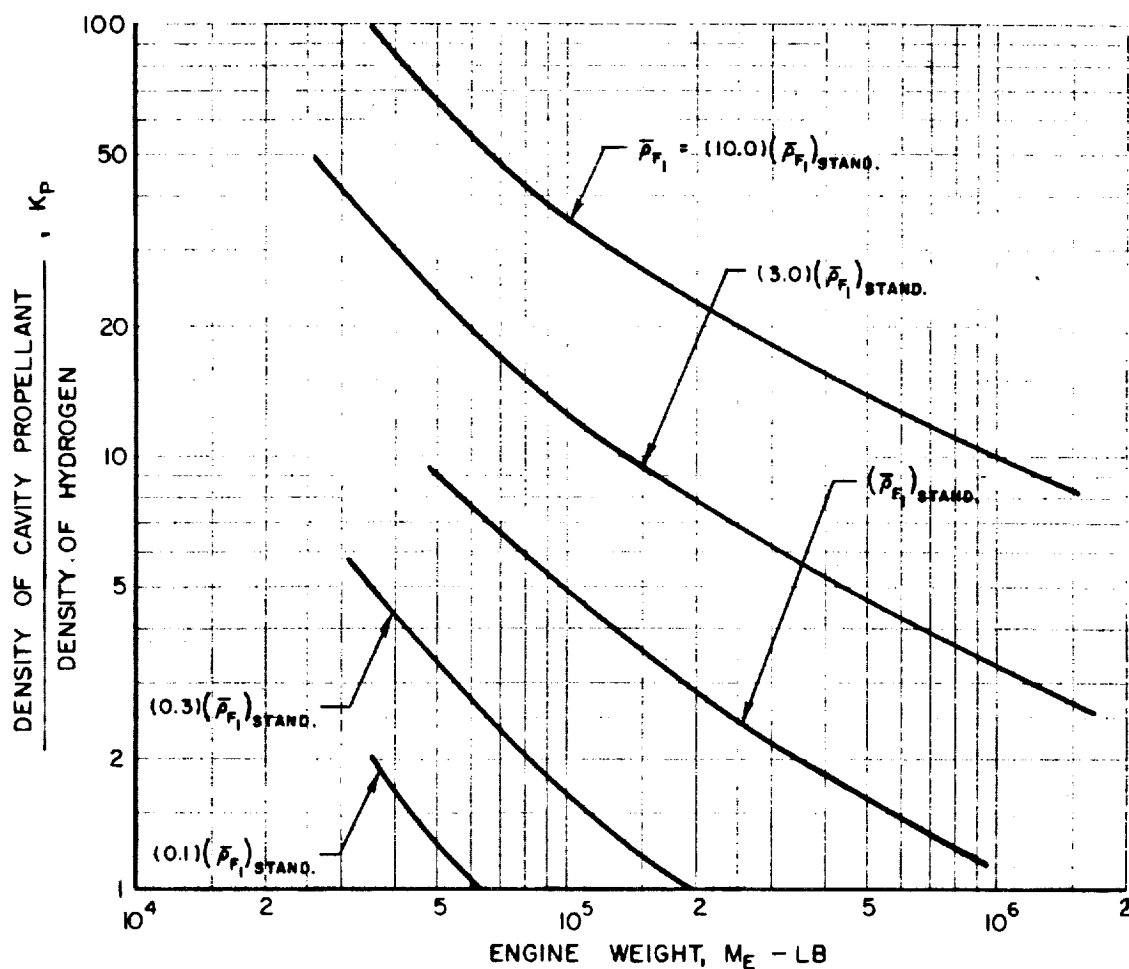


FIG. 31

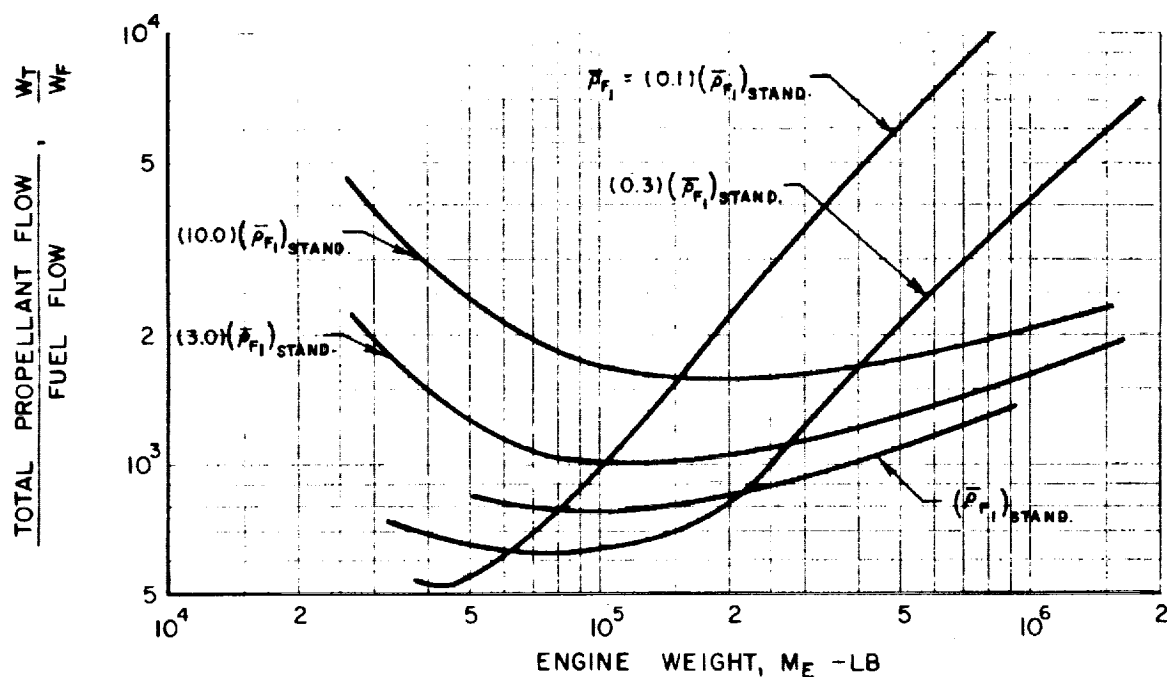
EFFECT OF ENGINE WEIGHT ON RATIO OF PROPELLANT TO FUEL FLOW FOR FIXED CRITERIA FOR CRITICAL FUEL DENSITY

SEE APPENDIX B

CURVES CALCULATED USING STANDARD VALUES OF PARAMETERS
EMPLOYED IN REF.36(SEE TEXT)

$(\bar{\rho}_{F_1})_{\text{STAND.}}$ GIVEN IN FIG. 10 OF REF. 36

$\tau_{F_1} = 0.01$

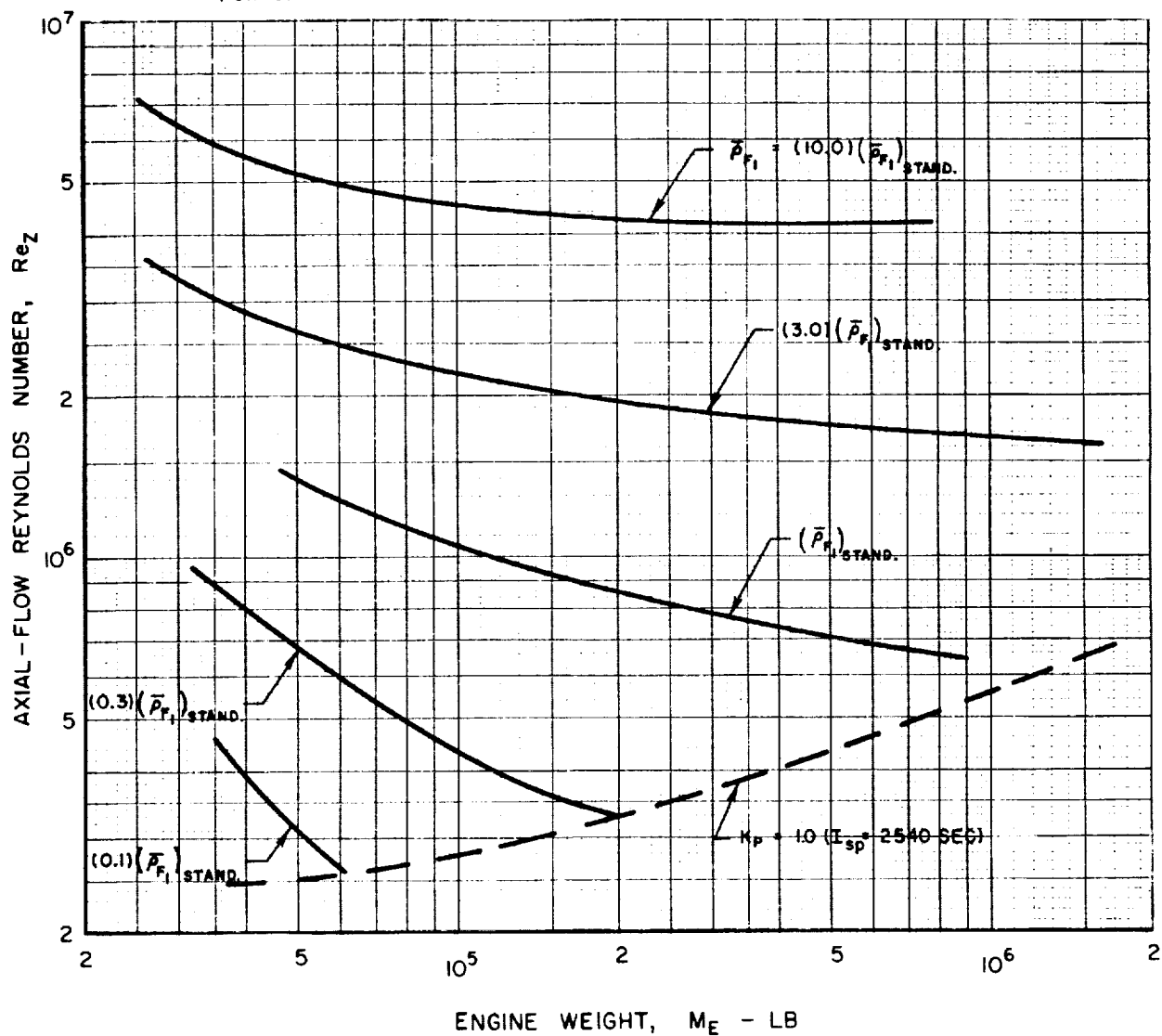


EFFECT OF ENGINE WEIGHT ON AXIAL-FLOW REYNOLDS NUMBER FOR FIXED CRITERIA FOR CRITICAL FUEL DENSITY

SEE APPENDIX B

CURVES CALCULATED USING STANDARD VALUES OF PARAMETERS
EMPLOYED IN REF.36(SEE TEXT)

$(\bar{\rho}_{F_1})_{\text{STAND.}}$ GIVEN IN FIG. 10 OF REF. 36



EFFECT OF ENGINE WEIGHT ON AXIAL-FLOW DYNAMIC PRESSURE FOR FIXED CRITERIA FOR CRITICAL FUEL DENSITY

SEE APPENDIX B

CURVES CALCULATED USING STANDARD VALUES OF PARAMETERS
EMPLOYED IN REF. 36 (SEE TEXT)

$(\bar{p}_1)_{\text{STAND}}$ GIVEN IN FIG. 10 OF REF. 36

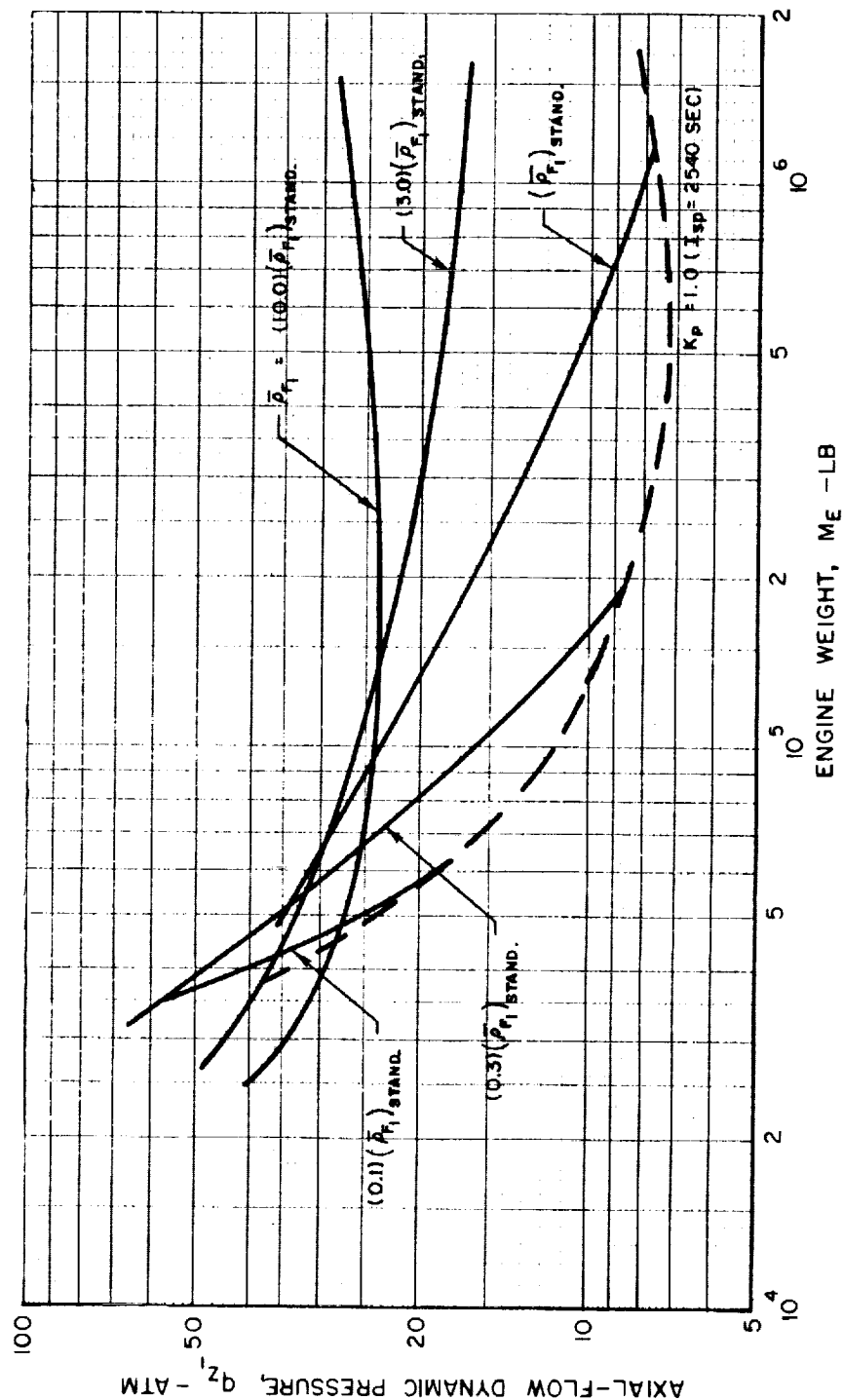


FIG. 33

EFFECT OF ENGINE WEIGHT ON FRACTION OF PROPELLANT FLOW PASSING THROUGH CAVITY FOR FIXED CRITERIA FOR CRITICAL FUEL DENSITY

SEE APPENDIX B
CURVES CALCULATED USING STANDARD VALUES OF PARAMETERS
EMPLOYED IN REF. 36 (SEE TEXT)

$(\bar{P}_F)_{\text{STAND.}}$ GIVEN IN FIG. 10 OF REF. 36

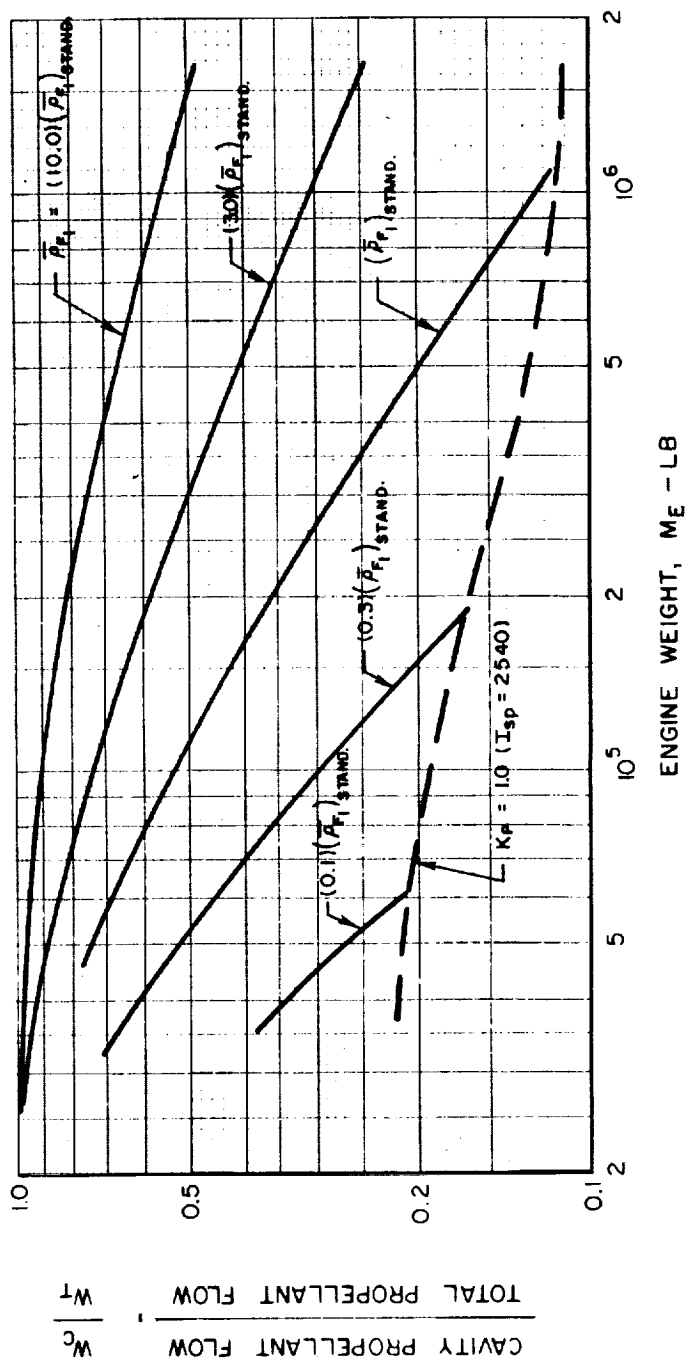


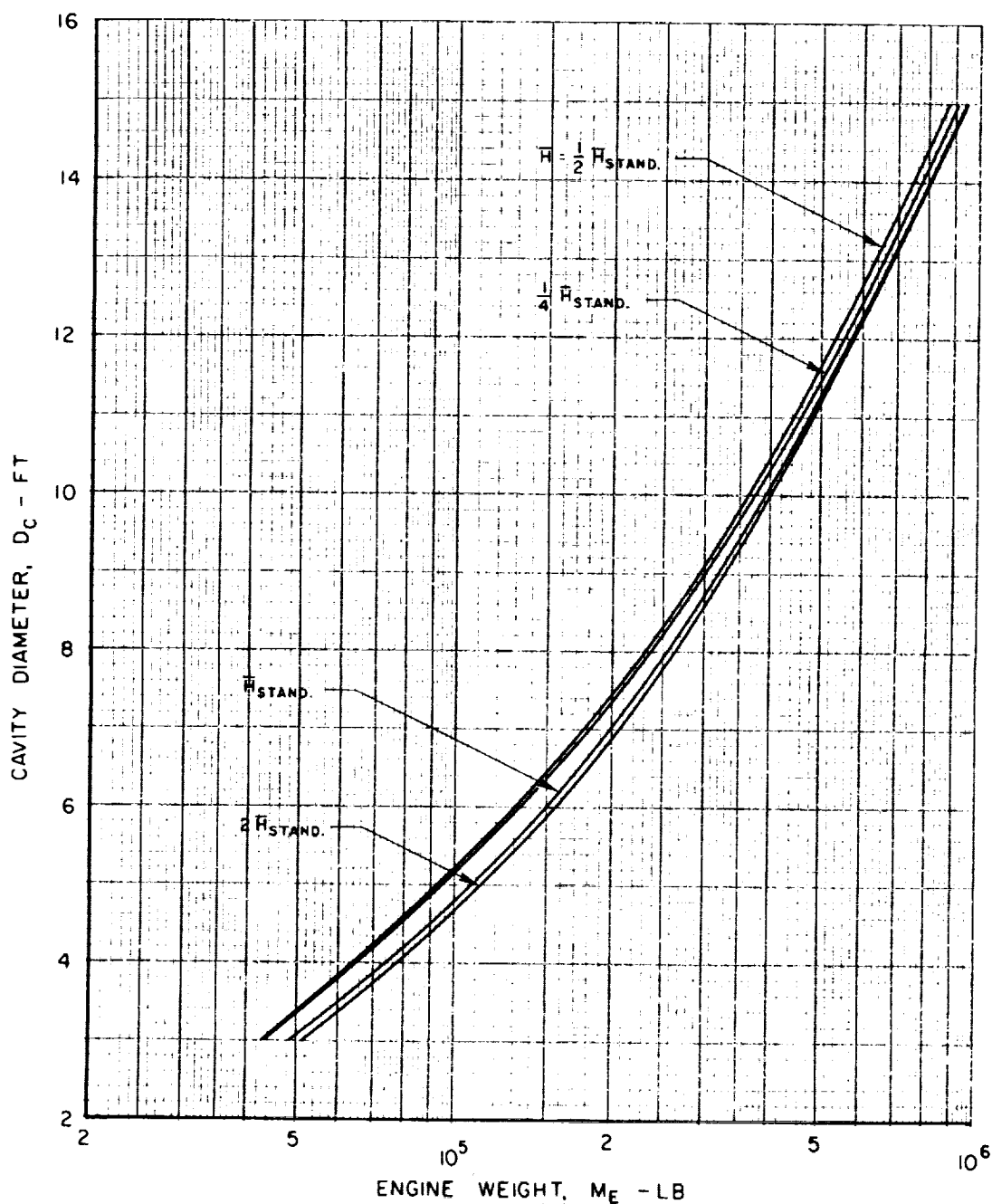
FIG.34

EFFECT OF ENGINE WEIGHT ON CAVITY DIAMETER FOR FIXED CRITERIA FOR CAVITY PROPELLANT ENTHALPY

SEE APPENDIX B

CURVES CALCULATED USING STANDARD VALUES OF PARAMETERS
EMPLOYED IN REF. 36 (SEE TEXT)

STANDARD VALUE OF CAVITY PROPELLANT ENTHALPY,
 $\bar{H}_{\text{STAND.}}$, GIVEN IN FIGS. 4 AND 5 OF REF 36



EFFECT OF ENGINE WEIGHT ON SPECIFIC IMPULSE FOR FIXED CRITERIA FOR CAVITY PROPELLANT ENTHALPY

SEE APPENDIX B

CURVES CALCULATED USING STANDARD VALUES OF
PARAMETERS EMPLOYED IN REF. 36 (SEE TEXT)

STANDARD VALUE OF CAVITY PROPELLANT ENTHALPY,
 $\bar{H}_{\text{STAND.}}$, GIVEN IN FIGS. 4 AND 5 OF REF. 36

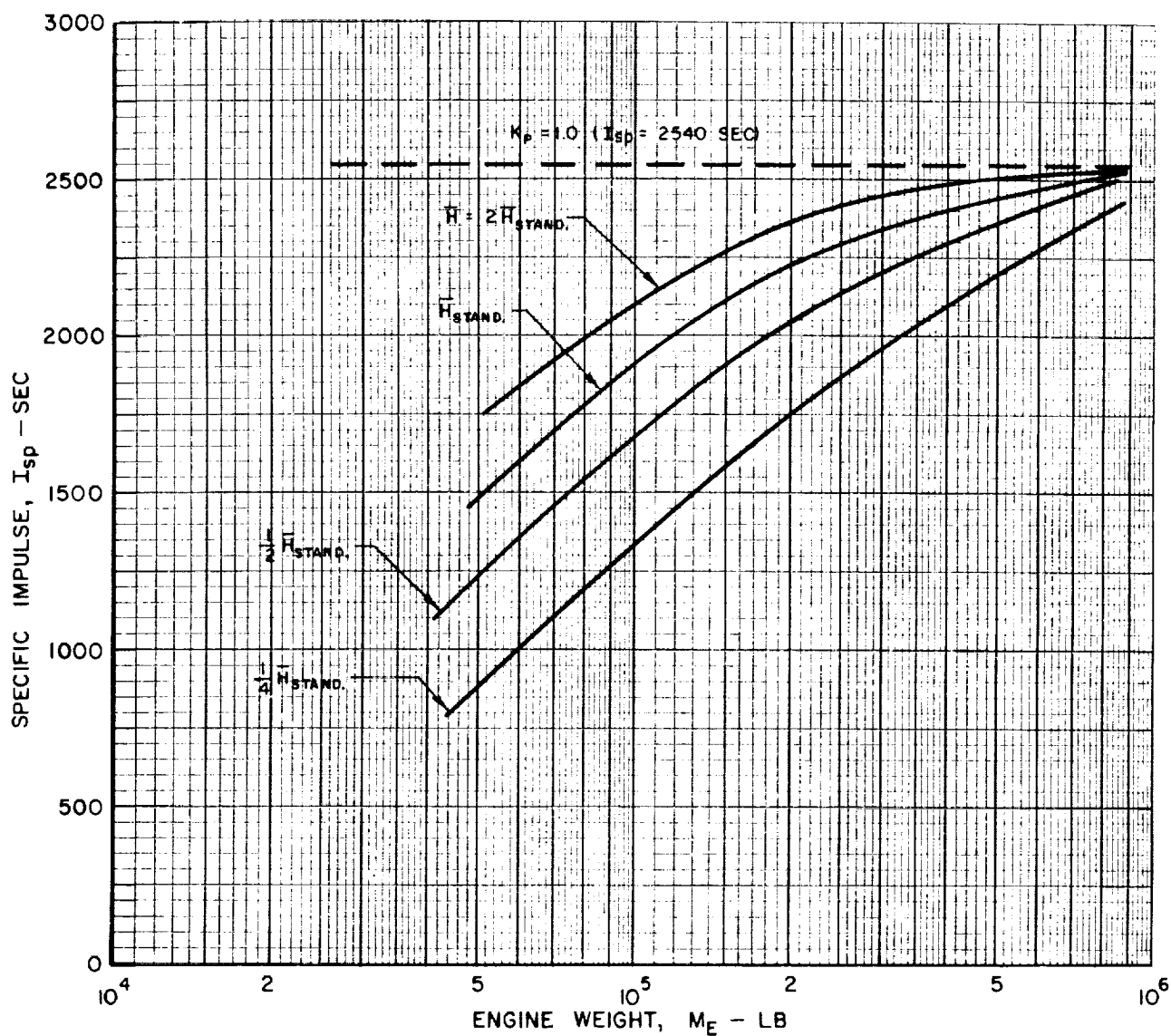


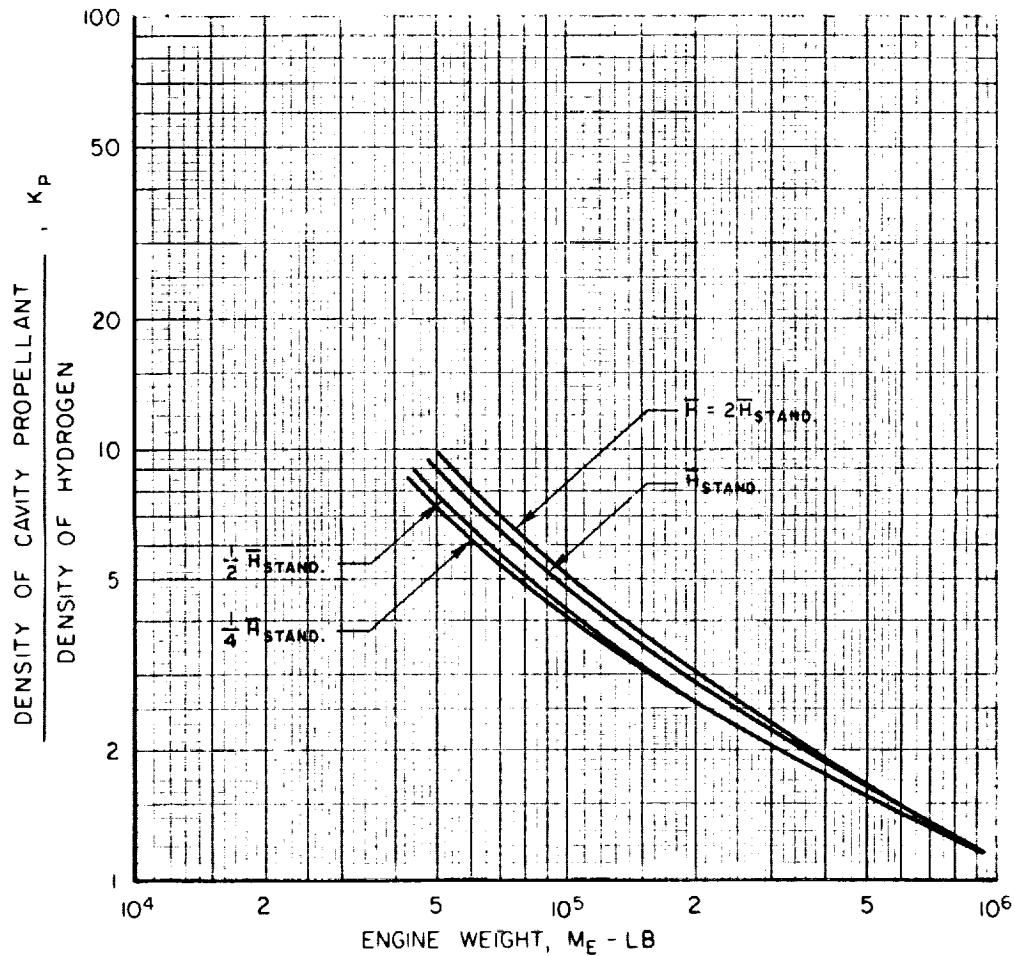
FIG. 37

EFFECT OF ENGINE WEIGHT ON RATIO OF CAVITY PROPELLANT DENSITY TO HYDROGEN DENSITY FOR FIXED CRITERIA FOR CAVITY PROPELLANT ENTHALPY

SEE APPENDIX B

CURVES CALCULATED USING STANDARD VALUES OF PARAMETERS
EMPLOYED IN REF 36 (SEE TEXT)

STANDARD VALUE OF CAVITY PROPELLANT ENTHALPY,
 \bar{H}_{STAND} , GIVEN IN FIGS. 4 AND 5 OF REF. 36



EFFECT OF ENGINE WEIGHT ON RATIO OF PROPELLANT TO FUEL FLOW FOR FIXED CRITERIA FOR CAVITY PROPELLANT ENTHALPY

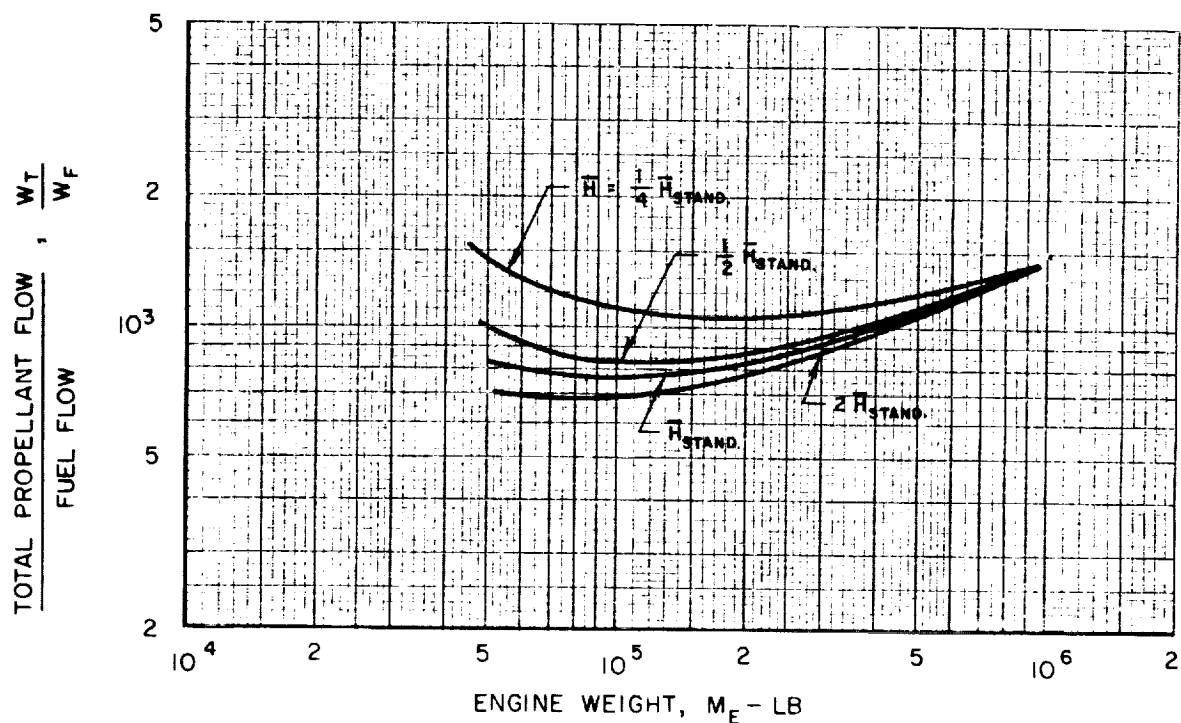
SEE APPENDIX B

CURVES CALCULATED USING STANDARD VALUES OF PARAMETERS

EMPLOYED IN REF. 36 (SEE TEXT)

STANDARD VALUE OF CAVITY PROPELLANT ENTHALPY, $\bar{H}_{\text{STAND.}}$,

GIVEN IN FIGS 4 AND 5 OF REF. 36



EFFECT OF ENGINE WEIGHT ON AXIAL-FLOW REYNOLDS NUMBER FOR FIXED CRITERIA FOR CAVITY PROPELLANT ENTHALPY

SEE APPENDIX B

CURVES CALCULATED USING STANDARD VALUES OF PARAMETERS

EMPLOYED IN REF. 36 (SEE TEXT)

STANDARD VALUE OF CAVITY PROPELLANT ENTHALPY, $\bar{h}_{\text{STAND.}}$,
GIVEN IN FIGS. 4 AND 5 OF REF. 36

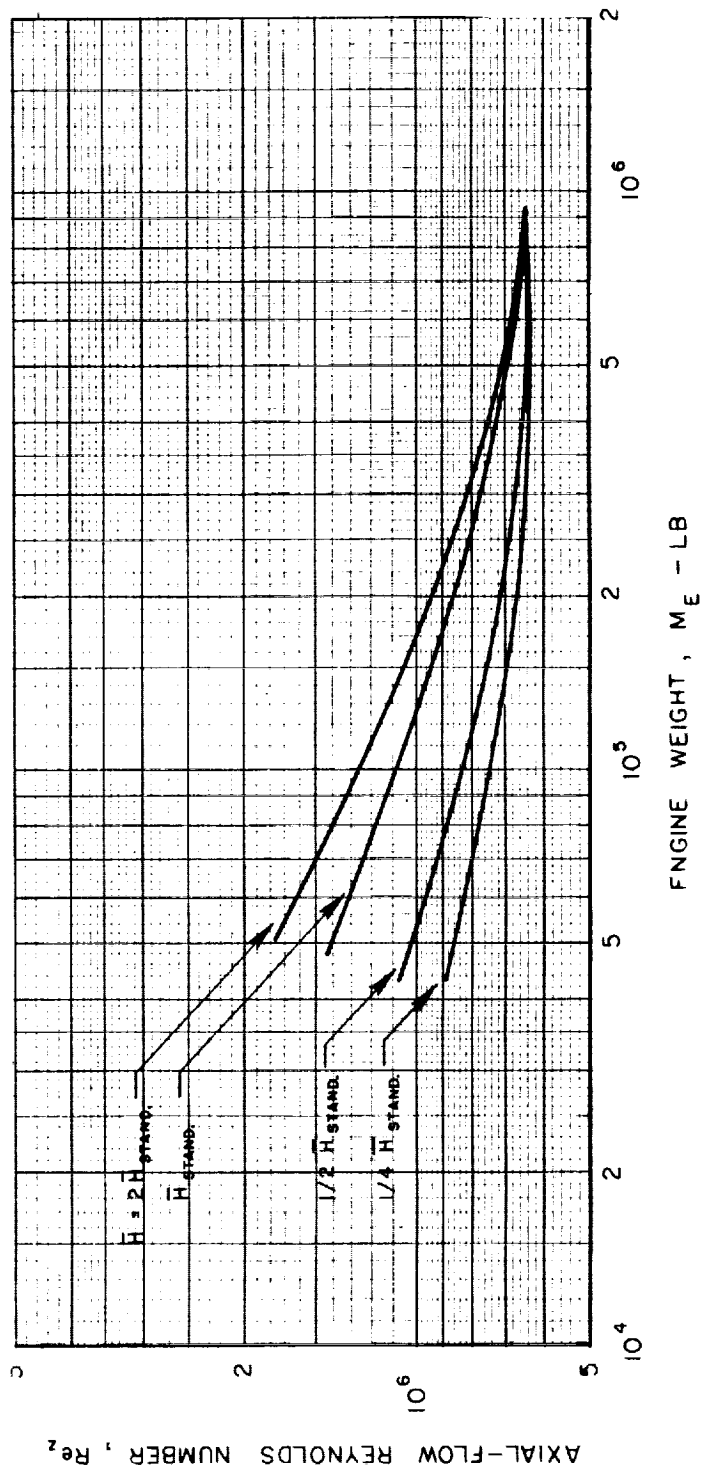


FIG 39

EFFECT OF ENGINE WEIGHT ON AXIAL-FLOW DYNAMIC PRESSURE FOR FIXED CRITERIA FOR CAVITY PROPELLANT ENTHALPY

SEE APPENDIX B

CURVES CALCULATED USING STANDARD VALUES OF PARAMETERS
EMPLOYED IN REF. 36 (SEE TEXT)

STANDARD VALUE OF CAVITY PROPELLANT ENTHALPY, $\bar{H}_{\text{STAND.}}$
GIVEN IN FIGS. 4 AND 5 OF REF. 36

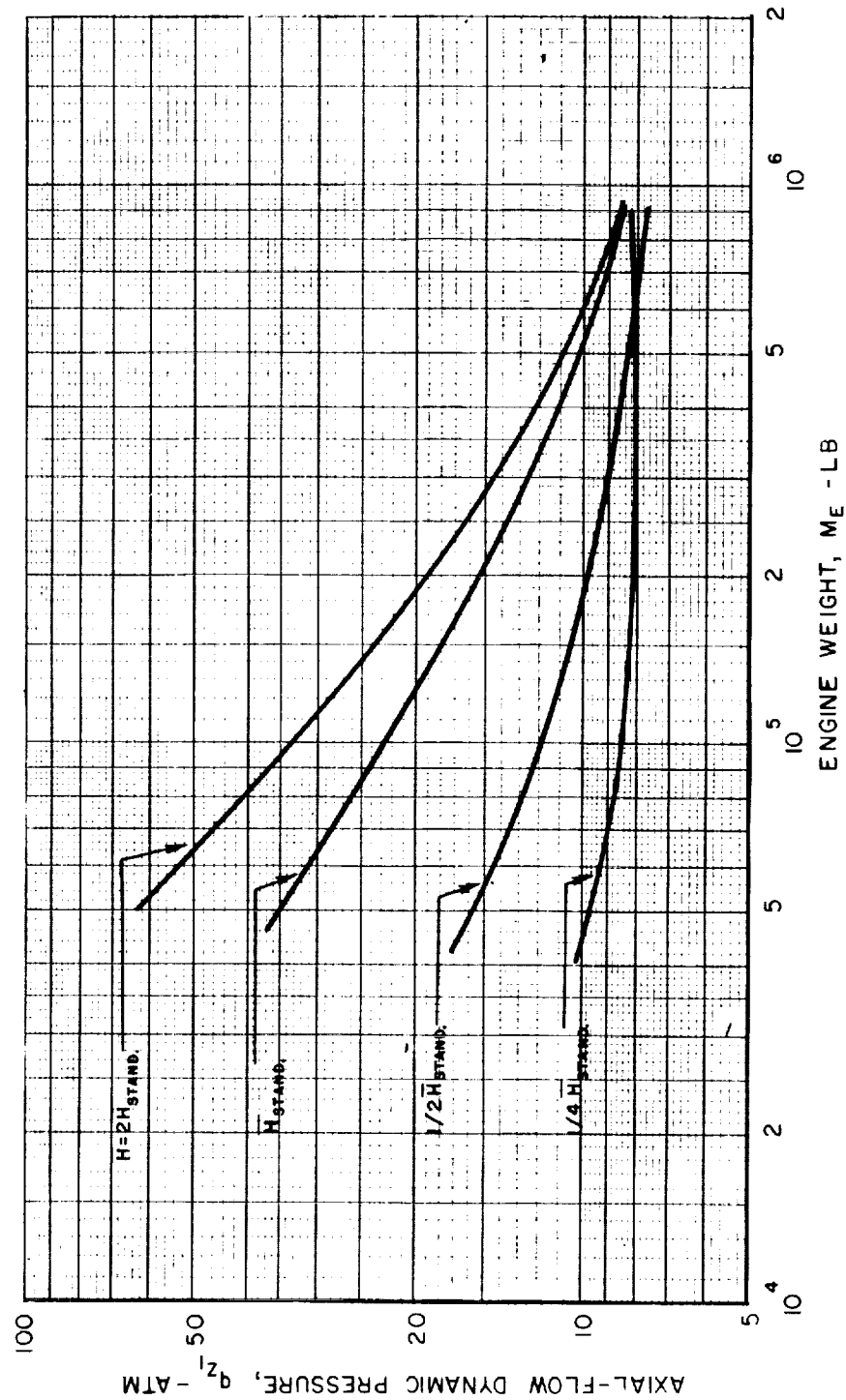


FIG. 40

EFFECT OF ENGINE WEIGHT ON FRACTION OF PROPELLANT FLOW PASSING THROUGH CAVITY FOR FIXED CRITERIA FOR CAVITY PROPELLANT ENTHALPY

SEE APPENDIX B

CURVES CALCULATED USING STANDARD VALUES OF PARAMETERS EMPLOYED IN REF. 36 (SEE TEXT)

STANDARD VALUE OF CAVITY PROPELLANT ENTHALPY, $H_{\text{STAND.}}$, GIVEN IN FIGS. 4 AND 5 OF REF. 36

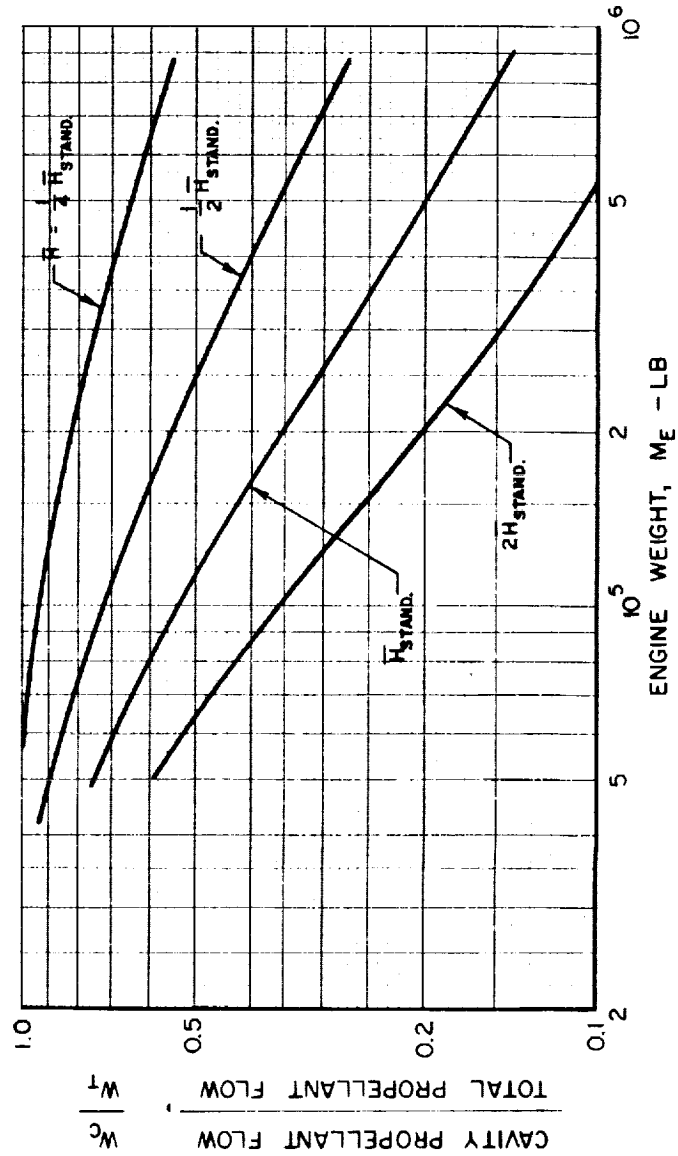
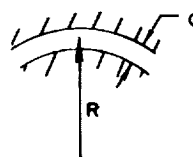


FIG. 41

COMPARISON OF FRICTION COEFFICIENTS IN STRAIGHT AND CURVED DUCTS

$$f \sim (Re_d)^n$$



DATA FOR CURVED DUCTS FROM REFS. 59 AND 60

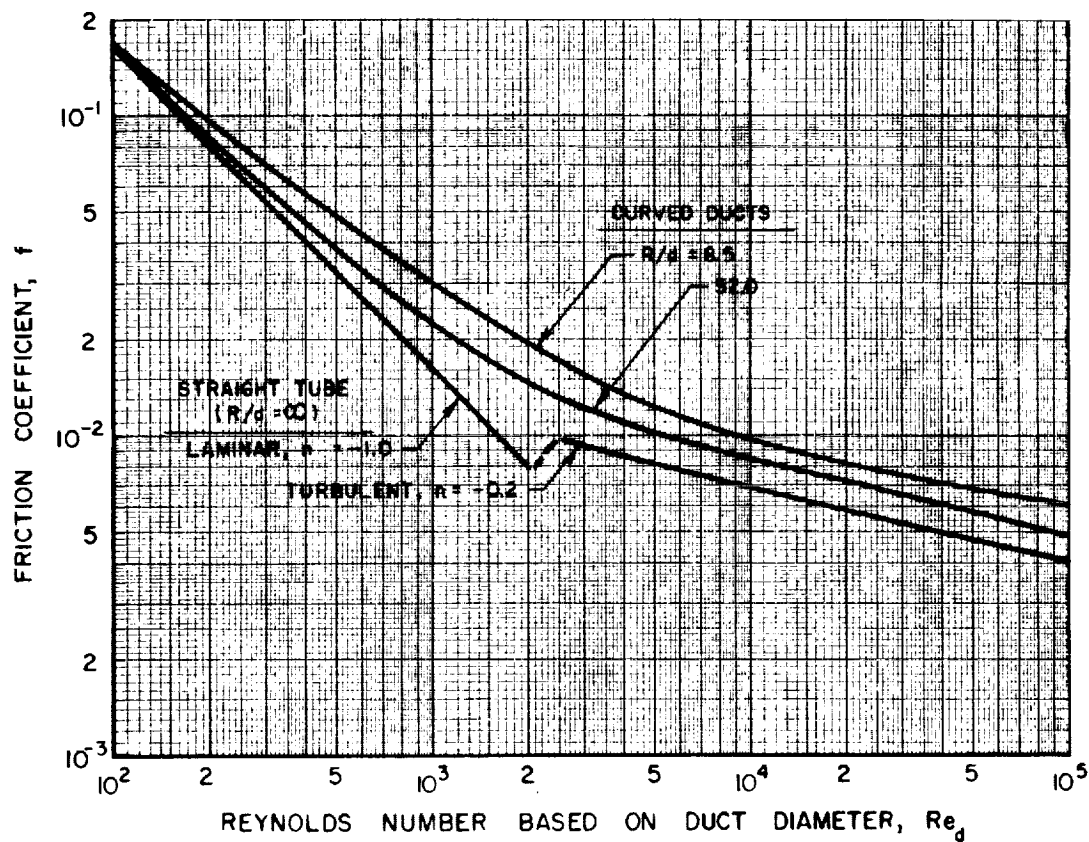
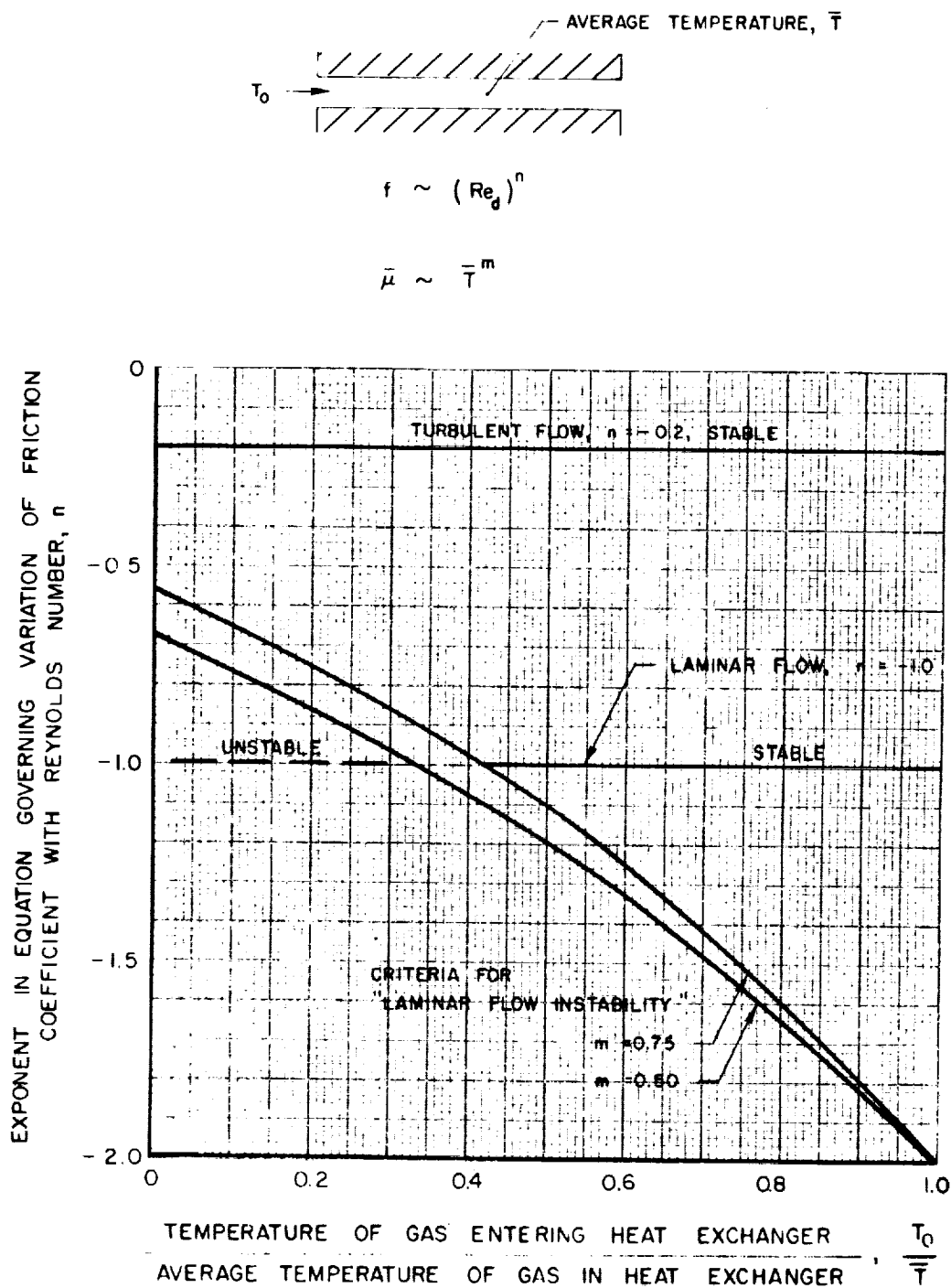


FIG. 43

APPROXIMATE CRITERIA FOR LAMINAR FLOW INSTABILITY IN HEAT EXCHANGER



[REDACTED]

[REDACTED]